ON THE RELIABILITY OF THERMOLUMINESCENCE DATING APPLIED TO BEACH DUNES DEPOSITED 0-700,000 YEARS AGO

OR

THE SANDS OF TIME

by

Jennifer J. Kirkey

B.Sc. Trent University 1983

THESIS SUBMITTED IN PARTIAL FULFILLMENT OF

THE REQUIREMENTS FOR THE DEGREE OF

MASTER OF SCIENCE

in the Department

of

Physics

SIMON FRASER UNIVERSITY

1988

APPROVAL

Name: Jennifer J. Kirkey

Degree: Master of Science

Title of thesis: On The Reliability Of Thermoluminescence Dating Applied To Beach Dunes Deposited 0-700,000 Years Ago or The Sands Of Time

Examining Committee:

Chairman: Dr. D. Boal

Dr. E. Nelson
Senior Supervisor

Dr. D.J. Huntley

Dr. G. Kirczenow

Dr. J.M. D'Auria
External Examiner
Professor
Department of Chemistry
Simon Fraser University

Date Approved: February 12, 1988

PARTIAL COPYRIGHT LICENSE

I hereby grant to Simon Fraser University the right to lend my thesis, project or extended essay (the title of which is shown below) to users of the Simon Fraser University Library, and to make partial or single copies only for such users or in response to a request from the library of any other university, or other educational institution, on its own behalf or for one of its users. I further agree that permission for multiple copying of this work for scholarly purposes may be granted by me or the Dean of Graduate Studies. It is understood that copying or publication of this work for financial gain shall not be allowed without my written permission.

Title of Thesis/Project/Extended Essay

On the Reliability of Thermoluminescence Dating Applied to Beach Dunes Deposited 0 - 700,000 Years Ago or The Sands of Time

Author: (signature)

Jennifer Kirkey (name)

Feb 15/1988 (date)

ABSTRACT

There is a need for an absolute, chronological dating technique which could be generally applied to sediments from fifty thousand to one million years old. Thermoluminescence dating has great potential to fill this need, but it will not be considered a valuable technique until it has been shown to be reliable.

The research presented in this thesis was done to see if thermoluminescence can be used to date sediments in this crucial age range. A series of thermoluminescence measurements was done on 100 μm quartz grains which had been extracted from a sequence of stranded beach dunes in south-east South Australia. The dunes have been independently dated, and their age estimates ranged from 0 to 700,000 years.

Three separate methods were used in an attempt to determine the radiation doses to which the dunes were exposed since their deposition. These methods were the partial-bleach method of Huntley and Wintle, a technique which involved matching growth curves from modern and old samples, and a "new" technique which attempted (unsuccessfully) to use an aspect of the pre-dose behaviour of the high temperature 375° peak.

The dose-rate for each dune was determined from in situ measurements, alpha counting and chemical analyses. The dose-rates were less than one Gray (Gy) per thousand years. The

presence of heavy minerals, which contained a large fraction of the below average amounts of uranium and thorium, made correction factors to the usual dose-rate equation necessary. A large fraction of the total error in the age equation was due to uncertainties in the dose-rate.

The age of each dune was calculated by dividing the total dose estimate by the dose-rate. Reasonable dates in the 0 to 200,000 year age range were found using the partial-bleach method and the "growth curve matching" technique, although the latter technique required the use of scaling factors. The behaviour of the pre-dose effect was erratic, so no dates were obtained with this technique.

The results obtained demonstrate that thermoluminescence dating can produce reliable ages which partially fill the "age gap" left by other sediment dating techniques.

ACKNOWLEDGEMENT

I must acknowledge my senior supervisor D.J. Huntley for his introduction to this topic. I found the research fascinating, and I learned a lot from him. His insightful comments helped clear up both research and writing problems. It has been a most interesting experience.

Without the advice, help and friendship of Glenn Berger this work would never have been completed. John Prescott and John Hutton from the University of Adelaide were invaluable, as they helped collect samples, did much of the geochemical analysis, and brought timely ideas and encouragement.

Many thanks to Stuart Cowan who wrote many of the computer programs used in the analysis of the data, to Ranjith Divigalpitiya for some of the figures used in this thesis, and to my patient proofreaders; Stuart Cowan and Dorothy Godfrey-Smith.

I would like to gratefully acknowledge the partial financial support from my supervisor through a research grant from the the Natural Sciences and Engineering Research Council of Canada, the teaching assistantships and the Graduate Research Fellowship from Simon Fraser University.

I wish to thank all the people whose friendship helped to keep me laughing throughout the course of this work, with special thanks to Vernon Hale for his support and patience.

QUOTABLE QUOTES

I could upon a light affriction easily perceive the stone to shine.

I also brought it to some kind of glimmering light, by taking it to bed with me, and holding it a good while upon a warm part of my naked body.

Sir Robert Boyle in "Observation made this 27th of October, 1663, about Mr. Clayton's Diamond"

(Ancient TL, 1981)

...the earth was held in thrall by relentlessly probing fingers of ice - ice that drew its power from frigid strongholds in the north, and flowed southward to bury forests, fields, and mountains. Landscapes that were violated by the slowly moving glaciers would carry the scars of this advance far into the future. Temperatures plummeted, and land surfaces in many parts of the world were depressed by the unrelenting weight of the thrusting ice. At the same time, so much water was drawn from the ocean to form these gargantuan glaciers that sea levels around the world fell by 350 feet, and large areas of the continental shelf became dry land.

John Imbrie and Katherine Imbrie, in Ice Ages, 1979

TABLE OF CONTENTS

List of Tables

LIST OF FIGURES

CHAPTER I

INTRODUCTION

1.1 Nature Of The Problem

Geologists need an absolute, chronological, dating technique which can be generally applied to sediments which are 50,000 to 1,000,000 years old. Currently, the main source of information about the ages of sediments comes from radiocarbon dating, which can be used to date organic materials which are 200 - 50,000 years old. Other techniques, such as potassium-argon, fission track and uranium-series dating can be used in materials more than 100,000 years old. Unfortunately, these techniques require materials which are not commonly found in geological sediments. Furthermore, they date the time since the material was formed, which is not necessarily the time since it was deposited in the formation under study. These techniques are limited in both their range of applicability and temporal scope.

Thermoluminescence dating has the potential to fill this age gap. Thermoluminescence is used to measure the radiation dose which a mineral has received since it was formed, or since its last exposure to sunlight or high temperatures ($\simeq 500^{\circ}C$). The environment around the sample is analyzed to determine the dose-rate, and the age is calculated from the following equation:

$$\text{Age} = \frac{\text{Dose}}{\text{Dose-Rate}}$$

The thermoluminescent signal from common minerals such as quartz and feldspar can be used to measure doses on the order of 1 to ≃200 grays (Gy). A typical dose-rate for rocks with 2 ppm of uranium and thorium and 1% by weight of potassium oxide is about 2 Gy per 1000 years. Samples up to ≃ 100,000 years can be dated.

Thermoluminescence has great potential, but it will not be considered a useful technique until it has been shown to be reliable in a variety of situations. This can be done by working with independently dated sediments to see if the expected ages can be obtained.

1.2 Summary Of Purpose, Scope And Method

A stranded beach dune sequence in south-east South Australia had been independently dated and was found to range in age from 0 to 700,000 years (Schwebel, 1978). The work described in this thesis used samples from this sequence to test the upper limit and accuracy of thermoluminescence dating.

Three separate methods were used in the attempt to determine the dose the samples had received in the environment. The first method had been developed in the late 1970's (Wintle and Huntley, 1979, 1980) while the other two were new techniques.

Various methods were used to find the dose-rates. Chemical analysis was done to determine the percentage weight of

potassium oxide in the samples while alpha counting and chemical analysis were used to find the uranium and thorium contents. In situ dosimetry was done at a few of the sample sites. The cosmic ray contribution was calculated using a knowledge of the depth at which the sample was collected.

1.3 Most Significant Outcome Of The Investigation

Reasonable dates were obtained for samples less than 200,000 years old. Few thermoluminescent dates in the 100,000 year range have been obtained, and rarely has there been the opportunity to check the validity of the thermoluminescent dates with dates obtained by other techniques. The older samples could not be dated with the techniques used in this thesis.

1.4 State of the problem at the end of the Investigation

There still exists a need to date sediments which are older than 200,000 years. More work should be done to see if a technique can be found which will increase the upper age limit.

There was evidence that the radioactive elements were not evenly distributed throughout the samples. Corrections were made to the dose-rate calculations, but further work could be done to quantify the extent to which the distribution was non-uniform and the effect on the dose received by the samples.

Improved sample preparation techniques helped increase the reproducibility of the data, but the causes of scatter in thermoluminescent measurements should be studied further.

CHAPTER II

BACKGROUND INFORMATION AND REVIEW

The following chapter will provide some background information for the work done in this thesis. Those who are familiar with sediment dating techniques, both TL and otherwise, may not find it necessary to read this chapter. The "jargon" of thermoluminescence will be introduced and explained. The physics of thermoluminescence will be discussed, and a brief review of the last 20 years in the thermoluminescence dating of sediments will be presented. This chapter will lay the groundwork for the specifics of the project which will be discussed in Chapter 3.

2.1 Review Of Non-Thermoluminescence Dating Techniques

The following section will give a brief overview of the various methods used to date geological sediments. It will demonstrate the need for another generally applicable dating method which can be used in the 50,000 - 1,000,000 year age range, and it will also provide a description of the various types of techniques which were used to date the samples studied in this thesis.

2.1.1 Radiocarbon Dating

The ratio of ^{14}C to ^{12}C in the atmosphere is about 10^{-12} to 1 (Libby, 1955). This ratio is also found in living organisms

which incorporate CO_2. A similar situation applies to shell and to some carbonate deposits. After the organism dies, the weakly radioactive ^{14}C decays with a half-life of 5730 years, causing the $^{14}C/^{12}C$ ratio to decrease. Measurement of the present day ratio can give some idea of the time since the organism died. This technique has an upper age limit of ≃50,000 years, (Libby, 1967) although very sophisticated apparatus and specialized techniques have been used to increase this age limit to ≃70,000 years (Grootes, 1978). Radiocarbon dating is the prime source of dates for young geologic sediments, though the age restriction and the need for organic samples limits its usefulness.

For a more thorough explanation and review of this important technique, the reader can consult the references cited above or almost any introductory archaeology or geology textbook.

2.1.2 Uranium-Series Dating

Uranium's radioactive decay processes have been extensively studied (See Appendix A for an abbreviated list of the daughter products). If uranium is deposited in rock or shell, the concentrations of the parent and daughter atoms begin to reach equilibrium. The equilibrium amounts are proportional to the half-lives of the decay product. Present-day concentrations can be measured and decay equations (Rosholt, 1967, York and Farquhar, 1972) can be used to determine the time since the original equilibrium was upset.

Shell, stalagmites and bone can be dated if it is assumed that the water-soluble uranium was incorporated at formation, but that the insoluble ^{230}Th or ^{231}Pa was not. These radionuclides, with the respective half lives of 75 ka and 33 ka, are the two most often used to U-series date geological sediments.

For further reading, Hamilton (1965) and Hamilton and Farquhar (1968) are recommended.

2.1.3 Palaeomagnetism

The intensity and direction of the earth's magnetic field vary with time. When materials such as clay or lava cool, or sediments are deposited, they acquire a weak magnetization in the same direction as the external magnetic field.

As well as small-scale secular variations of the earth's magnetic field which occur on the order of decades or centuries, there have been global reversals in the magnetic field direction. While the exact dates for such reversals are difficult to establish precisely, it is generally accepted that the last major reversal occurred ≃730,000 years ago (Tarling, 1983).

While this technique cannot give a direct estimate of the age of a sample, palaeomagnetic measurements can be done on sediment sequences. If a reversal is found, age limits can be assigned to the sediments.

The book Palaeomagnetism by Tarling (1983) provides a good introduction to this topic.

2.1.4 Amino-Acid Dating

Amino-acid racemization dating uses a chemical change to date organic materials such as bone and shell. The amino acids which form the protein of living organisms are entirely of one type or "orientation". As time passes, the amino acids slowly racemize (change orientation). The ratio of the two types is thus a measure of how much time has passed since the organism died. Each amino acid has a different racemization rate, and all the rates are highly temperature and species dependent. Changes of 1°C can cause a 15-20% change in the transformation rate (Masters and Bada, 1978).

Recent results have demonstrated that there are some major problems with amino acid dates which have been obtained in the past (Taylor, et al, 1985).

2.1.5 The Oxygen-Isotope Record

The ratio of $^{18}O/^{16}O$ atoms in seawater is about 1/500 (CRC Handbook, 57th ed.). The ratio of $^{18}O/^{16}O$ atoms in deposited materials which have incorporated oxygen extracted from the surrounding water depends on many factors, the dominant ones being the isotopic concentration of the surrounding water and the water temperature. The isotopic concentration changes as ^{16}O is preferentially evaporated from the ocean water due to its

lighter mass, then deposited in glacial ice (Covey and Schneider, 1984) When calcium carbonate ($CaCO_3$) is inorganically deposited or incorporated into a shell, the concentration of ^{18}O drops as the water temperature increases (Imbrie, et al., 1984).

Ocean cores contain sediments deposited over a long period of time, sometimes several million years. If shells from top-dwelling species are measured, the change in the isotope ratio can give information about surface sea water temperature fluctuations as a function of time. Study of bottom-dwelling species (which live in water whose temperature is always 4°C) can yield information about changes in the isotopic oxygen concentration of the surrounding water, which can be used to determine global sea level fluctuations, and thus the amount of glacial ice on earth, as a function of time (Imbrie et al., 1984). See Chapter 3 for some examples of these isotope curves.

The last reference cited above is an excellent article which gives some background information as well as presenting some of the latest results in oxygen-isotope dating.

While this technique cannot be used to date directly land based sediments, in a few cases, shoreline erosion or deposition events can be matched to sea level changes and assigned probable dates.

2.1.5.1 The Milankovitch Theory

Data from the oxygen-isotope record has been found to be periodic. It has lent support to an interesting astronomical theory of the ice ages, which will be briefly outlined below.

The earth's pole precessess, completing one revolution in ≃26,000 years. Its orbit is slightly elliptical, and the ellipse rotates slowly counterclockwise, with the four cardinal points shifting in cycles of 23,000 and 19,000 years. The axial tilt varies independently with a 41,000 year period and the eccentricity of the earth's orbit changes with variations of ≃0-6% over a 100,000 year cycle.

In the early twentieth century, Milutin Milankovitch assumed that the cyclic variations of the orbital eccentricity and axial tilt and the precession of the equinoxes were the important factors influencing the global climate. This led him to propose a cyclic theory of the ice ages which went against the then accepted theory of catastrophism. There was hope that his theory could be tested someday when absolute dating techniques became available.

In the 1970's CLIMAP, an interdisciplinary, inter-institutional project to map the surface of the earth during the last ice age and to measure the changes in the Pleistocene climate was begun. Variations in the oxygen-isotope ratio from ocean cores were studied and the first evidence for sea level changes which contained dominant cycles of 100,000,

43,000, 24,000 and 19,000 years was found. This was clear evidence for an astronomical influence on the climate and the ice ages (Imbrie and Imbrie, 1979).

Greater understanding of the cause of ice ages could lead to more accurate estimates of the date when such events occured, and may occur again.

2.1.6 Summary of the Review

Figure 2.1 illustrates the age gap left by the methods discussed in this section. As this age gap is of great interest to many geologists and archaeologists, there is a need for another dating method which will be generally applicable in this age range. Thermoluminescence dating has the potential to fill this gap, and will be be discussed in the following section.

2.2 Principles Of Thermoluminescence

2.2.1 Introduction

Thermoluminescence (TL) is the name given to thermally stimulated emission of light from an insulator or semiconductor following previous radiation energy absorption. It is caused by trapped electrons recombining with holes in the crystal lattice. It should not be confused with incandescence, the light which is spontaneously emitted from a substance when it is heated (Figure 2.2).

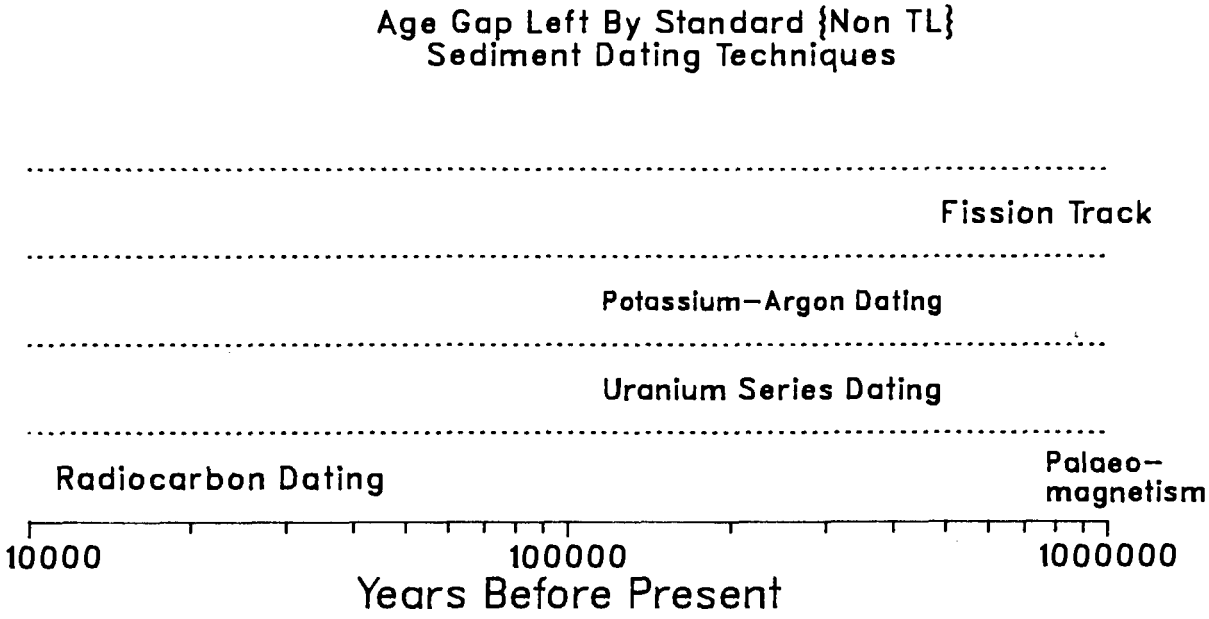

Figure 2.1

This schematic diagram shows the need for a sediment dating technique which is generally applicable in the 50 – 100,000 year age range.

There is no single existing dating technique which can be applied to both the marine and the terrestial sedimentary record. The techniques which have been devolped for dating the last million years are limited both by the time periods when they are useful, and by the few materials to which they can be applied.

TL Glow Curves
{TL Intensity vs. Temperature}

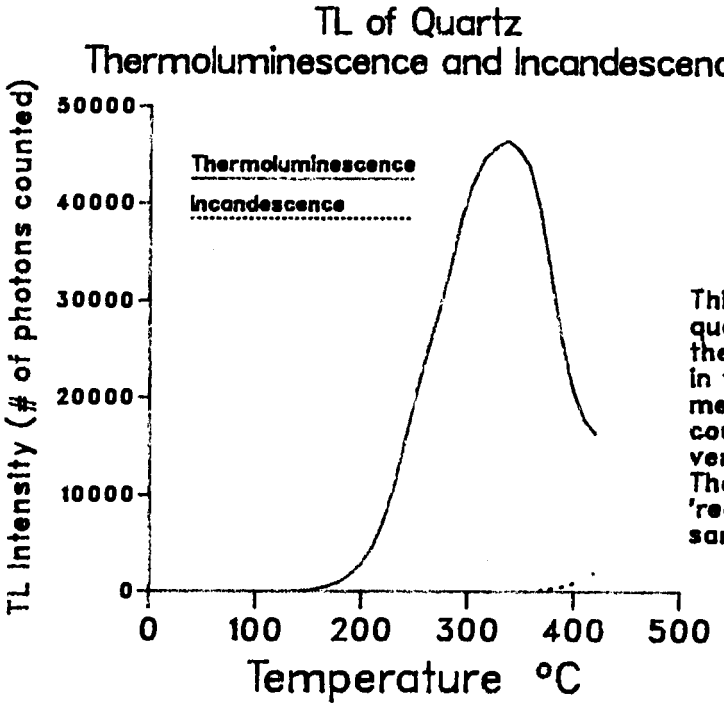

Figure 2.2a

This is an example of a typical quartz TL glow curve from one of the old (120 ka) samples studied in this thesis. The TL intensity was measured as the number of photons counted by the photomultiplier tube versus the temperature of the sample. The incandenscence is the 'red hot glow' from the sample as it is heated.

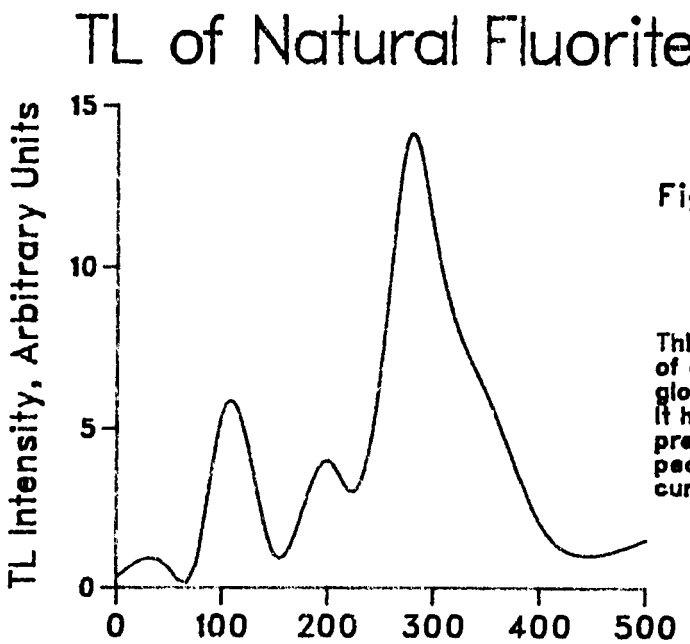

Figure 2.2b

This is an example of a more complex TL glow curve {Aitken, 1985}. It helps illustrate the presence of many different peaks present in the glow curve.

TL is acquired by a mineral as nuclear radiation passes through a crystal and strips electrons from the lattice atoms. Most of these are immediately recaptured by an atom, but a few get trapped at defects in the lattice. Note that a "defect" may also be an impurity atom. This process stores energy because a trapped electron is in a higher energy state than a ground-state (recombined) one. As the crystal is heated, the lattice vibrates. Some of the electrons become excited and are free to travel through the conduction band. They can then be captured by a deeper trap, recombine at a non-luminescent ("killer") centre (thermal quenching), or end up at a luminescent centre, emitting light in the recombination process (See Figure 2.3).

Luminescent centres are a special type of lattice defect. Often they are impurities like silver or manganese. The colour of light emitted depends on the impurity and its surroundings. The colour does not depend on the depth or type of trap in which the electron was originally captured.

TL can be used to measure the amount of radiation to which a sample has been exposed since its electron traps were last emptied. When a mineral or crystal is exposed to radiation from its surroundings and from cosmic rays, its electron traps slowly fill, and the number of trapped electrons increases as time passes. The TL signal is proportional to the number of trapped electrons, so the signal strength is proportional to the total dose which the sample has received.

Figure 2.3
The TL Process - Simple two-level model
Illustrates the trap depths and allowed transitions

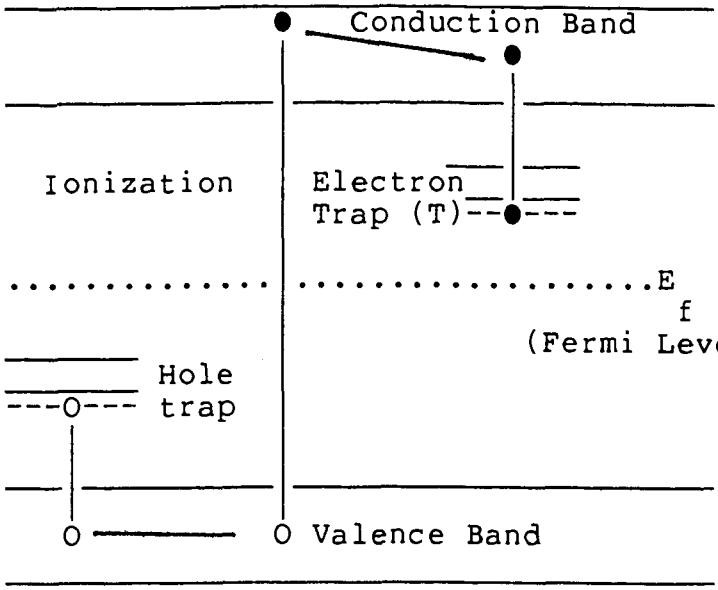

a) Irradiation:
Ionization occurs and the traps fill with electrons and holes.

O Electrons
O Holes

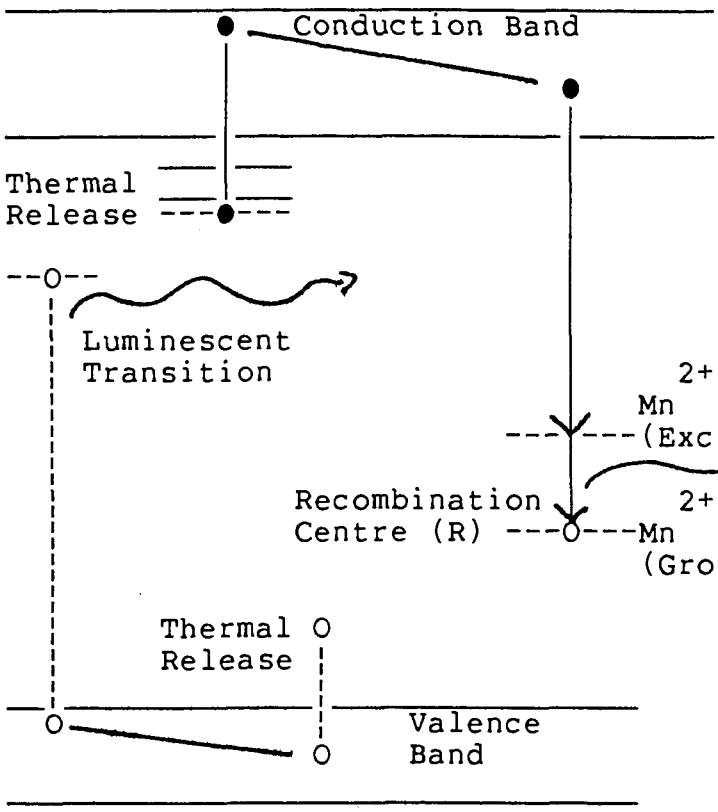

b) Heating:
The thermally released electrons (holes) recombine with luminescent centres and emit light (TL). The wavelength of the light is a characteristic of the luminescent centre.

(Divigalipitiya 1984, McKeever 1985)

The important phrase in the above description is "since the traps were last emptied". TL can measure the dose since the sample's formation, last heating, shock or exposure to light.

2.2.2 Mathematical Descriptions of some Important TL parameters

2.2.2.1 Length of time spent in a trap

If TL is to be used to date the ages of various materials, the length of time which the electrons are expected to remain trapped is an important parameter. One must be certain that the TL signal is stable over the time period being dated.

If Schrodinger's equation for electrons in a periodically varying potential is solved, one finds that there are only certain allowed energies for the electrons. In the Kronig-Penny model of a crystal, where a periodic array of potential wells is assumed, the number of electrons in each band is:

$$N(E) = Z(E)\, f(E)$$

$N(E)$ = Density of occupancy of energy level

$Z(E)$ = Density of available states

$f(E)$ = Fermi-Dirac distribution function

$$= \frac{1}{\exp((E-E_f)/kT) + 1}$$

E_f = Fermi Level, the chemical potential

At absolute zero in thermodynamic equilibrium, those energy levels less than E_f are full, while those greater than E_f are

empty. Electronic conduction occurs only when the electrons get enough energy to reach the conduction band. For an ideal crystal, $Z(E)=0$ for $E_{conduction} > E > E_{valence}$. However, in real crystals, with structural defects, impurities, etc., electrons can possess energies in the gap (McKeever, 1985, Figure 2.3).

This band gap description explains why electrons will remain trapped in a crystal. For a sample held at a constant temperature, the rate of electron escape from a trap depends on the probability of escape and the number of electrons which are still trapped (Fleming, 1974).

$$\frac{dn}{dt} = - pn \qquad (1)$$

n = number of electrons remaining at time t
p = probability of escape

The number of trapped electrons decays with time.

$$n = n_0 \exp(-pt) \qquad (2)$$

n_0 = number trapped at t=0

2.2.2.2 Simple Two-Level Model of TL

There are two localized energy levels; one level T acts as a trap, the other R as a recombination centre (Figure 2.3). The electron trap is empty before irradiation, and the recombination centre which full of electrons before irradiation is a potential hole trap. If the absorbed radiation energy is greater than the band gap energy, valence electrons can become free to travel through to the conduction band and free holes can be formed in

the valence band. These charge carriers can recombine with each other, or become trapped.

If the free electron becomes trapped at a trap T, recombination can take place only if the trapped electron absorbs enough energy E to be released back into the conduction band. The luminescence emission is delayed, the amount of delay being governed by the amount of time spent in the trap.

From thermodynamic arguments, the probability of escape p is related to the mean time by:

$$\frac{1}{\text{mean time}} = p = s \exp(-E/kT) \qquad (3)$$

s = constant, the frequency factor
E = trap depth
k = Boltzmann's constant

If a trap T is deep enough so that E is much greater than kT_0 (T_0 is the temperature of irradiation), its electron will, on average, remain trapped for a long period of time. The traps irradiated at a temperature T_0 will tend to be stable if the trap depth E satisfies $E >> kT_0$. To be useful in TL dating, the trap depth, storage temperature and frequency factor must combine such that the mean time spent in a trap is on the order of, or greater than, the age of the sample being studied.

As the free electrons and holes are created and annihilated in pairs, there are equal populations at T and R. In general, $(E_{\text{electron trap}} - E_f) > (E_f - E_{\text{recombination centre}})$ (McKeever 1985). The trapped electrons and holes are in a non-equilibrium state, and they will attempt to return to equilibrium, but the

relaxation rate is slow, as the perturbation (irradiation) was performed at low temperatures. The electrons are in a meta-stable non-equilibrium state, whose relaxation time is determined by the trap depth (E) and the frequency factor (s).

For example, a certain glow curve peak (375°C) in quartz, is believed to correspond to a trap with a depth E = 1.7 eV, $s = 1.5 \times 10^{13}$ sec^{-1} (Aitken, 1974). With a storage temperature at 40 °C, this gives a mean lifetime equal to 4.8×10^{6} years.

2.2.2.3 TL Intensity

If the temperature of the sample is raised so that that $E \simeq kT$, then electrons will be released from the traps, recombination will occur and thermoluminescence will result.

The mean time spent in a trap is the inverse of the probability of escape from a trap (Equation 3), so there is an exponential dependence on temperature. The TL intensity (I) is proportional to the rate of recombination of electrons with the luminescence centres, which is proportional to the rate of release of electrons from the trap.

$$I(t) = -C\frac{dn}{dt} = Cnp \quad C=\text{arbitrary constant} \qquad (4)$$

From equations (2) and (4)

$$I(t) = I_0 \exp(-pt) \qquad I_0 = \text{the intensity at } t=0 \qquad (5)$$

This equation describes the decay of TL intensity at a constant temperature.

2.2.2.4 Shape of a Glow Curve

If this exponential decrease in intensity is combined with a linear increase in temperature, then one can find an equation which describes the characteristic glow curve shape. While the electrons are metastable in their traps at low temperatures, their return to equilibrium can be speeded up by increasing the temperature of the sample.

Once an electron is freed from its trap, it is much more likely to return to the ground state than to return to the trap (McKeever, 1985). The intensity of the TL is therefore directly proportional to the recombination rate of holes and electrons, which is proportional to the rate of release of electrons from the trap.

As the temperature begins to rise, electrons are freed from their traps, and recombine with the trapped holes. As the traps empty, the recombination rate slows down and the intensity decreases. This is shown schematically in Figure 2.4.

There is a relationship between trap depths and the peaks of glow curves. Electrons in deep traps will (on average) remain trapped longer than those in shallow traps.

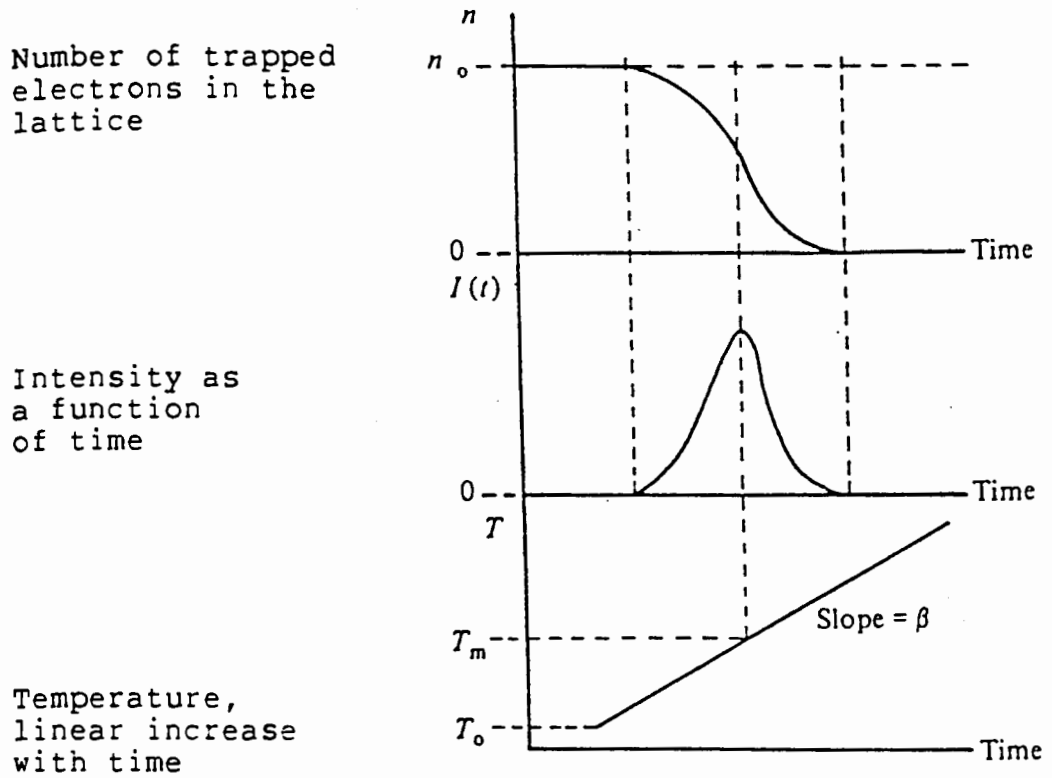

Figure 2.4

Schematic showing the formation of first order glow curves

As the temperature rises, more electrons escape from their traps. The number of recombinations increases, causing the TL intensity to increase. As the temperature continues to rise, the traps become depleted and the intensity decreases.

(McKeever, 1985)

When a sample is heated for a TL measurement (glowed) the electrons in shallow traps will escape and recombine to produce TL at a lower temperature than electrons in deep traps. Glow curves, the TL intensity as a function of the temperature of the sample, can indicate the presence of distinct traps (Figure 2.2a), but in many cases the electrons are escaping from so many traps that it is extremely difficult to sort out the presence of different specific traps which are contributing to the TL (Figure 2.2b).

A more precise mathematical description can be found by solving (4) for the non-isothermal case of a linear increase in temperature. In this case, $\beta = dT/dt$ and the shape of a first-order TL glow peak can be described by:

$$I(t) = C\, n_0\, s \exp(-E/kT) \exp\{\frac{-s}{\beta} \int_{T_0}^{T} \exp(-E/kT)dT\} \quad (6)$$

where n_0 = the number of trapped electrons at T_0 (McKeever, 1985).

2.2.2.5 Position of the Peak

The eviction rate of trapped electrons at a temperature T is found by combining equations 1 and 3.

$$\frac{dn}{dt} = - ns \exp(-E/kT) \quad (7)$$

As the TL intensity is proportional to the rate of eviction of the electrons, the temperature at which maximum TL intensity occurs can be found by setting $\frac{d^2n}{dt^2}$ equal to zero.

$$ns \exp(-E/kT) \{ (E/kT^2)\frac{dT}{dt} - s \exp(-E/kT) \} = 0$$

If there is a linear rise in temperature,

β (a constant) = dT/dt then

$$\frac{E}{kT} \exp (E/kT) = sT/\beta \qquad (8)$$

The equations presented in this section give some idea of the relationship between the various trap parameters. A range of trap depths will complicate this picture even further. The difficulties in separating the effects of the various parameters is one of the reasons why there is not yet a clear and definite picture of the physics of TL.

2.3 TL Of Quartz

The TL dates described in this thesis were obtained from 100μm quartz grains extracted from beach dune sands. The following is a brief description of the TL of quartz, largely taken from The Thermoluminescence of Solids (McKeever, 1985).

Quartz, SiO_2, occurs naturally at temperatures below 870°C. α-quartz is stable below 573°C and β-quartz between 573-870°C.

The α-β transition involves small adjustments in the atomic position. The change is reversible and involves no bond rearrangement (Figure 2.5).

The α-quartz crystal lattice is rhombohedral with the Si atoms tetrahedrally sharing the oxygen atoms. Two of the Si-O bonds are .1598 nm long and make a 66° angle with the c-channel. The other two bonds, at 44°, are .1616 nm long.

The Si-O bond is ≃40% ionic and ≃60% covalent. The mineral is rigid, so while dislocations and intrinsic defects exist, they are complex and poorly defined. Quartz is damaged by radiation in two main ways. Ionizing radiation can damage the Si-O bond and direct collision with nuclear particles can create vacancies and interstitials. The defects caused by ionizing radiation tend to occur at imperfections (mainly impurities) which are already present in the lattice.

TL requires the presence of two defects, the trap and the luminescent centre. The intensity of the peak is proportional to the smaller of the two defect concentrations. In a sample with many types of traps, competition effects make interpretation of the defect structure difficult.

TL, when combined with other experimental methods involving dielectric loss, electrical conductivity, ionic thermal currents, thermally stimulated polarization currents, optical absorption, electron spin resonance, etc. can yield information about certain defect structures.

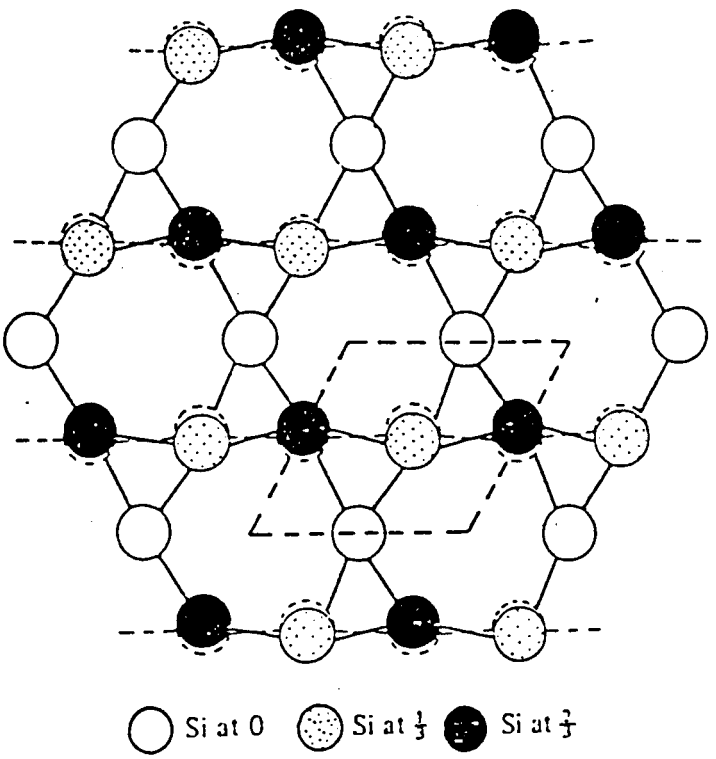

Figure 2.5
Crystal Structure of Quartz (SiO_2)

The above diagram illustrates the silicon atoms in quartz and indicates the rhombohedral structure of alpha-quartz.

Solid circles = alpha-quartz, stable below 573°C
Dashed circles = beta-quartz, stable above 573°C

The oxygen atoms are arranged in a tetrahedral formation around the silicon atoms.

(McKeever, 1985)

Since different experimental techniques may be sensitive to different types of defects, information gained from one technique may not be generally applicable. One must be very careful about generalizing results from these different methods. These techniques also give information about specific defects, but if relationships among various defect concentrations and certain TL peaks are found, one does not know if it is traps or luminescent centres which are being studied.

The E_1' and E_2' defects have been extensively studied. E_1' (E_2') defects are oxygen vacancies with an unpaired electron (proton) on one of the two adjoining silicon atoms. Optical and ESR data suggest that E_1' and E_2' centres have energies of 5.8 eV and 5.3 eV respectively. A 7.6 eV absorption band is believed to be caused by trapped holes at oxygen interstitials or a dangling oxygen bond (See Figure 2.6a).

Impurities influence the properties of intrinsic defects and can act as traps themselves. Monovalent alkali ions such as Na^+, Li^+, and K^+ act as network modifiers as they induce non-bridging oxygen bonds (See Figure 2.6b). These ions can easily diffuse through the open c-axis channel.

If aluminum is present, the optical absorption decreases. This is believed to be due to the trivalent Al^{3+} which, after substituting for Si^{4+}, captures an alkali ion to complete the charge compensation. This prevents the alkali ion from

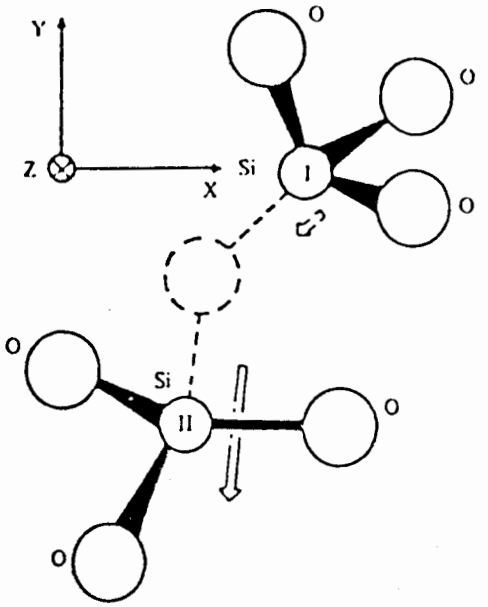

Figure 2.6a
E_1' Defects in Quartz

The dotted circle shows the oxygen vacancy. The unpaired electron is at the Si(I) site. The arrows indicate the movement of the Si atoms from their normal positions.

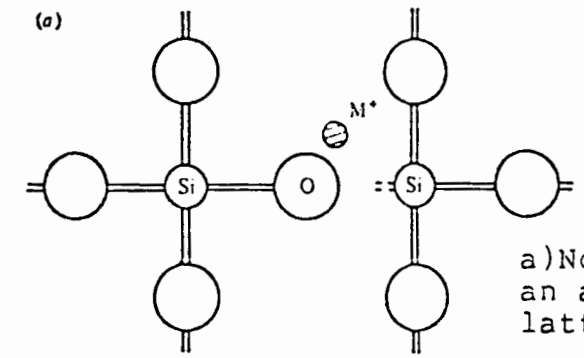

Figure 2.6b
Alkali Defects in Quartz

a)Non-bridging oxygen bond due to an alkali ion M^+ in the SiO_2 lattice.

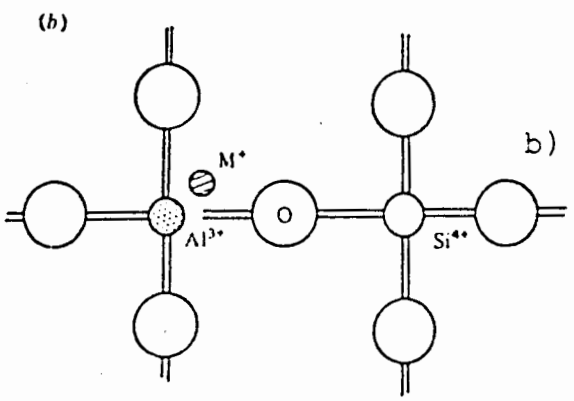

b) An alkali-aluminum centre.

(McKeever, 1985)

becoming a network modifier. Al is also believed to cause the "smoky colour" of irradiated quartz. No clear relationship has been found between the absorption bands, the ESR signal and the Al concentration. This has led some researchers to suggest that impurities such as Fe^{3+}, Ge^{3+} and Ti^{4+} are important.

At room temperature and above, the TL intensity increases with the irradiation temperature. Alkali ions can diffuse away from the Al site during irradiation, forming an $(Al^{3+})^{0}$ centre, which suggests that the TL above room temperatures is related to these centres. Phototransfer studies show that all the glow peaks above room temperature are related to electron traps. This suggests that $(Al^{3+})^{0}$ is the recombination centre.

TL emission spectra vary greatly from sample to sample so only general conclusions can be made.

No unambiguous correlations between impurities and specific glow peaks have been found. For example, the 380°C peak is believed to be related to an oxygen vacancy. However, one researcher introduced different impurities into a quartz lattice and observed little change in the TL, he concluded that except for Ti, impurities are not important in the production of TL.

Thermally stimulated current (TSC) studies indicate that traps and luminescent centres are close together, which give some justification for first order kinetics for the glow curves.

In summary, the TL above room temperatures appears to be related to electrons recombining with holes trapped at $(Al^{3+})^{o}$ sites.

2.4 TL Dating

2.4.1 Introduction and a simple example

To illustrate how TL can be used to date something, an "ideal" case shall be described. The "object" undergoes a treatment which releases all the electrons from their traps. Heating to a temperature of 500°C would do this, as might happen in the case of a fired clay pot.

The object is collected immediately after the event which emptied all the traps, sub-divided into several identical samples, each of which is given a different dose (eg. 0 to 10 units in 1 unit steps) of radiation in the laboratory. The samples are then glowed - heated to ≃450°C while the TL intensity is recorded, usually as the number of photons counted with a photomultiplier tube.

No TL would be emitted from the sample which had received no dose in the laboratory, but the other samples would. The greater the lab dose, the more the traps would have filled, and the more TL would be emitted. The glow curves (TL intensity vs. temperature) would increase with the lab dose. From the set of glow curves, a single curve which represented the change of TL intensity with lab dose at a certain temperature could be drawn.

This is a growth curve, and is illustrated in Figure 2.7a. A growth curve is a compilation of data from several glow curves. For the sample whose traps had just been emptied in nature, the growth curve would pass through the origin, and increase as a function of the dose. In this ideal case, the growth curve is a straight line.

But if the sample had been left alone in nature, not collected immediately after its traps were emptied, the mineral inclusions would be subjected to radiation from radioactive elements in the environment and from cosmic rays. Its traps would slowly fill. Such an "old" sample would be collected, prepared and measured as described above. All the prepared samples would now emit TL. The fraction of the sample which did not receive a dose in the laboratory would emit TL as some of its traps would have been filled in nature. The growth curve of the old sample would be like the one shown in Figure 2.7b. It would not pass through the intercept. The growth curves from the modern and old samples would be similar. By extrapolating the old sample's growth curve back until it intercepts the dose axis, an estimate of the dose the sample had received in nature could be made. This dose estimate is often called the "equivalent dose" (D_{eq}).

While this illustrates an "ideal" case, it should be noted here that many pottery samples do behave similar to the sample described above. Pottery dating is a successful application of TL dating (Aitken, 1974, 1985).

Method Of Determining The Dose Received In Nature By An Ideal Sample

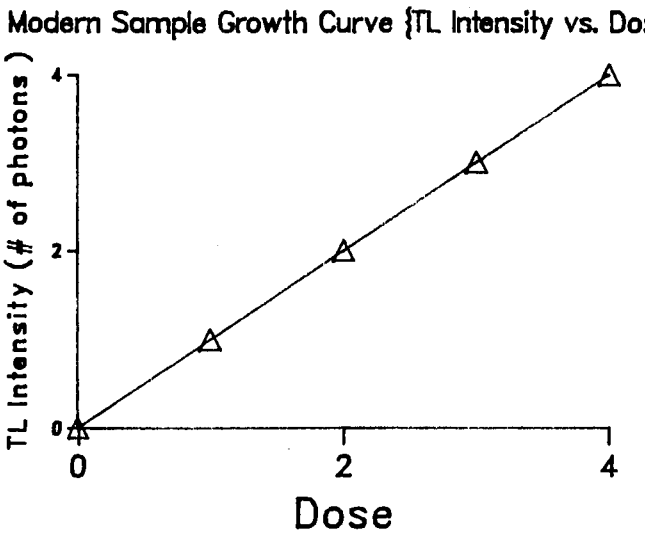

Figure 2.7a
This is an example of a growth curve, TL intensity vs. dose, of a modern sample.

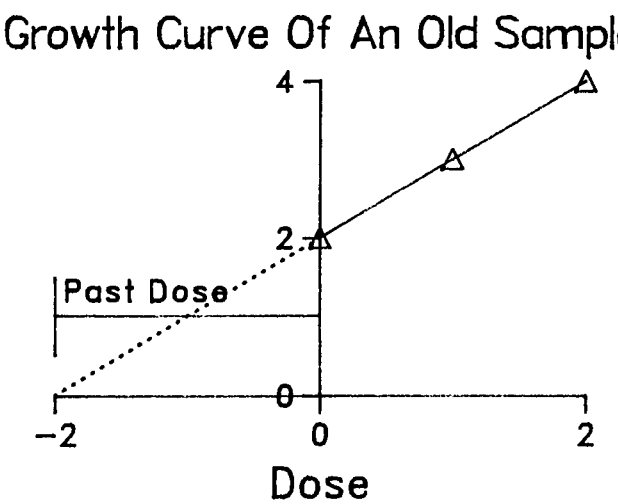

Figure 2.7b
Growth curve of an old sample. Also shown is the extrapolation used to determine the dose received in the past by the sample.

To determine the dose received by a sample whose initial TL is zero. As Figure 2.7a shows, the growth curve is a straight line which intersects the origin. If the growth curve in Figure 2.7b is extrapolated back until it intersects the dose axis, the distance from the origin to the intersection point gives a measure of the dose the sample received before being irradiated in the laboratory.

2.4.2 The Plateau Test

The D_{eq} is determined for a number of temperatures along the glow curve, which corresponds to measuring different traps (the trap depth increasing with the temperature). At the end of the analysis, the measured D_{eq} are plotted versus the temperature, and if a "plateau" is formed, one can be reasonably confident about the measured D_{eq} value.

Higher temperatures correspond to deeper traps. An electron will (on average) remain in a deep trap longer then in a shallow one. The TL signal must be stable over long periods of time, so the D_{eq} obtained from different traps should be the same. A successful plateau test indicates that different traps, with different average lifetimes, have been exposed to the same amount of radiation since the initial, zeroing event. This increases the confidence in the final result.

If a plateau is not obtained, it indicates that something was wrong with the method or sample.

2.4.3 TL Dating of Sediments

The method outlined above cannot be directly applied to most sediments. In that ideal case, all the trapped electrons were emptied during the firing. The vast majority of sediments have not undergone such high-temperature heating. Most likely, the event being studied is the last exposure to sunlight, although there is some evidence that grinding or weathering can be

responsible for the emptying of some of the traps. (From now on, sunlight will be assumed to be the relevant "zeroing" mechanism.) Either way, not all the traps were empty when the sediment was deposited. This means that a modern, zero-age sample will have a non-zero TL signal. If this is not taken into account, the D_{eq} will be incorrectly measured, as is shown in Figure 2.8. The dating technique must be modified to take this "depositional" TL into account.

After exposure to light, some electrons still remain in traps, the number left depending on the length of the sunlight exposure, the wavelength of the incident light, the trap depths (thermal activation energy), and the mineral type. Wintle and Huntley (1980) divided the TL of sediments into two parts, $I_{total} = I_o + I_d$, where the I_d was from traps which were easily bleached (i.e. had probably been emptied before deposition), and the I_o was from light insensitive traps. In real sediments there is a continuum of trap types between these two extremes.

There are three main methods of separating I_o and I_d in use today (Aitken, 1985): the regeneration method of Wintle and Huntley, the total-bleach method of Singhvi, and the partial-bleach method of Wintle and Huntley.

Growth Curves Of A Modern And Old Sample
Which Have Some TL Present At Deposition, Such As Sediments

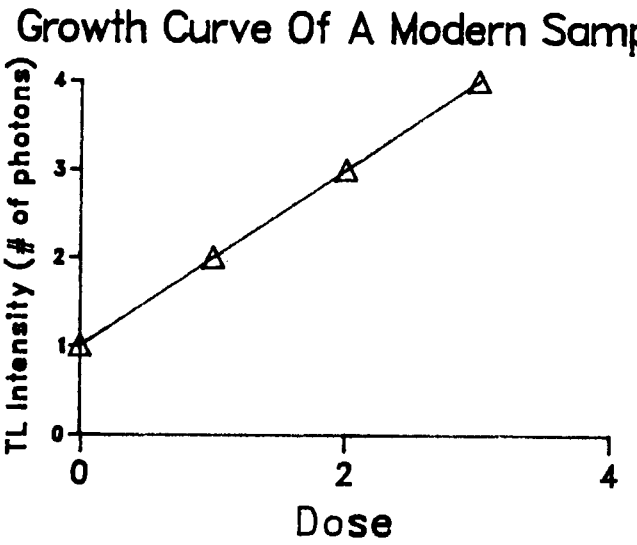

Figure 2.8a
Growth curve (TL intensity vs. dose) for a modern sample with non-zero initial TL intensity.

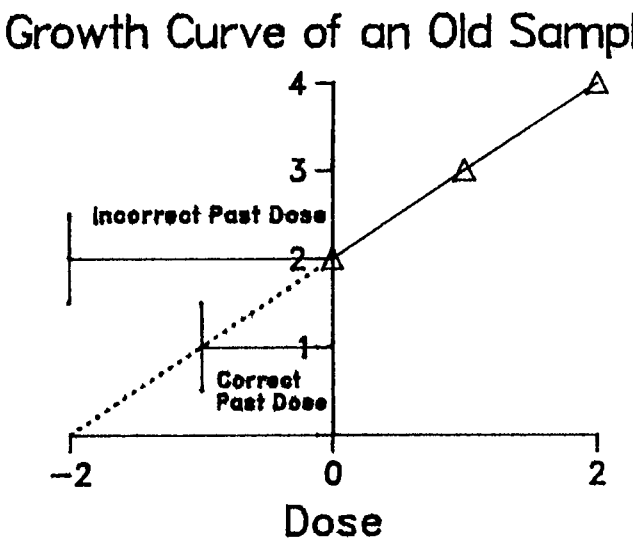

Figure 2.8b
Growth curve of an old Sample. As in Figure 2.7, the growth curves of the modern and old sample are both linear.

If the past dose received by the sample is measured from the distance between the y axis and the intercept of the extrapolated curve and the dose axis (as was shown in Figure 2.7), an incorrect value will be obtained. The method used to determine this past dose must take the non-zero initial TL intensity into account. Various methods of dating such samples of which sediments are a prime example will be described further in the text.

2.4.3.1 Method 1: Regeneration

With the regeneration method, most of the sample is bleached (exposed for a long time to an artificial light source). The bleached sample is then divided out amongst several discs or planchets which are then artificially irradiated and then glowed. This procedure "regenerates" the TL growth curve. The amount of sample which was not bleached is then glowed to provide a measure of the natural TL intensity. The D_{eq} is measured from the intersection of the horizontal line drawn through this natural TL intensity and the regenerated growth curve (Figure 2.9a). Sensitivity changes which result from the bleaching often occur with this method. If the regenerated growth curve does not accurately reproduce the growth characteristics that the grains underwent in nature, then the evaluated D_{eq} will not be correct. Non-linear growth curves do not cause a lot of difficulty with this method.

2.4.3.2 Method 2: Total-Bleach

In the total-bleach method, a small part of the sample is given an arbitrarily long bleach to remove all the electrons from light sensitive traps. It is glowed to determine I_o. The rest of the sample is given a series of increasing doses. The TL intensity versus dose is plotted, and this curve is extrapolated back until it intersects the horizontal (dose) axis. D_{eq} is determined from the intersection of the extrapolated growth curve and the I_o from light insensitive traps (Figure 2.9b).

Methods For Determining The D_{eq} Of Sediments

Method 1: Regeneration

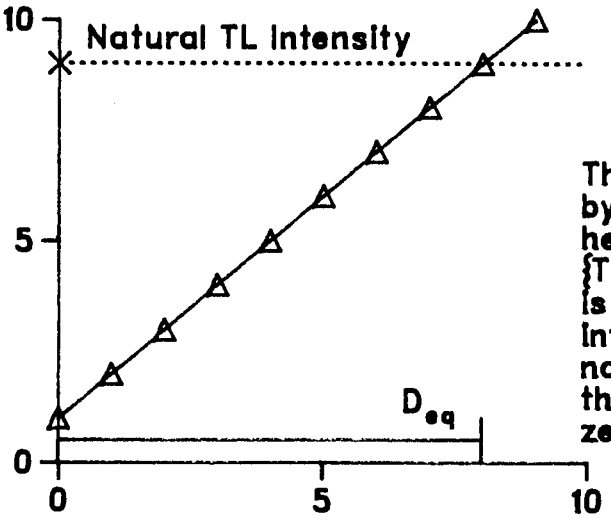

Figure 2.9a
The sample is zeroed by a long bleach or heating. A growth curve {TL intensity vs dose} is then constructed. The intersection of the natural TL intensity and the growth curve of the zeroed sample gives D_{eq}.

..... Extrapolations to data

Method 2: Total–Bleach

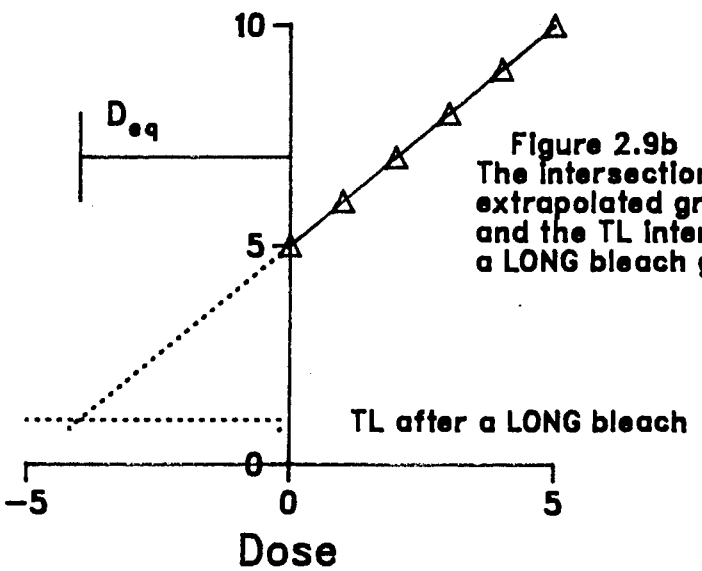

Figure 2.9b
The intersection of the extrapolated growth curve and the TL intensity after a LONG bleach gives the D_{eq}.

The main problem with this method is the arbitrary assumption that the sample has been totally bleached. This is hard to justify when zero-age samples from a variety of sediments and locations have been measured and found to have substantial TL, which can sometimes be reduced by a sunlight exposure on the order of a few hours (Prescott 1983, Berger 1984, Huntley et al. 1983). This method may therefore give D_{eq} values which are too large.

2.4.3.3 Method 3: Partial-bleach

In the partial-bleach method, the TL from highly light-sensitive traps (which are the most likely to have been emptied at deposition) is separated from the TL arising from the rest of the traps. If a modern sample is given a set of increasing doses in the lab, a growth curve such as the one shown in Figure 2.10a will be formed. If a similar set of samples is exposed to a small amount of bleaching there will be no significant change in the TL from the natural (lab dose=0) samples, as most of their light-sensitive traps have already been emptied. But the samples which have received a lab dose now have some electrons in their light sensitve traps, and even a brief light exposure will cause a significant reduction in their TL. The two curves, Natural+Dose and Natural+Dose+Bleach intersect at the y (zero dose) axis. If the sample is overbleached, traps which were not emptied during deposition will be emptied, and the Natural+Dose and Natural+Dose+Too Much Bleach curves will intersect beyond the zero dose axis.

Method 3: Partial–Bleach
Growth Curves and Extrapolations

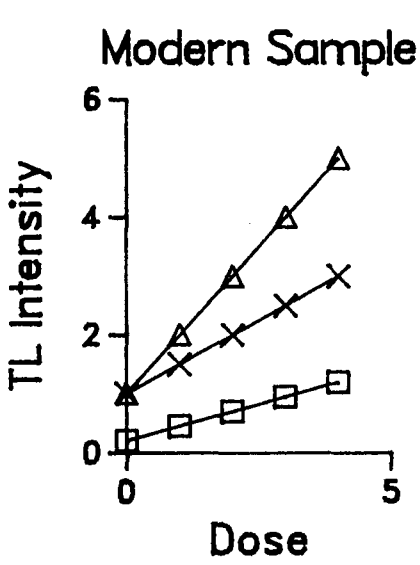

Figure 2.10a
After the samples have been irradiated there is an optimal amount of bleach which will not significantly effect the natural unirradiated samples, but will reduce the TL for the irradiated samples. Too much bleaching will empty traps which were not emptied at deposition.

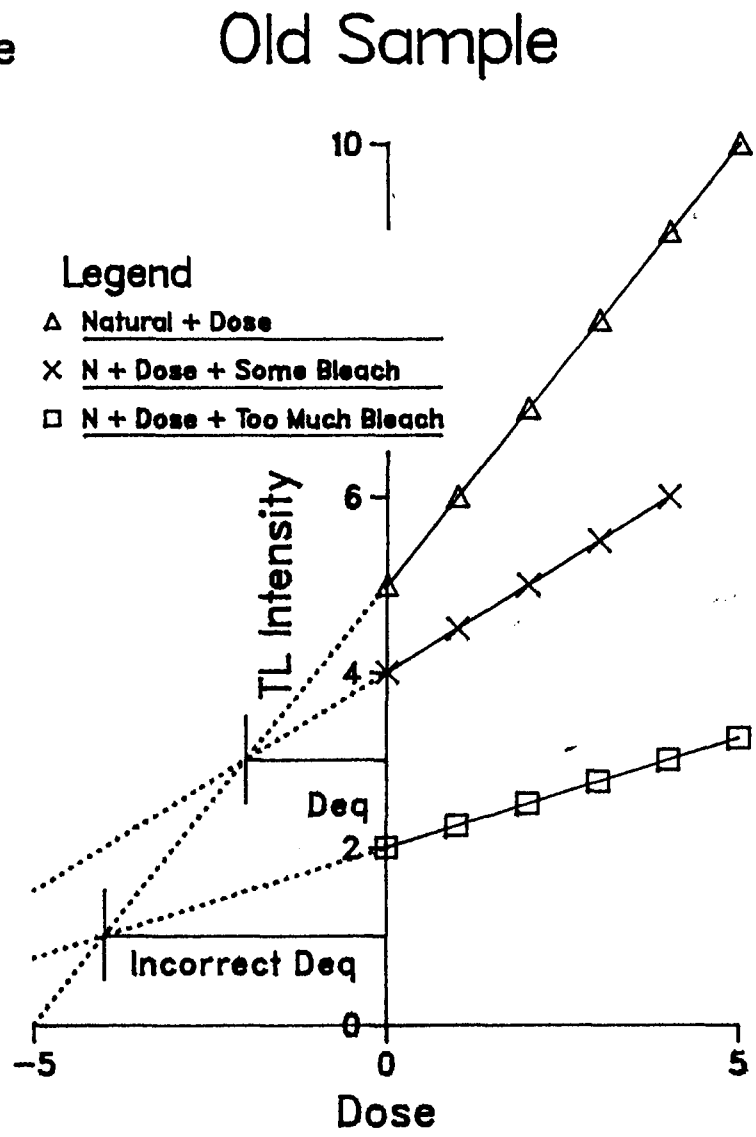

Figure 2.10b

With the partial–bleach method, two growth curves are constructed. One is the natural+laboratory dose curve and the other is the natural+lab dose+bleach curve. These curves are extrapolated back, and the intersection of the extrapolated curves is a measure of the dose the sample has received since it was last bleached (See Figure 2.10a). The distance from the y axis to the intersection point is the Deq (Refer to the text for a more detailed explantion).If the sample is over–bleached, an incorrect value will be obtained.

This method can be applied to old samples which have recieved an appreciable radiation dose in nature (Figure 2.10b). The Natural+Dose and Natural+Dose+Bleach curves will no longer intersect at the y (zero-dose) axis, but the distance between their intersection point and the y axis gives the D_{eq}. Also shown in the figure is the effect of overbleaching and the total-bleach method. They both yield D_{eq} which are too large.

The difference between the Natural+Dose and Natural+Dose+Bleach curves is the reduction in TL caused by the bleaching. It represents the TL from light-sensitive traps. The partial-bleach method can be thought of as an extrapolation to determine where this reduction is equal to zero (Huntley, 1985). This method assumes that all the highly light sensitive traps have been emptied in nature, and that the lab bleaching empties a fraction of these traps, but no others.

If there are doubts about the bleaching time chosen the experiment can be repeated with different bleaching times, the D_{eq} obtained should be the same. If only a small amount of sample is available, this is not always practical.

2.4.4 Fitting curves to Experimental Data

If the growth curves are non-linear (as was the case with the samples studied in this thesis) the total-bleach method and the partial-bleach method become more difficult to use. The regeneration method is not greatly affected by non-linear data, but non-linear curve fitting routines become necessary in many

cases. The growth curve of quartz is similar to that of a saturating exponential. Figures 4.2 and 4.4 are examples of real, non-linear growth curves. There is a physical explanation for an exponential growth curve. A sample without any electrons in its traps will not emit TL when glowed, but when exposed to increasing doses, the traps fill. As there are lots of empty traps available, the most important factor is the dose. If the dose increases linearly, the number of trapped electrons will increase linearly. As the traps become more full, the number of spaces available for the electrons decreases and the dose is no longer the limiting factor. When all the traps are full, more radiation will not increase the number of trapped electrons, and the growth curve levels off.

This is a very simple explanation. The presence of many traps with different trap depths which saturate at different doses will complicate this picture immensely.

Many models have been suggested which yield mathematical descriptions of growth curves (McKeever, 1985) with linear, supralinear and sublinear behaviour at low doses, and exponential behaviour at high doses, but so far, only broad agreement with experimental results has been obtained.

It is difficult to choose the best curve to fit growth curve data. At low doses, a linear fit is adequate. As the doses increase and the growth curve becomes non-linear, another choice must be made.

If a modern sample of the same type as the old sample being studied is available, its growth curve can provide a guide to choosing the type of fit. Some work (Prescott, 1983) has been done using the second glow growth curves as a guide to choosing the shape of the first glow growth curves.

A combination of physical and experimental reasons should be used when justifying the type of fit chosen (quadratic, cubic, exponential). Just because a certain type of fit (eg. cubic spline) will give a curve which goes through all the data points, it does not mean that the extrapolations from such a curve will be valid.

At very high doses (>1000 Gy) the growth curves begin to increase again. The behaviour has not been throughly studied (Aitken et al., 1968).

2.4.5 Bleaching

All the methods outlined above use some type of light exposure (bleaching) as an integral part of the D_{eq} determination. Extreme care must be taken during the laboratory bleach. Overbleaching can occur if the sample is exposed to wavelengths not encountered in nature, so the laboratory lamps must not employ wavelengths not found in the solar spectrum (especially at the high-energy blue end of the spectrum). Many lamps have UV components which must be filtered out. But overbleaching can occur even if a solar simulator is used for laboratory bleaching. The grains may have had a coating which

filtered out certain wavelengths during deposition, but sample preparation techniques remove this coating and overbleaching can occur if the now "bare" mineral is exposed to wavelengths it had never before experienced. A similar problem exists with water laid sediments. Water strongly attenuates the red and blue ends of the solar spectrum, so the laboratory bleaching light should be carefully filtered.

2.4.5.1 Comparison Of The Extent And Effect Of Bleaching Between Different TL Dating Methods

The regeneration method is very prone to overbleaching as most of the samples have been zeroed using light. In the total-bleach method the sample is exposed to an arbitrarily long light exposure to make sure that all the light-sensitive traps are emptied. Like the regeneration and total-bleach method, the partial-bleach method assumes that the sample was exposed to sunlight at deposition, but it is the only method that makes no assumptions about the extent of this original bleaching. The lab light exposure is kept to a minimum, and great care is taken to ensure that the bleaching apparatus does not contain wavelengths to which the sample has not been previously exposed.

2.4.6 Common types of Minerals used in TL dating

The three methods outlined above have been applied to different minerals in a variety of sizes and sediment types. The most common minerals used for TL dating are quartz and feldspar. They are relatively abundant, and their TL properties are fairly

well researched. Some work has been done with zircon grains. Water-laid sediments (ocean, lake and river), loess, organic rich sediments, and sand dunes have been investigated.

2.5 Present State Of Affairs In TL Dating Of Sediments: A Review Of The Last 20 Years

Many attempts were made in the 1950's and 1960's to date rocks, but few meaningful dates were obtained, possibly due to a lack of understanding of the subtleties and complexities of TL. In the mid 1960's, G.V. Morozov and V.N. Shelkoplyas began publishing TL dates for sediments in the U.S.S.R. (Dreimanis, et al., 1978). The following section will review the current state of affairs in the TL dating of geological sediments.

Two main grain size fractions are studied, the "fine grains" ($\simeq 10\mu m$ in diameter) and those which are $\simeq 100\mu m$ in diameter. The reasons for this will be discussed more thoroughly in Chapter 5, which deals with dose-rate calculations, but it should be noted here that fine-grains are irradiated by α, β and γ rays while most of the α rays contribute relatively little to the TL of the larger grains.

2.5.1 Ocean Sediments

In the 1970's Huntley and Johnson (1976) measured the natural TL of the siliceous shells separated from two North Pacific Ocean deep sea cores. They found that the TL intensity

increased with depth up to a limiting value. This showed that TL was potentially useful for dating deep sea cores.

A few years later, Wintle and Huntley (1980) reported the first successful application of TL dating to sediments. They had discovered that the TL emission measured by Huntley and Johnson was from silt that clung to the shells, so all further analysis was done on the fine-grain (4-11 μm) fraction of the sediment. They obtained TL dates of 9-140 ka, which agreed satisfactorily with a $\delta^{18}O$ marker and with Cycladophora Davisiana variations in the core. This paper proposed that sunlight reduced the pre-depositional TL to a small residual value, and outlined three different methods to obtain D_{eq} which took this residual into account.

Berger, Huntley and Stipp (1984) published TL dates for a marine core whose age range of 0-25 ka had been independently established by radiocarbon dating. The R-Γ technique was performed on the fine-grain polymineral fraction of the sediments. Though reasonable ages were obtained, the analysis was complicated by the presence of quartz in the sample. Quartz does not bleach as quickly as feldspar. The bleaching spectrum, duration of light exposure, and the glow curve region used for analysis had to be carefully selected. Radon losses from the dry powders used for α-counting were overcome by glassing the samples.

2.5.2 River, Lake and Glacial Sediments

Berger and Huntley (1982) published acceptable TL dates for some fine-grained water laid sediments. It was found that the fine-grain fraction from modern river silts gave acceptably low D_{eq} when the laboratory bleaching spectrum was modified to take into account the attenuation of the solar spectrum by the water. Great care was needed to prevent overbleaching.

Later work (Huntley et al. 1983) showed that good results could be obtained from river and lake sediments if the laboratory light was filtered with an orange Corning 3-67 filter, which cuts off wavelengths <550 nm. Zero-age river silts were measured and TL ages of <1-3 ka were obtained. A TL age of 64 ± 11 ka for an old river silt compared favourably with a radiocarbon date of 58.8 +2.9/-2.1 ka from materials immediately overlying the silt. Glacial lake and till sediments were found to produce unsatisfactory results, probably due to incomplete bleaching at deposition.

TL dating of lake silts (Berger, 1984) initially did not appear to work for silts which had been deposited at rates >4 mm/year. Using the R-Γ techniques on the 4-11 μm feldspars from a mud flow silt which had been more slowly deposited at ≃ 1 mm/year, an acceptable TL date of 7.8 ± 0.5 ka was obtained. Further work (Berger, 1985) with the 2-4 μm feldspar-dominated grain fraction from the thick varve gave a TL age of 14.2 ± 2.3 ka, which was in good agreement with the expected age of

10-11 ka.

With glacial silts, the feldspar-dominated component of the terrigenous sediments was a practical TL clock for sediments which were approximately 36 and 66 ka old. The poor results from quartz were most likely caused by quartz's low bleaching sensitivity (Berger, 1984).

A laboratory experiment was done (Gemmell, 1985) to measure the bleaching of the TL signal from sediments undergoing fluvial transport. The speed and turbulence of the stream flow was found to affect the amount of bleaching by attenuating the red and blue ends of the solar spectrum. The study was carried out with suspension densities greater than 10 g/l which is much larger than the <2 g/l carried by most rivers.

More work on the zeroing of the TL of sediments was done by Huntley (1985). Using the partial-bleach (R-Γ) method and yellow-orange UV filters with a cutoff at 540 nm (Corning 3-67), he was able to obtain D_{eq} as low as 5 Gy for river silts, using the fine grain feldspar-dominated grain fraction.

River silts were also studied by Divigalpitiya (1982). Using the fine grain portion of the sediments (2 - 8 μm), which was feldspar-dominated, correct ages in the range of 0 - 60 ka were obtained, though some difficulty was experienced with a few of the samples. Incomplete bleaching was given as the probable reason for obtaining TL ages which were much too old.

2.5.3 Loess Deposits

A.G. Wintle applied TL dating to the fine grain fraction of late Devensian loess in southern England (Wintle, 1981 and 1982). The site had been dated by correlating it with other northern European deposits which had radiocarbon dates of 14-30 ka for interstadial deposits. The R-β technique was used on fine grains, and data from the 260-320° range of the glow curves were analyzed to obtain a date of 14.8 ± 3 ka. Some sensitivity changes were noticed, possibly caused by the laboratory bleaching lamp (which had a UV component in its spectrum).

Loess from Pakistan was studied by Rendell (1983). Good relative ages were obtained with the 2-10 μm fraction using the total bleach method. The residual TL measured depended on the exposure time and wavelength of the bleaching lamp. This caused problems in determining the absolute TL ages.

Wintle and Proszynska dated loess from Germany and Poland (1983). Using 4-11 μm grains and the regeneration method, they obtained acceptable ages of 18.6 ± 1.9 and 32 ± 5 ka, though there were some problems with sensitivity changes.

Ages of volcanic tuff in Germany were obtained by TL dating of loess (Wintle and Brunnacker, 1982). A TL date of 19.5 ± 0.7 ka was obtained for a sediment which was stratigraphically correlated with the Eltviller Tuff radiocarbon dated at 18.5 ±0.95 and 21.2 ± 1.4 ka. Another reasonable age of 43.2 ± 4.3 ka was obtained from the same site.

2.5.4 Organic Rich Soil Horizons

A-horizons from soils have been found to yield acceptable TL dates. For example, a soil radiocarbon dated at 4.4 ka was TL dated at 4.3 ka (Berger and Huntley, 1982). Three modern A-horizon soils from archaeological sites were studied. A TL age of <0.7 ka was obtained for one soil which had been radiocarbon dated at <1.6 ka. One coastal midden site gave an acceptable TL age of 1.2 ± 0.5 ka, while another midden was TL dated at 23 ± 4 ka - unacceptably old (Huntley, 1985).

Peat from a bog known to be less than <0.5 ka was found to yield an acceptable TL age of of <0.5 ka (Huntley, et al. 1983).

The R-Γ technique on 2-8 μm grains from peat horizons yielded results comparable to ^{14}C dates. The ages ranged from 7-25 ka. One sample was TL dated at >480 ± 90 ka. This was is comparison with a ^{14}C date of 71.5 +1.7/-1.4 ka and a fission track age of 870 ± 210 ka for a layer of ash which was 1 m below the peat layer (Divigalipityia, 1982). These results were quite encouraging.

2.5.6 Sand Dunes

Singhvi et al. (1982,1983) reported one of the first applications of TL dating to dune sands. They used the total bleach method on aeolian dunes from the Rajasthan desert. They measured the 1-8 μm and the 90-105 μm fraction. Similar results were obtained for the two size ranges. Zero age samples from the

tops of the dunes gave D_{eq} of 1.5 ± 1 Gy. Acceptable TL ages in the 3-16 ka age range were obtained.

100 μm quartz from aeolian dunes in Roonka, Australia gave TL ages consistent with archaeological features (Prescott, 1983). 65 ± 12 ka TL dated dunes were found under an archaeological feature which had been radiocarbon dated at 18 ka. Other TL ages, 2.7 ± 0.3 and 14.5 ± 2 ka were also found to be acceptable and supported previous archaeological work. A variation on the total-bleach method was used to obtain these dates, but high residual TL in modern samples led the author to warn that the published ages may be too old and call for futher clarifying work.

100-300 μm feldspar grains from a sand layer in Finland were TL dated (Jungner, 1983). The sand layers framed an organic deposit which was radiocarbon dated at 63.2 (+5.5 -3.2) ka. The grains were preheated at 200°C for 10 seconds, and the glow curve temperatures between 250-400°C were analyzed. The R-Γ method was used, but strong evidence for a mixture of bleached and unbleached grains was found, and some corrections had to applied to the plateaus. The corrected TL ages for the sands above and below the organic layer were 98 ± 18 ka and 150 ± 30 ka.

Mejdahl (1985) dated glacial sand deposits with an expected age of 20 ± 5 ka. Using a new method which involved determining the 'correct' sunlight exposure by bleaching quartz and feldspar

grains from the same sample until they yielded the same TL age, an age of 21.5 ± 2 ka was found.

TL dating using single large grains (0.2 mm) of feldspar to date beach and dune sands was investigated by Southgate (1985). Using the total bleach method on alkali feldspars, he obtained reasonable D_{eq}. Unfortunately, he did not work out dose-rates for the various grains, so no absolute ages were available.

2.5.7 Anomalous Fading

The problem of anomalous fading, where the TL from a sample irradiated a short time (less than 1 year) ago is less than that from an identical sample which has been recently irradiated, is common with volcanic feldspar, but rare with metamorphic rock. It must be taken into account when calculating the D_{eq}. Anomalous fading has rarely been observed in unheated quartz, although Mejdahl (1985) reported fadings on the order of 10% for quartz from heated rocks. Readhead (1984) also observed anomalous fadings in some quartz, but admitted that the data was of poor quality and often contradictory due to variations in the output from disc to disc. Averaging over three sample sites, no net fading was observed (though one of the samples exhibited a fading of 15 ± 3 %). In addition, the TL from the stored discs was compared with TL from discs which had been irradiated just a few minutes previously. Such recently irradiated discs often exhibit large variations in their TL output. It is becoming a common practice to wait at least 24 hours after irradiation

before glowing, and this practice was followed with the work done in this thesis.

2.5.8 Summary of the TL Review

Although there seem to be as many failures as successes in TL dating, some things are becoming clearer. The partial-bleach method appears to work quite well with the fine-grain feldspar-dominated grains from rivers, loess, and organic rich horizons. These sediments yield correct TL ages if care is taken to avoid overbleaching and the effects of anomalous fading.

Water laid sediments must be carefully bleached, as certain wavelengths of the solar spectrum are often attenuated by particles in the water and the water itself.

The 100μm quartz grains give satisfactory results if they have been extracted from sediments which have been well bleached before deposition (e.g. those in most sand dunes).

Work with large single grains of zircon and feldspar is promising, but is still in the preliminary stages of investigation. The large variations among the emitted TL and the dose-rates of the individual grains is a problem.

While there has been progress in the field of TL dating of sediments, more work needs to be done, especially at the higher age ranges.

2.5.9 Optical Dating

It should be noted here that a new method for dating sediments using light from a laser to excite electrons from thermally-stable light-sensitive traps and thus measure the D_{eq} has been introduced by D.J. Huntley, D.I. Godfrey-Smith and M.L.W. Thewalt of Simon Fraser University (1985). It shows great promise for dating sediments which have had a brief light exposure. It uses light, as opposed to heat, to stimulate the emission. This is theoretically more sensible, and makes automated sample analysis practical. Work is continuing on the new method.

CHAPTER III

THE PROJECT

3.1 Introduction

The work described in this thesis was done to test the accuracy and upper age limit of TL dating when applied to certain samples. A series of measurements was done on quartz extracted from a stranded beach dune sequence in south-east South Australia. This sequence had been independently dated and was found to range in age from 0 - 700,000 years (Schwebel, 1978).

The first part of Chapter III will describe the samples, the latter part will outline the preparation techniques and apparatus used for the TL measurements.

The age of a sample was determined from the equation Age = Dose / Dose-Rate. Chapter IV discusses the various TL methods used to determine the dose, and Chapter 5 deals with the dose-rates. The results of the age calculations are presented and discussed in Chapter VI, with some suggestions for further work.

3.2 The Samples

In south-east South Australia (SESA) there is a set of stranded beach dunes which range from the present coastline to more than 100 km inland. The gradient perpendicular to the coast is quite low, 1m/km (Idnurm and Cook, 1980) so the 30-50 m high dunes which run parallel to the coastline are clear topographical features (Figure 3.1).

3.2.1 Historical Review

The origin of the dunes has been a matter of controversy for more than a century. Although Woods recognized that they were stranded coastlines as early as 1862, they were believed to be the result of tectonic uplift until the 1930's when Tindale noticed a general agreement between the high sea levels of the northern hemisphere Pleistocene interglacial periods and the dune formations (Sprigg, 1979). In the 1950's and early 1960's R.W. Fairbridge extensively studied ancient sea levels, and thought that the South Australian dunes supported the Milankovitch theory of the cyclic sea-level changes. Problems with determining absolute ages for high-sea level led to a disagreement between eustatic (global) and diastrophic (local) explanations (Imbrie and Imbrie, 1979). In 1952 Sprigg used the Milankovitch radiation curves in an attempt to determine absolute ages for the dunes (Sprigg, 1979).

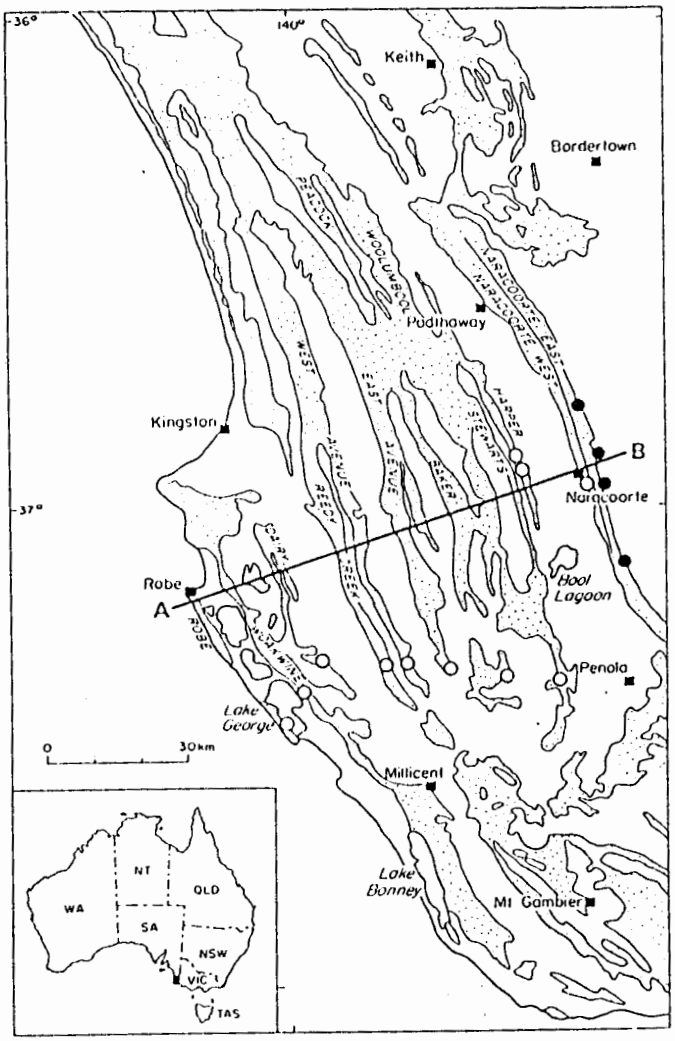

Figure 3.1

Map of the dune sequence in south-east South Australia (SESA). The circles show the sampling sites for palaeomagnetic measurements (Idnurm and Cook, 1980).

He went on to study the dune system, both stranded and submerged in greater detail, and correlated the aeolian desert cycle with $\delta^{18}O$ data and the Milankovitch theory.

3.2.2 The Ages of the Dunes

3.2.2.1 Age Measurements

A variety of methods were used to directly date some of the dunes. Palaeomagnetic measurements were done on the sequence (Idnurm and Cook, 1980). All dunes to the west of and including the West Naracoorte Barrier were of normal polarity, while the East Naracoorte dune was of reversed polarity (Figure 3.1) The dunes of normal polarity were assumed to have been deposited since the Brunhes-Matuyama magnetic reversal (Schwebel, 1978).

A radiocarbon age of 4330 ± 10 years was found for Robe I, one of the younger dunes in the sequence (Schwebel, 1978).

D. Schwebel used the uranium-series method on aragonite muds and molluscs from the Woakwine Barrier Lagoonal Unit (beside the Woakwine dunes) to obtain the respective ages of 100,000 ± 30,000 and 125,000 ± 20,000 years. A review in 1972 by Broecker and Bender indicated that uranium-series dating works well with coral and stalagmites, but is generally unreliable for shell and bone due to the differences in the uranium content (coral contains about 1000 times as much uranium as shell) and the 'open system' behaviour of bone and shell.

Amino acid racemization (AAR) dates were done on mollusc samples from both sides of the Woakwine range (von der Borch, et al., 1980). Ages of ≃120,000 and ≃92,000 years were assigned to two of the samples on the basis of the similarity of their AAR ratio with that of similar molluscs from a California terrace which had been uranium-series dated (with coral) at 120,000 ± 10,000 years. AAR dating is highly temperature dependent and problems have been discovered with some AAR dates which have been obtained in the past (See Chapter II).

3.2.2.2 Sea Level Change/$\delta^{18}O$ age estimates

Using the ages mentioned aboves as "markers", Schwebel estimated the ages of the other deposits by comparing $\delta^{18}O$ curves (previously published by Shackleton and Opdyke) with the stratigraphy of the dunes.

In developing the model used to assign the absolute ages, Schwebel assumed that the changing sea levels brought about by the ice ages acted on a slowly uplifting coastal plain to produce deposition of stranded barriers on flat, gently sloping bedrock (gradient only 1m/km (Idnurm and Cook, 1980)). He assumed that when the sea-levels peaked and stabilized, the sediments no longer migrated inward (up the beach), barrier shore-line deposition took place and the dunes became fixed in place by calcrete formation shortly after deposition. He then compared palaeo sea-level heights with the beach dunes and associated lagoonal deposits.

He concluded that lagoonal deposits were not always present, that deposition and erosion can occur simultaneously at the high sea-level stands and that there was evidence of extensive marine erosion. He identified eleven separate depositional events which formed the stratigraphy. These are illustrated and explained in Figure 3.2. The dune sequence can be quite complicated. He stated that "if the delicate balance of an uplift rate, sea-level height and coastal plain gradient is not maintained then strandlines will be superimposed" and erosion and deposition would modify their appearance (Schwebel, 1978). It was unlikely that a barrier would persist through more than 2 or 3 cycles of marine deposition unless there was simultaneous erosion and deposition.

Information about the different sea-level heights, the gradient of the land, and the uplift-rate can be used to predict the distance between the present shore line and the location (km inland) of the deposited dunes (Schwebel, 1978).

The heights above the present day sea-level were measured using a variety of criteria, the level of marine erosion surfaces, the absence/presence of marine sediments in the lagoonal deposits indicated the maximum/minimum sea-level, the boundaries between sediment layers in complex dunes (those with two or more different resolvable depositional events) and the lowest occurence of a beach dune in a barrier indicated the minimum sea-level height at that time.

Figure 3.2
Schwebel's Cyclical Model of the SESA Dune Formation

As the sea level fluctuated due to ice ages, with changes as great as 100 meters per cycle, the gently sloping land of south-east South Australia was tectonically uplifted. Dunes formed at the high water marks. The present dunes form a complex pattern which runs parallel to the present-day coast line.

Schwebel identified eleven separate depositional events (which are sketched on the next page). Each depositional event occurred at an inter-glacial high sea-level. The following description is condensed from his thesis (Schwebel, 1978).

1) Pre-Quaternary: No depostition, some erosion of Pliocene marine sand and Gambier limestone at the sea's edge.

2)The Woakwine V barrier was deposited directly on eroded Gambier limestone.

3) After many sea-level oscillations, which eroded Woakwine V and more Pliocene marine sand, Woakwine IV was deposited.

4) The sea-level rose and deposited the West Avenue barrier. 2 and 4 may have occurred in reverse order, but the δO^{18} records suggest otherwise.

5) East Dairy was deposited at the next high sea-level.

6) Reedy Creek was deposited. It is mostly carbonate, and indicated that most of the Pliocene marine sand had been removed. Woakwine IV and East Dairy were eroded.

7) Woakwine III was deposited. The area west of Reedy Creek was flooded. Lagoonal deposits can now be found there.

8) The cycle repeated, with Woakwine II being deposited over Woakwine III, and West Dairy being deposited.

9) Woakwine I deposited.

10) Robe III deposited.

11) Sea-level rose, eroded Robe III, deposited Robe II dune and formed a lagoon. This dune was judged to be relatively young as it has not been widely eroded yet.

12) The sea-level is at its present height, erosion occurs and Robe I is being deposited.

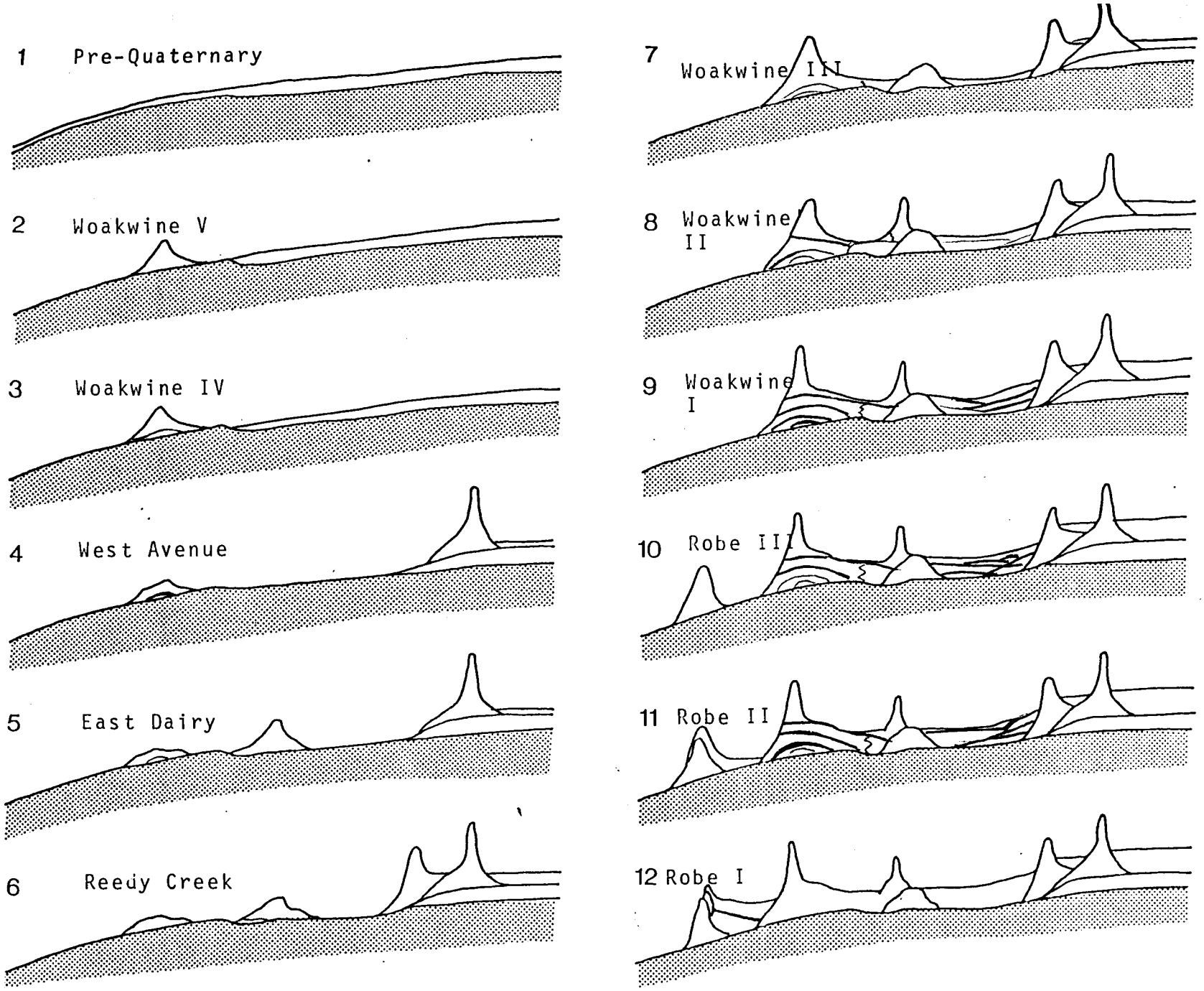
1 Pre-Quaternary
2 Woakwine V
3 Woakwine IV
4 West Avenue
5 East Dairy
6 Reedy Creek
7 Woakwine III
8 Woakwine II
9 Woakwine I
10 Robe III
11 Robe II
12 Robe I

Schwebel calculated the rate of continental uplift by setting the Brunhes-Matuyama reversal at 690,000 years ago. The base of the Naracoorte dunes are 35 m above the present-day sea level, which gave an uplift of 0.05 m/ka. The Woakwine complex which was uranium-series dated with a mean age of 120,000 years is 12 to 17 m above the present-day sea-level. Subtracting 6 m for the sea-level changes in the last 120 ka, yields uplift rates of 0.05 and 0.09 m/ka. He used the average value of 0.07 m/ka in his calculations, which agrees favourably with other tectonic uplift rates (Schwebel, 1978).

Using the model and data outlined above, Schwebel obtained absolute ages for the various dunes. He matched the various depositional events with data from $\delta^{18}O$ curves to obtain absolute ages for the dunes. These ages are given in Table 3.1. The stratigraphy of the dunes is quite complex. For ages less than abut 300 ka, a good stratigraphic match is possible (Idnurm and Cook, 1980). The ages of the older dunes are open to interpretation. Schwebel admits that he is not certain of the order of deposition of West Avenue/Woakwine V ($\simeq$350 ka). And dunes older than this are even harder to resolve. The palaeomagnetic data gives a definite upper limit to the sequence.

In summary, the dunes are land-based sediments which vary in age from 0 to 700,000 years old. They have been independently dated using $\delta^{18}O$ curves, uranium-series dates, magnetic reversal

data and amino acid dating.

The number of independently dated geologic formations in the world in the 100,000 to 1,000,000 year age range is limited. In this sequence, each dune was deposited in a similar way, and in a similar environment as the other ones. This gives a uniformity of deposition which most sequences that span similar time ranges do not have. These dunes form a very good test sequence for determining the reliability of TL dating.

3.2.3 Geochemical Information

An extensive study of the geography and the soils of south-east South Australia was done in the 1960's (Blackburn, et al., 1965). This study reported that calcareous sand which contained many small shells was dominant in the dunes. Shingle beaches were found only near Mount Gambier. Most of the ridges were consolidated, immobile structures. The calcareous components of the dunes were mainly fragments of marine organisms, such as molluscs, bryozoa, ostracods, foraminifera and reworked Tertiary and Pleistocene organisms. Land snail shells were found in a few of the dunes. The dunes are not just aeolian. Flat-bedded beach deposits containing entire large shells have been found. The SESA dunes have a mineral assembly which is similar to a raisin pudding. There is a matrix of calcite (calcium carbonate, $CaCO_3$) with quartz and a few heavy minerals scattered throughout.

Table 3.1

The South-East South Australia Sand Dune Sequence

List of Samples and Non-TL Age Estimates

(Age Estimates from Schwebel, 1978)

Name	Lab Code (SESA #)	Age Estimates (ka) $\delta^{18}O$	Other	
Robe	17	0		
Robe I	20		4.3±.1	Radiocarbon
Robe II	13	83		
Robe III	16	93		
Woakwine I	1	120	100 ± 30	U Series
			125 ± 20	U series
			≃120	AAR *
			≃92	AAR *
West Dairy	30	200		
Reedy Creek	4	248		
East Dairy	33	309		
West Avenue	42W	347		
East Avenue	36	380		
Cave	6	500		
Woolumbool	43	510		
Harper	8	575		
West Naracoorte	10		<700	(Magnetic Reversal)
East Naracoorte	35		>700	(Magnetic Reversal)

*Amino-Acid Racemization Dates (von der Borch, et al., 1978)

In general, the concentration of heavy minerals is quite low, rarely greater than 0.5% by weight and often less than 0.1% (Colwell, 1979). This is due to the large amount of shell and other carbonate material in the dunes and the lack of a mechanism for concentrating the heavy minerals when they were deposited. Colwell found that the heavy-minerals were a mixture of:

> 24-45% magnetite-plus-ilmenite, 5-20% leucoxene, 5-25% zircon, 5-30% tourmaline, and between 0-10% amphibole, epidote, rutile and garnet. Andalusite, sillimanite, kyanite and staurolite occur as minor components in many assemblages.

Few of the dunes had carbonate contents less than 30% by weight; in general it was 50% - 70%, with higher values for the younger dunes west of the Reedy Creek Range (Colwell, 1979).

3.3 Previous Thermoluminescence Work

In collaboration with J.R. Prescott and J.T. Hutton of the University of Adelaide, Australia, a set of samples was collected by D.J. Huntley in 1982. The natural TL glow curves of the 100μm quartz fraction showed increasing TL with age and were resolvable over a 600 ka age span. The dose-rates for the dunes were found to be approximately equal to 0.7 Gy/ka. These preliminary results suggested that the SESA dune sequence could be an ideal test site for the reliability of TL dating (Huntley, Hutton and Prescott, 1985).

3.4 Sample Preparation

3.4.1 Collection

Most of the samples were collected by D.J. Huntley, J.R. Prescott and J.T. Hutton in December 1982. Additional samples were collected over the next three years by Prescott and Hutton, some of which were sent to Simon Fraser University for analysis. Samples were taken from 15 of the dunes.

The samples were collected from as deep inside the dune as was feasible. Quarry and road and drainage cuts provided easy access to sand which had originally been in the centre of a dune.

The samples were collected using an auger a few cm in diameter. The first few centimeters of sample were discarded due to possible light exposure and contamination from other sediments. A black cloth was used as a shield against the sun while the sand was taken out of the dune and immediately placed in one litre paint tins. The tins were quickly sealed.

3.4.2 Preparation of the Samples for TL Measurements

The quartz was isolated using the standard quartz inclusion technique developed by Fleming (1968). The carbonate was removed by placing the sample in a dilute (15%) solution of HCl acid. The mixture was stirred and fresh acid was added until the

bubbling had stopped. After thorough rinsing in distilled water, the sample was dried at 40°C.

The grains were sorted according to size by shaking in sieves for a few minutes. Table 3.2 lists the percentage of quartz in the dunes, and the quartz size distribution for each sample.

One size fraction was then selected (normally the 90-125 μm), and placed in a solution of 48% HF for 40 minutes. It was stirred every 10 minutes. This treatment removed a thin (≃6 μm) outer layer of the quartz grain, the part of the grain which was most likely to have been contaminated by other elements and to have been exposed to α radiation. Besides etching the quartz grains, the HF dissolved any feldspars which may have been present. Feldspars are strong TL emitters, and their signal can swamp that of quartz.

The sample now consisted primarily of white shiny grains, though a few dark grains were visible. These were removed with a magnetic separator.

X-ray diffraction was done on three of the samples. Classic α-quartz spectra were obtained (Figure 3.3). Quartz diffracts X-rays quite strongly, so it would have been very difficult to detect the presence of other minerals (Hutton, private communication, 1985). As some heavy minerals may have been present in the sample, an additional step was added.

The remaining grains were separated by density using the simple "Sink-or-Float" method of gravity separation with sodium polytungstate[1], an odourless, non-toxic, water-soluble heavy liquid (specific gravity=3). The grains were placed in a separating funnel (Figure 3.4), thoroughly stirred and allowed to settle overnight in a solution of density ≈2.9 g/ml. the funnel, while the quartz grains floated on top. The two fractions (Heavy and Light) were decanted into funnels lined with filter paper, thoroughly rinsed and dried at 40°C.

Heavy minerals were obtained from all the samples, though often their mass was so small it could not be accurately measured. Most of the heavy grains were dark in colour, and were likely magnetite. A clear reddish grain, most likely garnet, was often observed. Single grains of the various types found were individually glowed in an attempt to find a strong TL emitter and thus estimate what amount of TL in a mixed (quartz and heavy grains) sample would be from the heavy grains. None of the grains were bright, and only a few produced a TL signal distinguishable above background.

A quick check for zircon (which tends to have a high concentration of uranium and thorium) was done using a technique which uses the grains' different indices of refraction for separation. No zircon was observed in the approximately 50 "likely" heavy grains which were viewed (Berger, personal communication, 1985).

---

[1]From Metawo, Falkenreid 1, D 1000 Berlin 33, West Germany

Table 3.2

Size Fractions of the SESA Dunes

SESA #	Quartz (% Remaining After Treatment with HCl)	Percentage (Weight) Fractions Grain Size in Micrometers <90	90-125	125-250	>250
17	26.5	2.3	13.0	84.6	0
20	30.6	1.6	3.9	94.5	0
13	22.9	.7	.5	58.4	40.3
16	27.3	.4	1.3	57.2	41.1
1	20.7	5.4	7.3	60.2	27.1
30	14.4	.5	.6	36.2	62.7
4	31.5	.8	2.7	96.5	0
42W	24.9	.5	.4	99.0	0
36	34.3	1.4	2.9	33.7	61.9
6	13.1	0	5.4	23.1	71.5
43	71.9	4.5	54.8	40.6	0
8	21.0	.7	.7	1.6	96.9
10	33.5	.9	8.1	90.9	0
35	60.8	.7	2.7	96.5	0

Heavy minerals were less than .1% of the sample, by weight. It was difficult to measure their mass accurately.

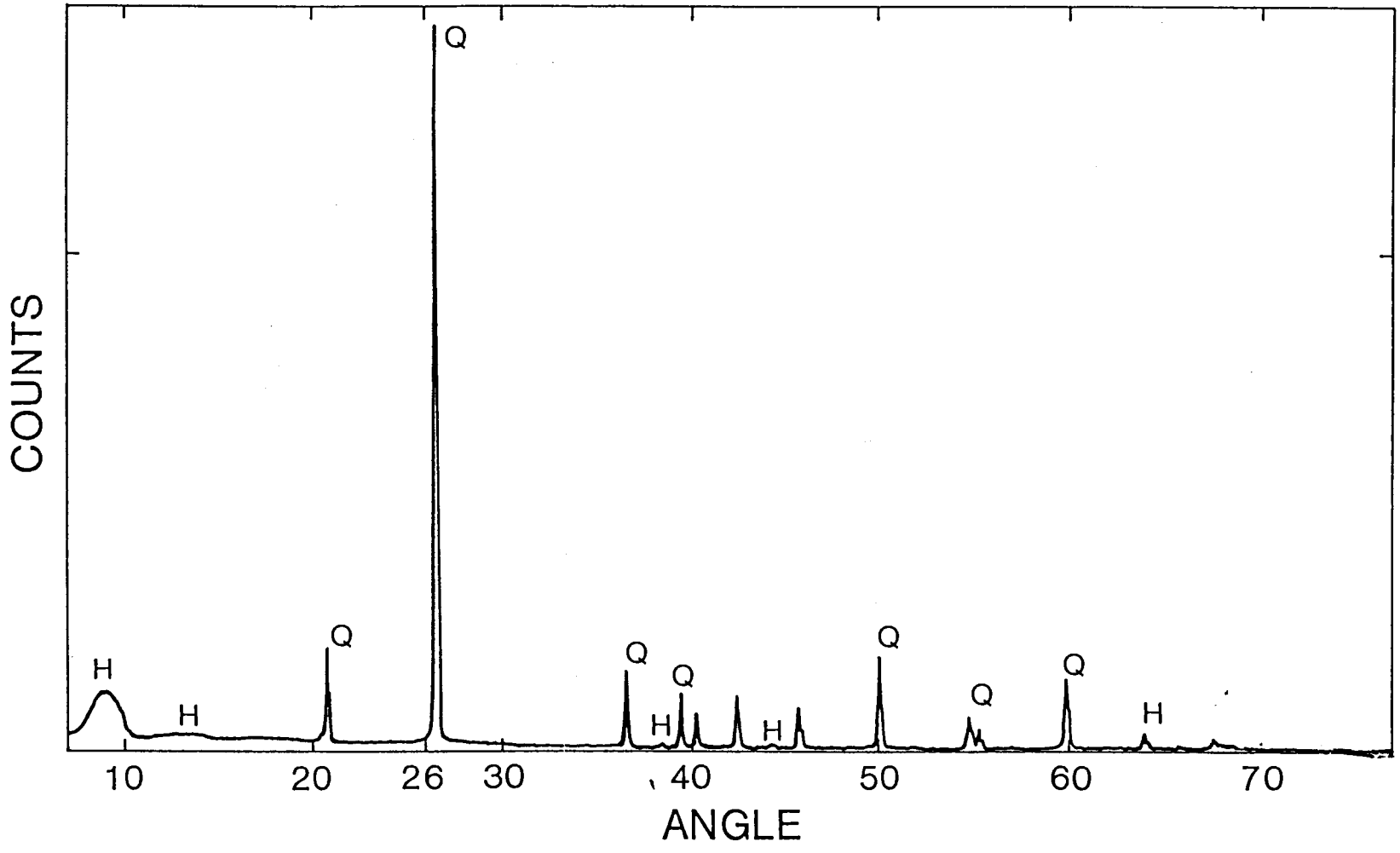

Figure 3.3

This is a copy of the x-ray diffraction results for a modern SESA sample, -17. The angle is 2θ degrees. Q refers to quartz and H refers to peaks from the holder.

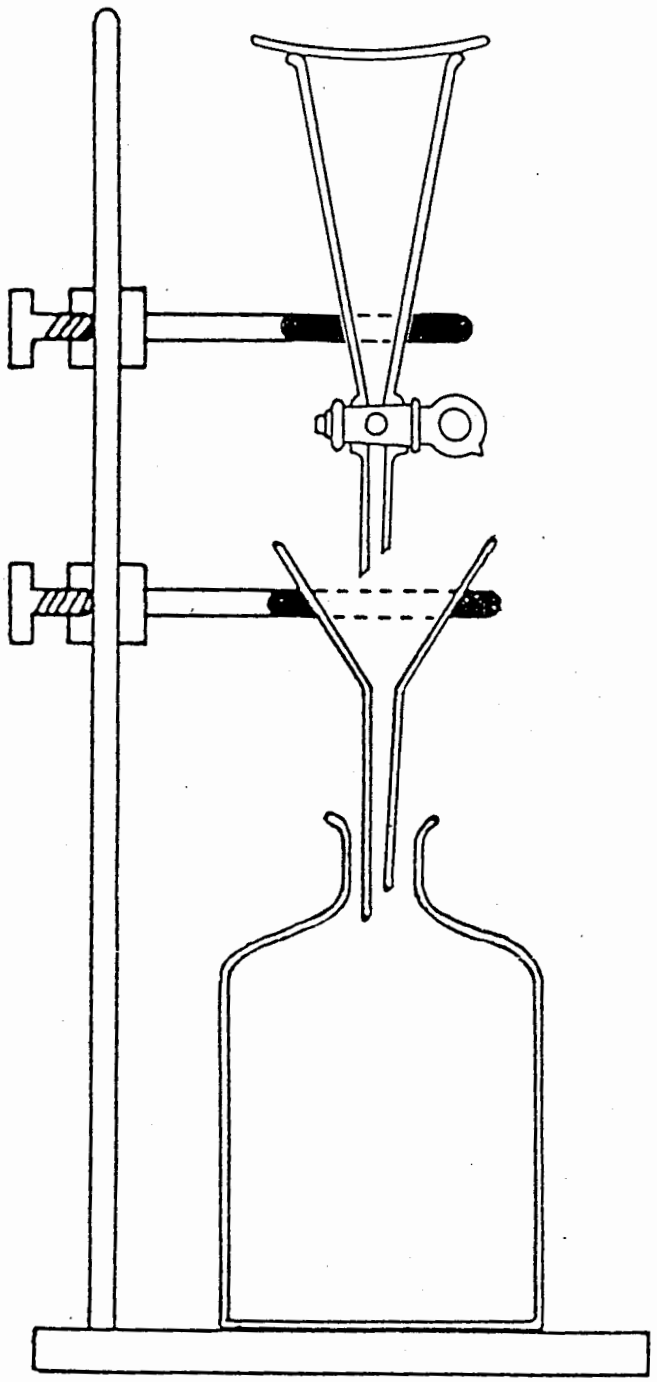

Figure 3.4

Apparatus For Heavy Liquid Separation

Preparation of the Samples for TL Measurments

The planchets[2] were made of 1/16th inch aluminum, with an outer diameter of 1/2 inch and a depth of 1/8 inch.

They were cleaned by ultrasonic agitation in a series of solvents - ethanol, acetone and then trichloroethylene. A few seconds of etching in dilute HF removed a thin surface layer of aluminum oxide. Before drying, the planchets were thoroughly rinsed in water, then methanol.

Dow Corning 200 silicon oil was spread on the planchets to hold the grains in place. After arranging 40 of the planchets on a hot plate, a drop of oil was placed in the centre of each with a 26-gauge syringe. This method has several advantages over spraying or wiping; only a small, controllable, consistent amount of oil was used and very little oil spread to the edges or sides of the planchet. After a few minutes heating at 70°C, the oil covered about half the bottom area. The planchets were then placed in a box and left to sit undisturbed. A wait of 24 hours was found to be best, with a minimum wait of 12 hours and a maximum of about 6 days being used. The sample tended to clump if the planchets were used too soon, and with too long a wait, the grains did not adhere well. This was probably due to the oil spreading too much and perhaps drying out.

---

[2]Manufactured by Hansen Industries, 202-111611 Bridgeport, Richmond, British Columbia, Canada

Mass normalization was used for all the experiments. The weighing procedure consisted of placing the empty, oiled planchet on a laboratory balance[3] and then zeroing. The planchet was taken off the balance and a small spatula was used to put ≃30mg of sample in the middle of the planchet. It was then gently tapped and shaken until the grains covered the bottom of the planchet. It was turned over, tapped and shaken firmly to dislodge any loose grains. The bottom and upper edge were wiped on a methanol soaked paper towel to remove any clinging grains. The planchet was placed on the previously zeroed balance and reweighed to determine the sample weight. The sample mass was thus determined very quickly and easily.

This technique gave an average mass of 18 ± 2 mg of 100 μm quartz grains per planchet. A low power microscope was used for quick visual inspections. It was found that the grains primarily formed a monolayer. It was very rare to see clumps which were three grains deep.

The TL signal was found to be reproducible within ±5% after this method of sample preparation was followed. See Appendix C for a more thorough discussion of reproducibility.

---

[3]From Mettler Instrument Corporation, Box 71, Hightstown, New Jersey, U.S.A. 08320 Model AE163, accurate to within ±10 μg

3.5 Apparatus

3.5.1 The TL Apparatus

The experimental apparatus was modelled on the glow oven developed by M.J. Aitken of Oxford, and is similar to the one shown in Figure 3.5. It consisted of an evacuable chamber 11.5 cm in diameter and 3 cm deep. The kanthal heating strip was 3.5 x 2.5 x 0.05 cm. The heater was powered by a Daybreak 520 TL Oven Control[4]. In all the experiments, the heating rate used was 5°C/sec from 20-450°C. An EMI 9635B photomultiplier tube was used with a Corning 5-58 blue filter to suppress the TL and incandescent emissions at wavelengths less than ≃300 nm and greater than 500 nm.

A Tracor Northern 1750 multichannel analayzer[5] was used to measure the glow curve (number of photons versus temperature), and a Hewlett-Packard 7035B X-Y Recorder[6] was used to record the curves during measurement. A dwell time of 400 ms was used when measuring the number of photons per channel. The channel counts were saved on magnetic tape for further data analysis with a Tektronix 4051 computer. One channel corresponded to a 2.16°C change in temperature. For ease of analysis, the data from five channels (10.8°C) were summed and stored as a unit.

---

[4]Daybreak Nuclear and Medical Systems, Inc. 50 Denison Drive, Guilford, CT, U.S.A. 06437

[5] Tracor Northern, 2551 West Beltline Highway, Middleton, Wisconsin, U.S.A. 53562

[6] Hewlett-Packard Company, 16399 W. Bernardo Drive, San Diego, California, U.S.A. 92127

Thermal compound[7] was used to ensure good thermal contact between the planchet and the heating strip. Before glowing, a fresh 5 ml beaker of P_2O_5 was put in the chamber. This is a strong dessicant, and helped remove traces of water vapour. For each planchet, the chamber was evacuated to <30 μm. Pre-purified argon gas, with <10 ppm O_2, was then flushed through the system. During the actual glowing, the pressure was ≃ 13 Pa (100 μm of mercury) with a flow rate of ≃0.1 L/min (Figures 3.5, 3.6).

3.5.2 Irradiation Apparatus

The gamma irradiations were done using an Atomic Energy of Canada Limited ^{60}Co "Gammacell".

The dose-rate was calibrated using an irradiated TLD phosphor which was obtained from the Laboratory for Research in Archaeology, 6 Keble Road. Oxford, England, OX1 3QJ. This calibration was done by A.G. Wintle in 1976 and extrapolated to the period 1983-1986.

3.5.3 Bleaching Apparatus

The bleaching apparatus used at the beginning of the work for this thesis was a filament from an automobile headlight. A concave lens was used to focus this light onto a circle approximately 4 cm in diameter. The samples were placed on a small rotating platform which was the magnetic stirring unit

---

[7]Wakefield Thermal Compound, Part # 120-2, from Wakefield Engineering Inc. Wakefield, Mass. U.S.A. 01880

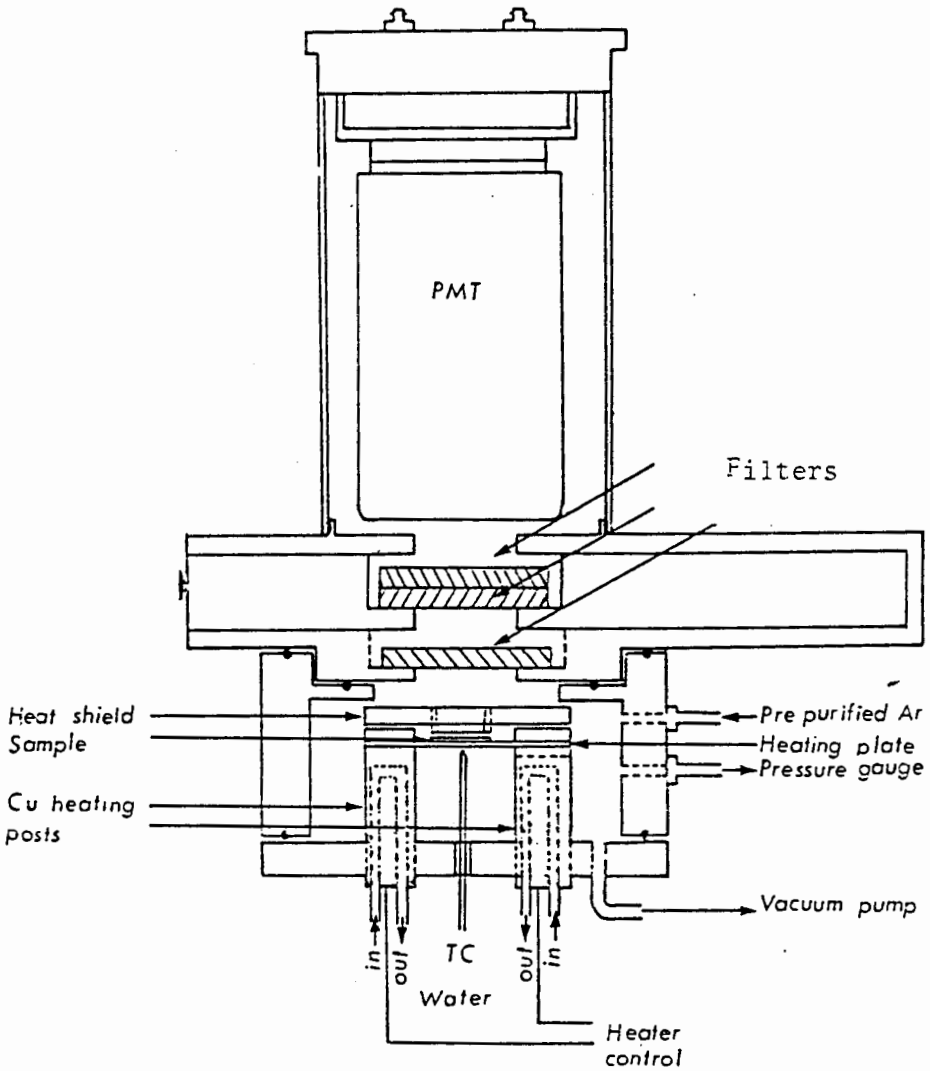

Figure 3.5

Glow Chamber

(Divigalpitiya, 1982)

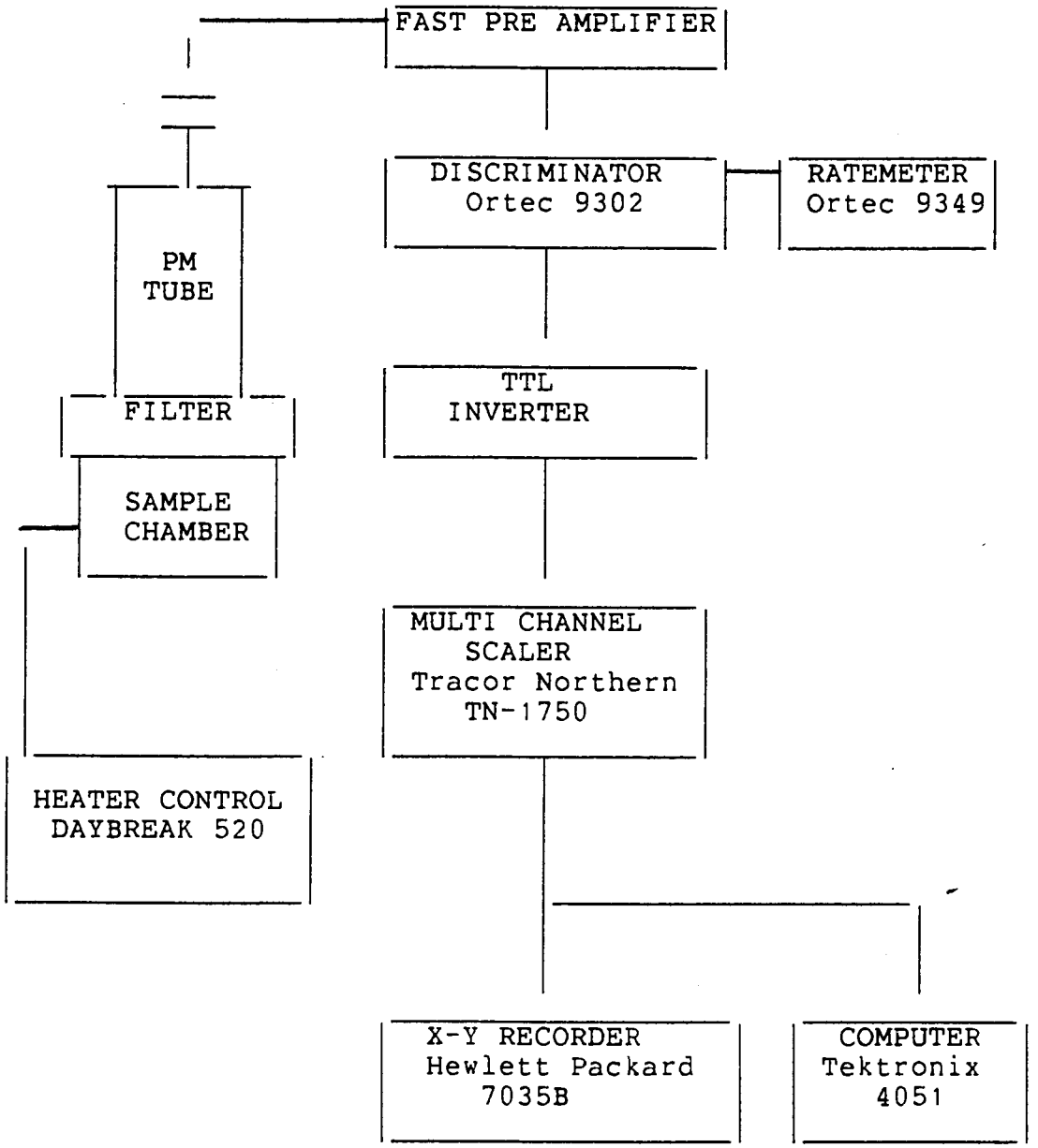

Figure 3.6
Schematic of the TL Apparatus

from a defunct hot plate. This reduced the variations in light exposure received by the the discs to less than 5%. When the light was filtered to remove any UV components, the intensity decreased to such an extent that it was more practical to use natural sunlight to bleach all the samples which were studied during the course of this work.

This helped ensure that all the samples (as many as 70 were bleached at one time) received the same light exposure. And since sunlight was assumed to be the original bleaching mechanism, the use of sunlight to bleach the experimental samples meant that there was little difference between the original and laboratory spectra.

CHAPTER IV

EQUIVALENT DOSE DETERMINATIONS

As outlined in the introduction, TL increases with the dose which the mineral has received. Figure 4.1 illustrates the natural (no laboratory dose) glow curves from the various SESA samples.

Note that the increase with age is non-linear, there appears to be a saturation point, and the zero-age samples have non-zero TL. In this case, as with most geological sediments, not all the TL traps were empty at deposition - the "TL clock" has not been totally reset. The exact zeroing mechanism for geologic sediments is still unknown, but sunlight is the most likely candidate, and was assumed to be the zeroing agent in this work.

4.1 Partial-bleach Method

Since one does not know the extent of the original bleaching one must use a method to determine the equivalent dose that does not depend on this knowledge.

The partial-bleach method involves a laboratory bleach which empties some of the light-sensitive traps (See Chapter II for a more detailed explanation of this method).

The bleaching times used were on the order of a half hour, no sample was exposed to more than one hour of sunlight.

Averaged Natural Glow Curves

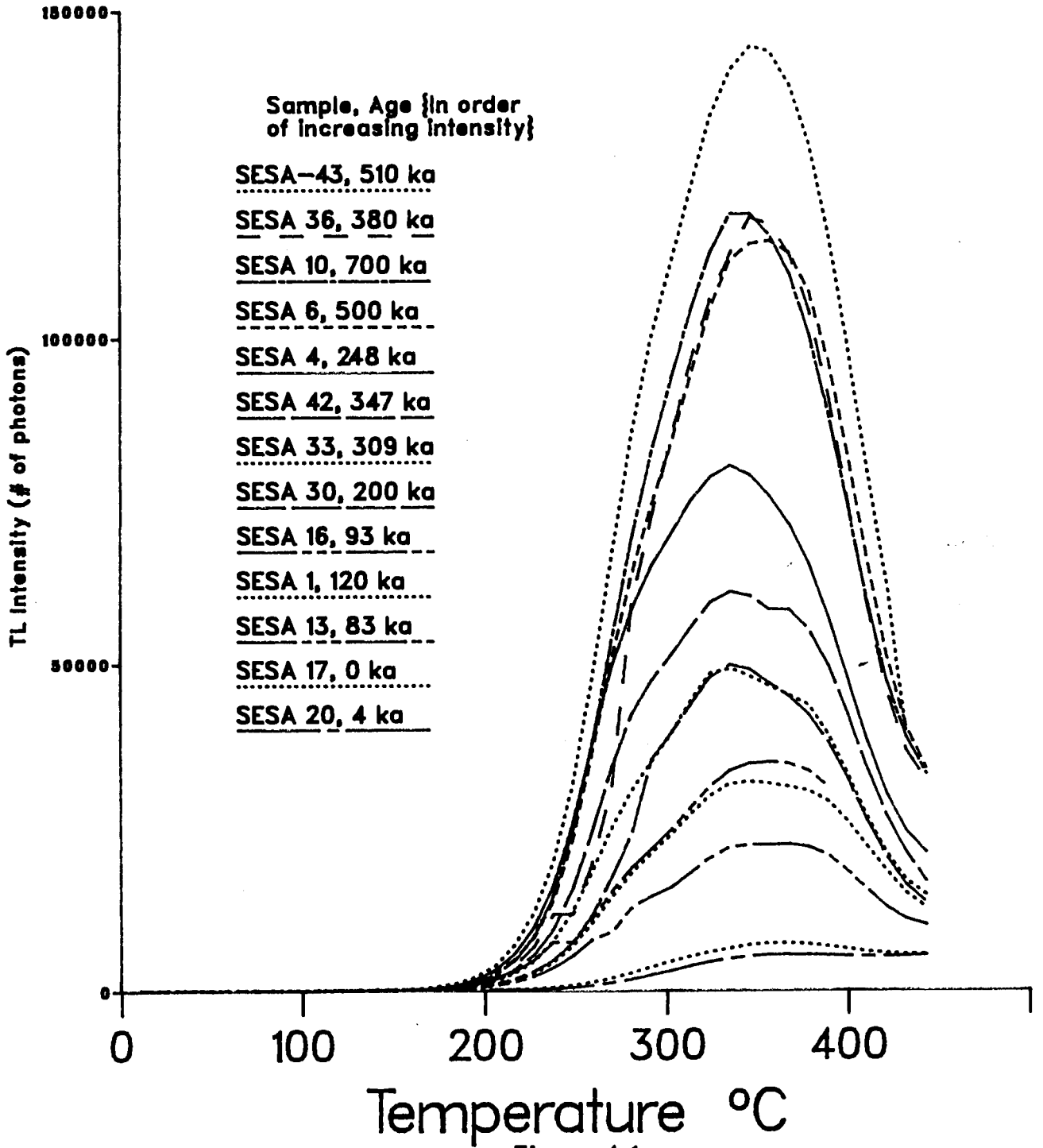

Figure 4.1

Various SESA glow curves, the average of 3 planchets. Note the increase of TL intensity with age.

4.1.1 Extrapolations

4.1.1.1 Fitting the modern sample's growth curve

A modern sample of the same type as the older samples was available for measurement (the presence of a modern sample was one of the reasons these sands were such a good test sequence). A growth curve was constructed from the modern sample, and quadratic and exponential curves were fitted to the data using the computer program outlined in Appendix C (Figure 4.2). The data had an intrinsic scatter of ≃±5% which made it difficult to fit curves to the experimental data. The figure shows that the exponential was a better fit. For this reason, exponential extrapolations were used throughout this thesis. As well, the exponential fit can be justified on physical grounds as part of the trap depth model of TL (Section 2.4.4).

4.1.1.2 Extrapolations

The modern growth curve shown in Figure 4.2 could also be used to check the validity of the extrapolations and give some idea of the errors involved in fitting the data. To do this, the data from doses 0 to D_x was ignored on the growth curve. The remaining data was fitted with either quadratic or exponential curves and extrapolated to obtain a value D_x'. D_x is the correct D_{eq}, while D_x' is the calculated D_{eq}. The difference in these values is plotted in Figure 4.3 for values of D_x from 0-75 Gy. It gives some idea of the error expected in the extrapolations used for the older samples.

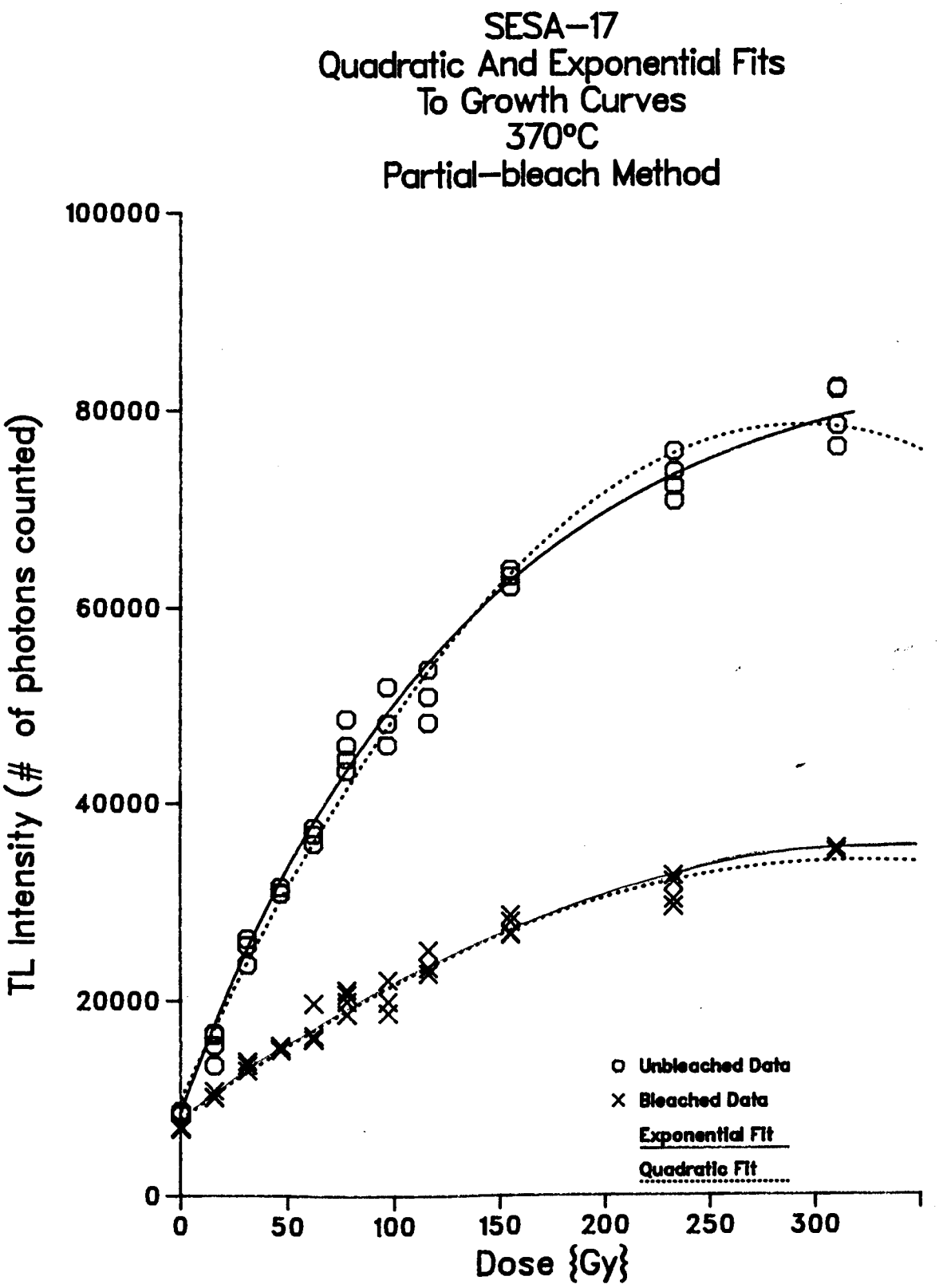
SESA–17
Quadratic And Exponential Fits
To Growth Curves
370°C
Partial–bleach Method
TL Intensity (# of photons counted)
100000
80000
60000
40000
20000
0
0
50
100
150
200
250
300
Dose {Gy}
Unbleached Data
Bleached Data
Exponential Fit
Quadratic Fit

Figure 4.2

The large errors in the higher dose ranges (especially 75 Gy) are more likely a function of this particular set of data than a true estimate of the error involved. Note the scatter (Figure 4.2) in the TL from doses 40-70 Gy. This made curve fitting at these D_x values difficult. A modern sample should have yielded a D_{eq} of 0. As Figure 4.3a showed, the calcuated D_{eq} range from -1 Gy to +3 Gy, with a average of about +2 Gy. The D_{eq} obtained for older samples using this method will be at least 2 Gy too large. The rest of the data shown in this figure gives some more details of the errors expected in the 15-45 Gy range. For temperatures less than ≃325°C, the calculated D_{eq} should be decreased by 3-7 Gy, while for temperatures greater than this, the calculated D_{eq} should be increased. For samples with an expected D_{eq} greater than 60 Gy, the D_{eq} calculated at temperatures less than ≃350°C should be decreased by ≃15 Gy. It would be useful to repeat this experiment, and to have more data points extending out to a higher dose range.

These results should not be interpreted too strongly. They indicate that the calculated D_{eq} for older samples will problably be too large by 2-≃15 Gy. It does indicate that error associated with the D_{eq} calculations is at least ±10 Gy for older samples.

Figure 4.2, 4.4a, b and c show the partial-bleach method applied to samples of various ages. Note that the growth curves from SESA-36 were close to saturation, making it difficult to fit an exponential. (See Section 4.1.4).

4.1.2 Intercept Check

Figure 4.1 furnishes a check on the validity of the extrapolations. It gives a rough indication of the ratio of natural TL for modern and old samples. If the ratio of the intercept obtained from the partial-bleach method to the natural (laboratory dose = 0) TL from an old sample is not similar to this, it indicates that something is wrong. This criterion casts doubt on the validity of the SESA 36 data.

4.1.3 Plateau Test

Plateau tests (Figures 4.5a-e) were done by plotting the D_{eq} as a function of temperature. The error bars (obtained by the computer program outlined in Appendix C) give approximate 95% confidence intervals for a specific temperature range of 5°C. The final D_{eq} values was obtained by looking at the figures and deciding which value was consistent with the data. The error limits were also estimated by eye, and cannot be represented in statistical language as no formal analysis was done.

4.1.4 Results and Discussion

Table 4.1 lists the D_{eq} plateau values (≃300° - 370°C) obtained from the partial-bleach method on the various samples. Values calculated from the data shown in Figure 4.5 as well as the corrections caused by the data shown in Figure 4.3 are listed in this table.

Differences Between The Expected And Calculated Values of D_{eq}

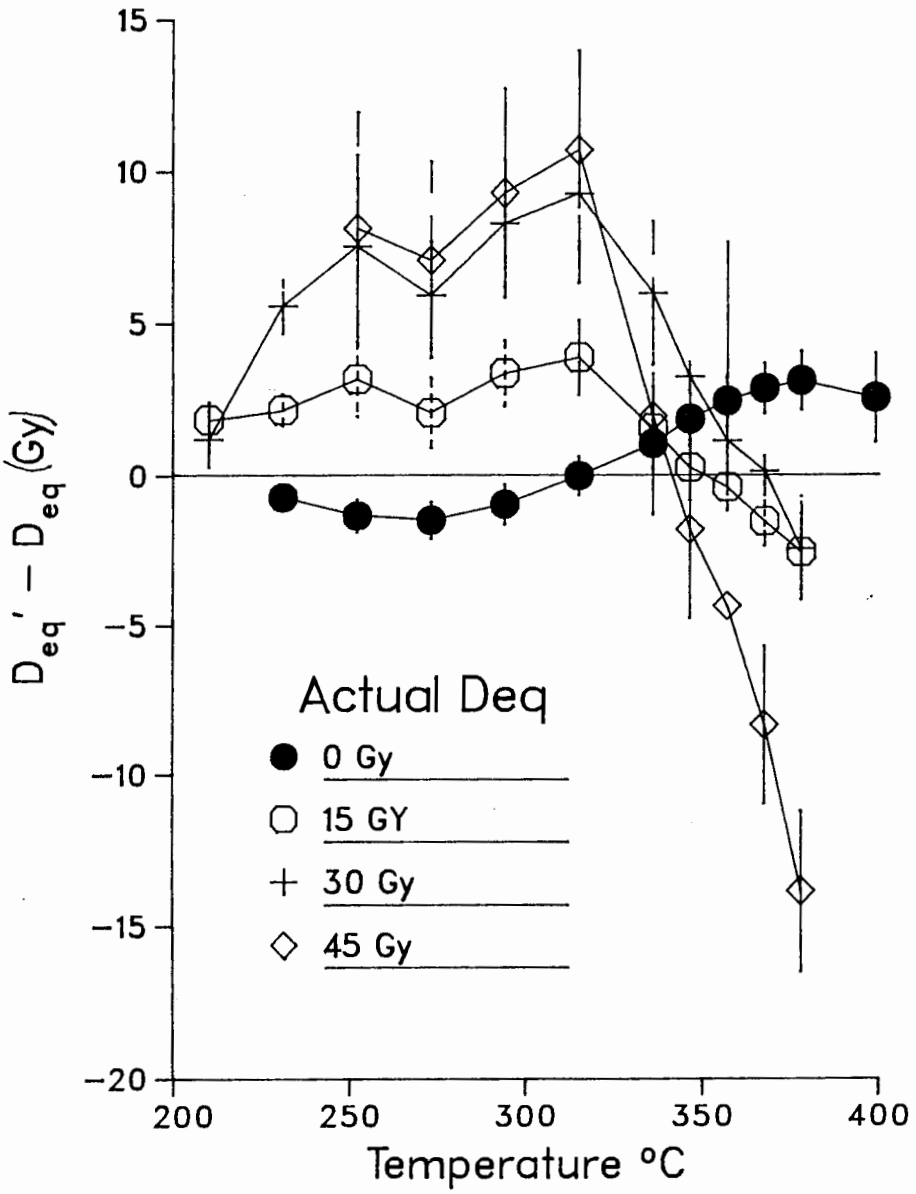

Figure 4.3a

Differences between the expected and calculated D_{eq} values. Expected errors due to extrapolations from the curve-fitting routine used in this thesis. $D_{eq}' - D_{eq}$ is the difference between the expected and actual values of D_{eq}.

Differences Between The Expected And Calculated Values Of The D_{eq}

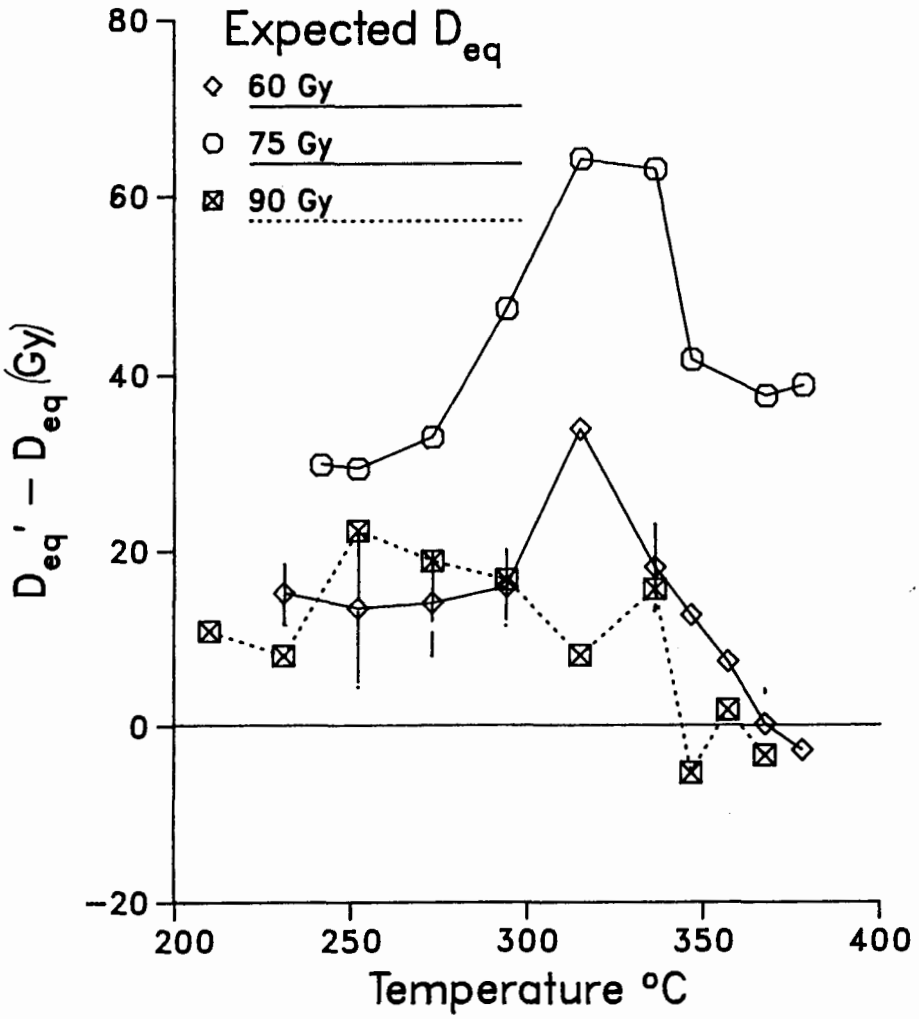

Figure 4.3b

Difference between the actual and calculated values of D_{eq}, from the curve-fitting routine used in this thesis. $D_{eq}' - D_{eq}$ is the difference between the calculated and actual value. The large range is the 75 Gy data is most likely due to scatter in the data used for the extrapolation {See Figure 4.2}.

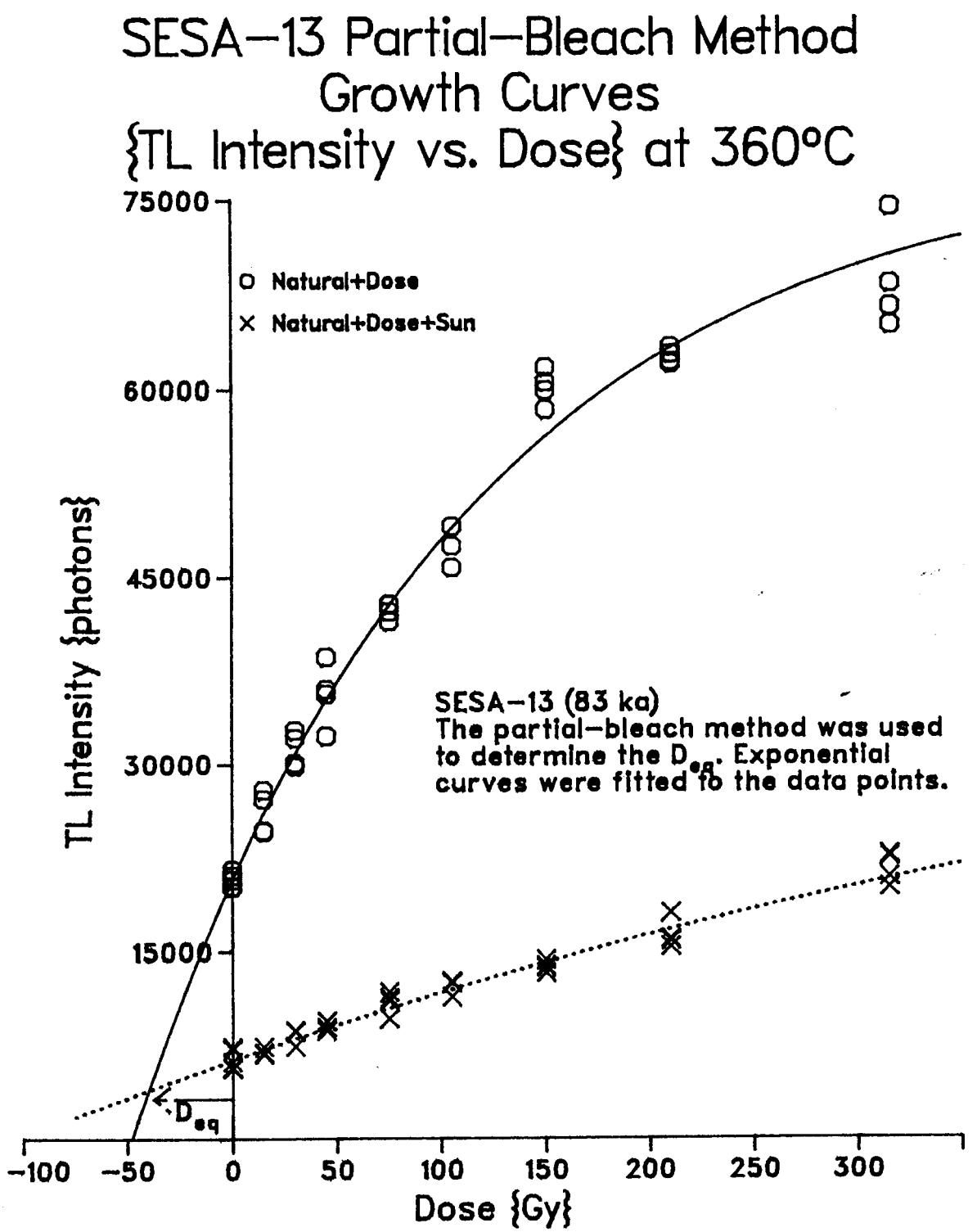
SESA–13 Partial–Bleach Method
Growth Curves
{TL Intensity vs. Dose} at 360°C
75000
60000
45000
30000
15000
TL Intensity {photons}
Natural+Dose
Natural+Dose+Sun
SESA–13 (83 ka)
The partial–bleach method was used to determine the D_{eq}. Exponential curves were fitted to the data points.
D_{eq}
–100
–50
0
50
100
150
200
250
300
Dose {Gy}

Figure 4.4a

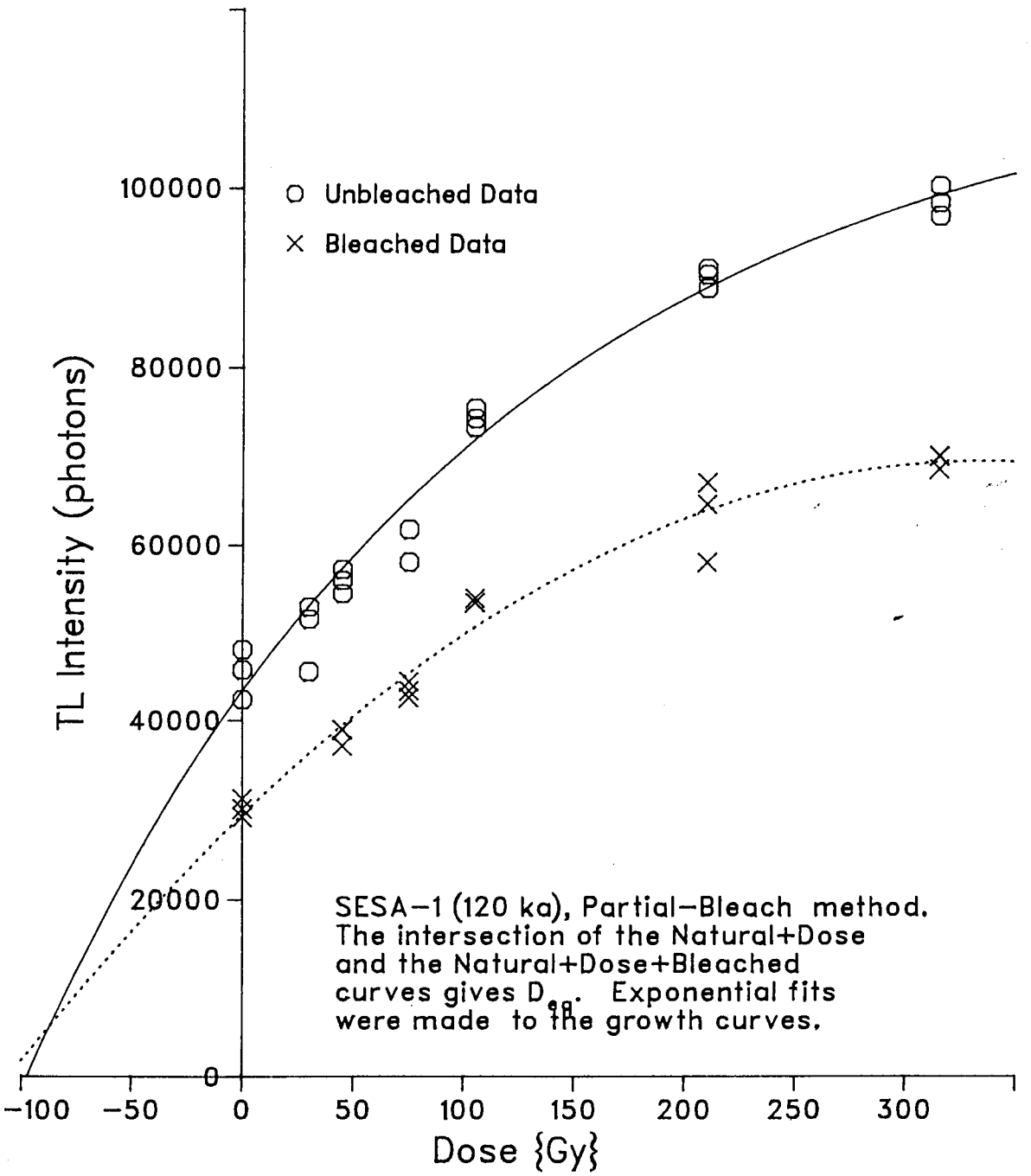
SESA–1 Partial–Bleach Method
Growth Curves
{TL Intensity vs. Dose} at 330°C
100000
80000
60000
40000
20000
0
TL Intensity (photons)
Unbleached Data
Bleached Data
SESA–1 (120 ka), Partial–Bleach method.
The intersection of the Natural+Dose
and the Natural+Dose+Bleached
curves gives D_{eq}. Exponential fits
were made to the growth curves.
–100
–50
0
50
100
150
200
250
300
Dose {Gy}

Figure 4.4b

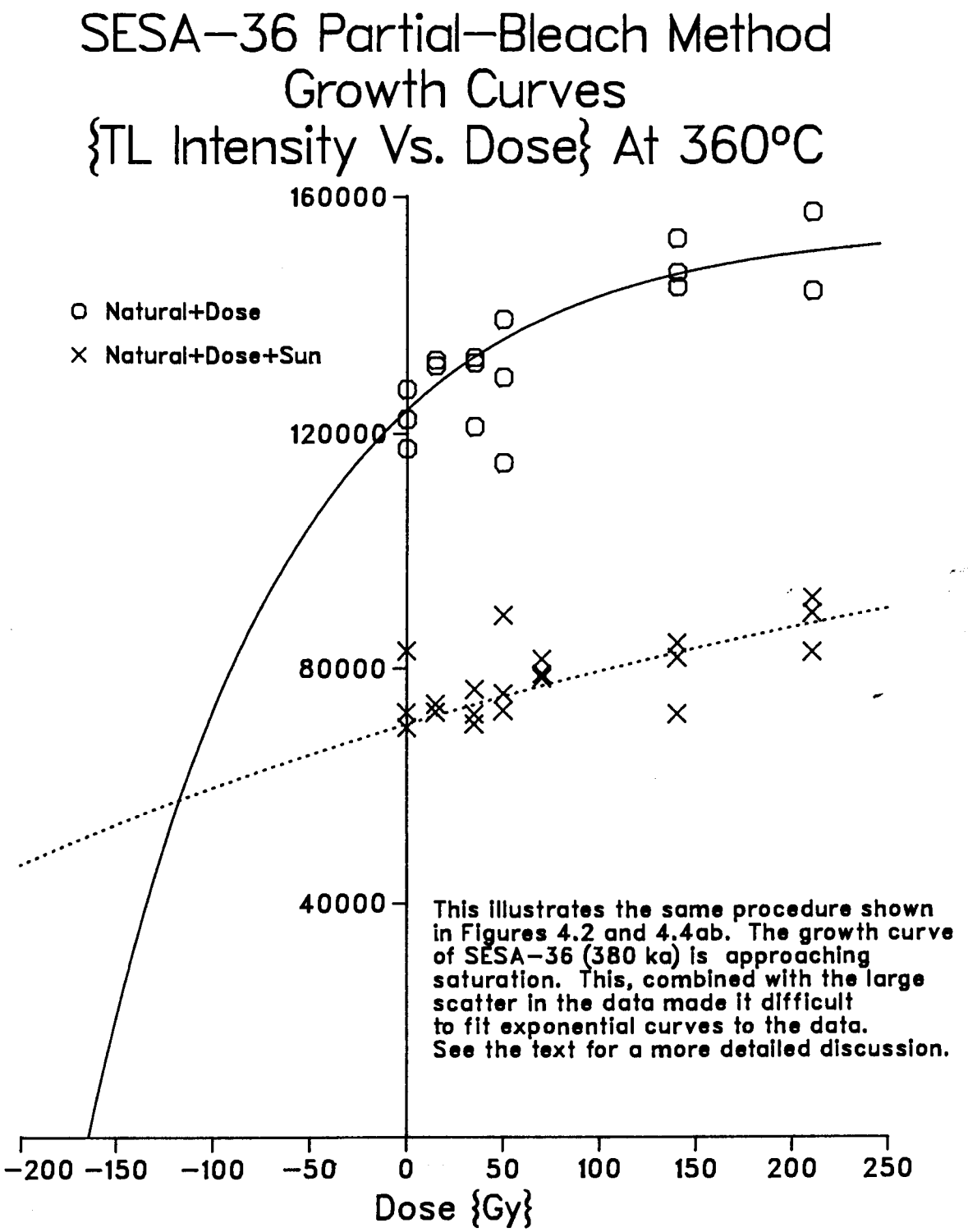
SESA–36 Partial–Bleach Method
Growth Curves
{TL Intensity Vs. Dose} At 360°C
160000
120000
80000
40000
O Natural+Dose
× Natural+Dose+Sun
This illustrates the same procedure shown in Figures 4.2 and 4.4ab. The growth curve of SESA–36 (380 ka) is approaching saturation. This, combined with the large scatter in the data made it difficult to fit exponential curves to the data. See the text for a more detailed discussion.
−200 −150 −100 −50 0 50 100 150 200 250
Dose {Gy}

Figure 4.4c

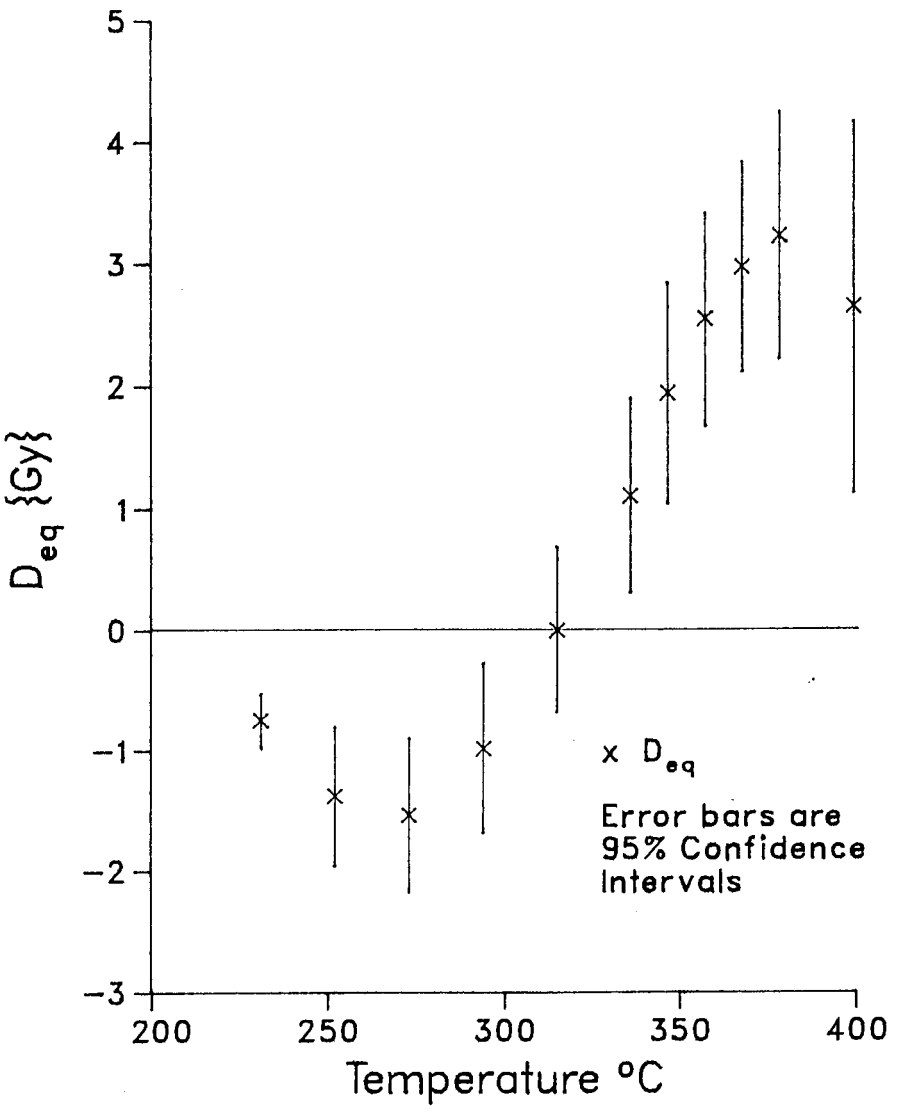

Figure 4.5a

Plateau test for SESA−17 (modern sample), D_{eq} vs. temperature, with exponential fits to unbleached and bleached data.

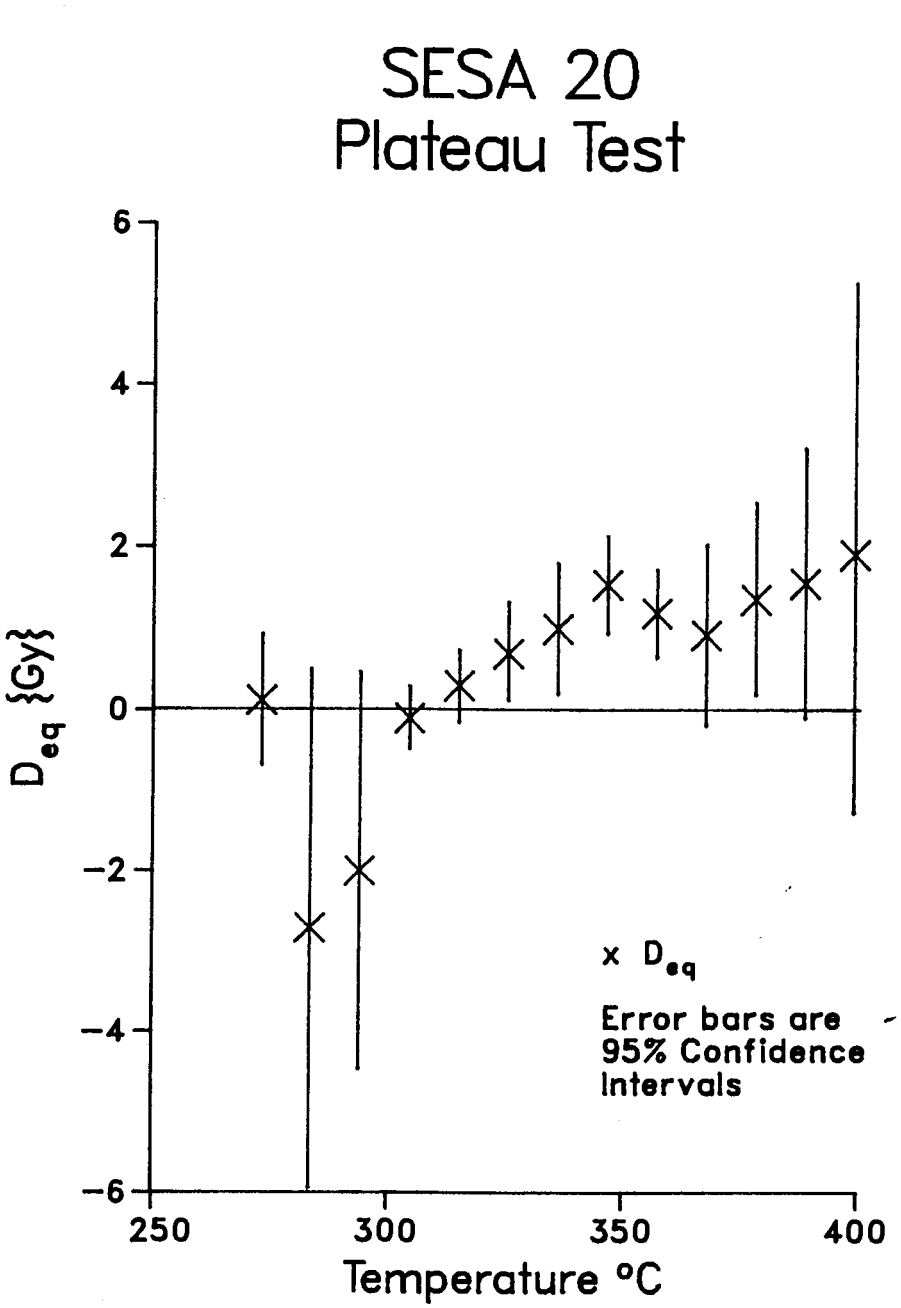

Figure 4.5b

Plateau test for SESA−20 (4 ka).
D_{eq} vs temperature
with exponential fits to unbleached and bleached data.

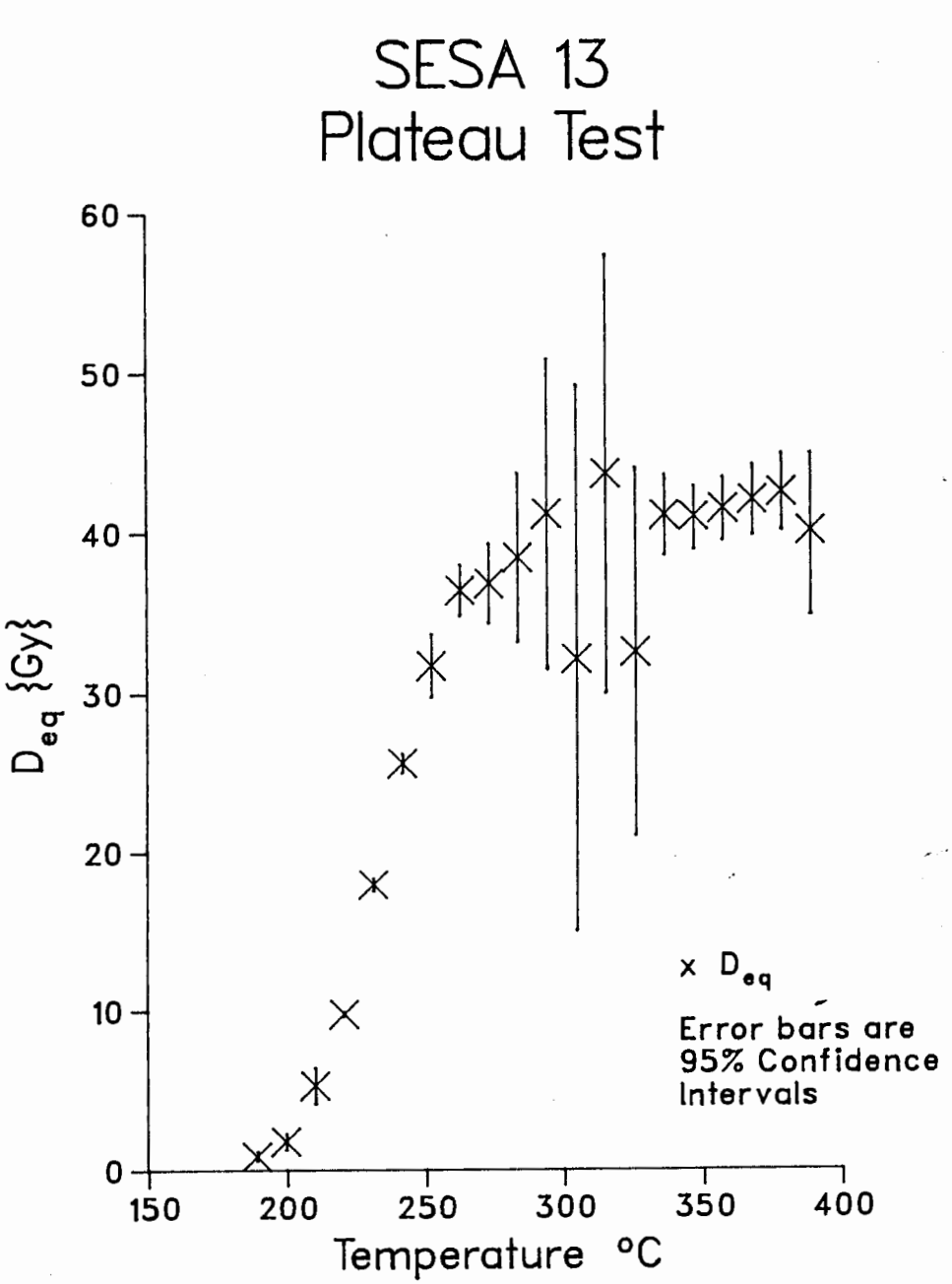

Figure 4.5c

Plateau test for SESA–13 (83 ka), D_{eq} vs. temperature with exponential fits to unbleached and bleached data.

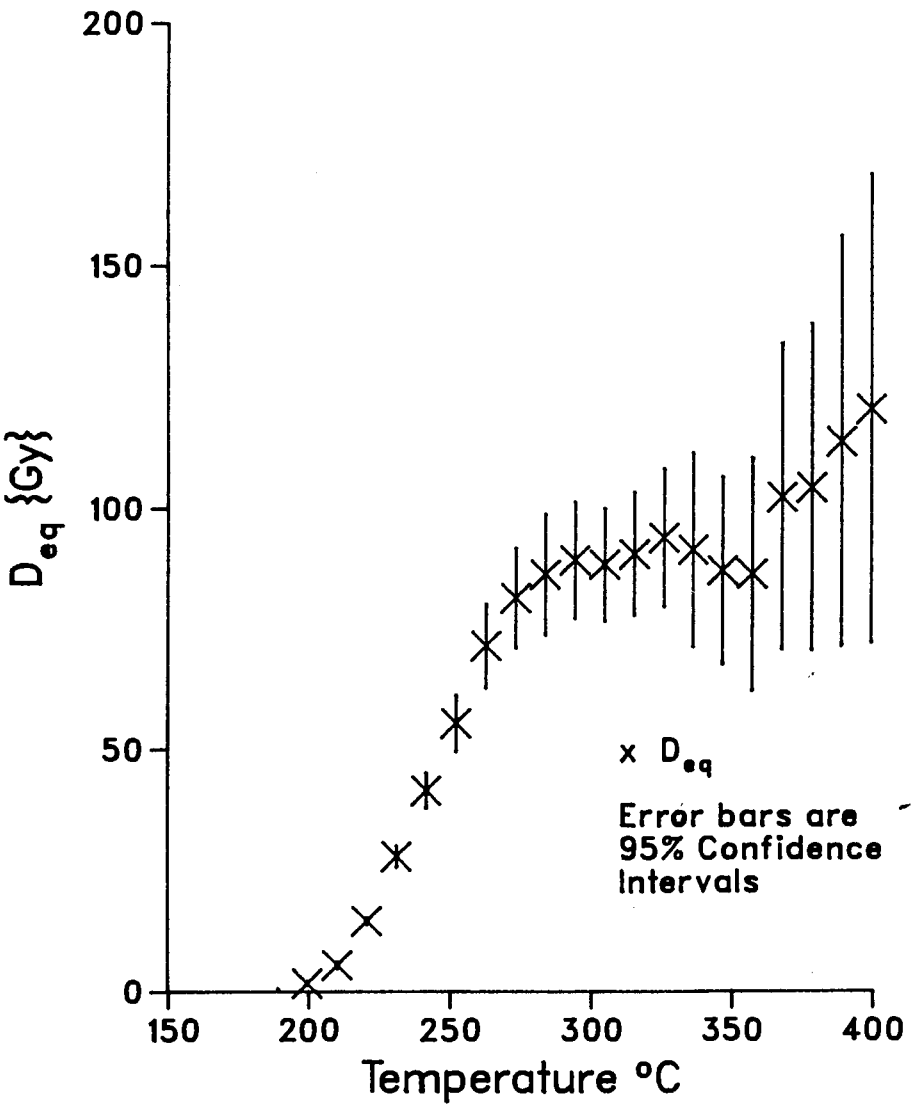

Figure 4.5d

Plateau test for SESA–1 (120 ka),
D_{eq} vs. temperature with exponential fits
to unbleached and bleached data

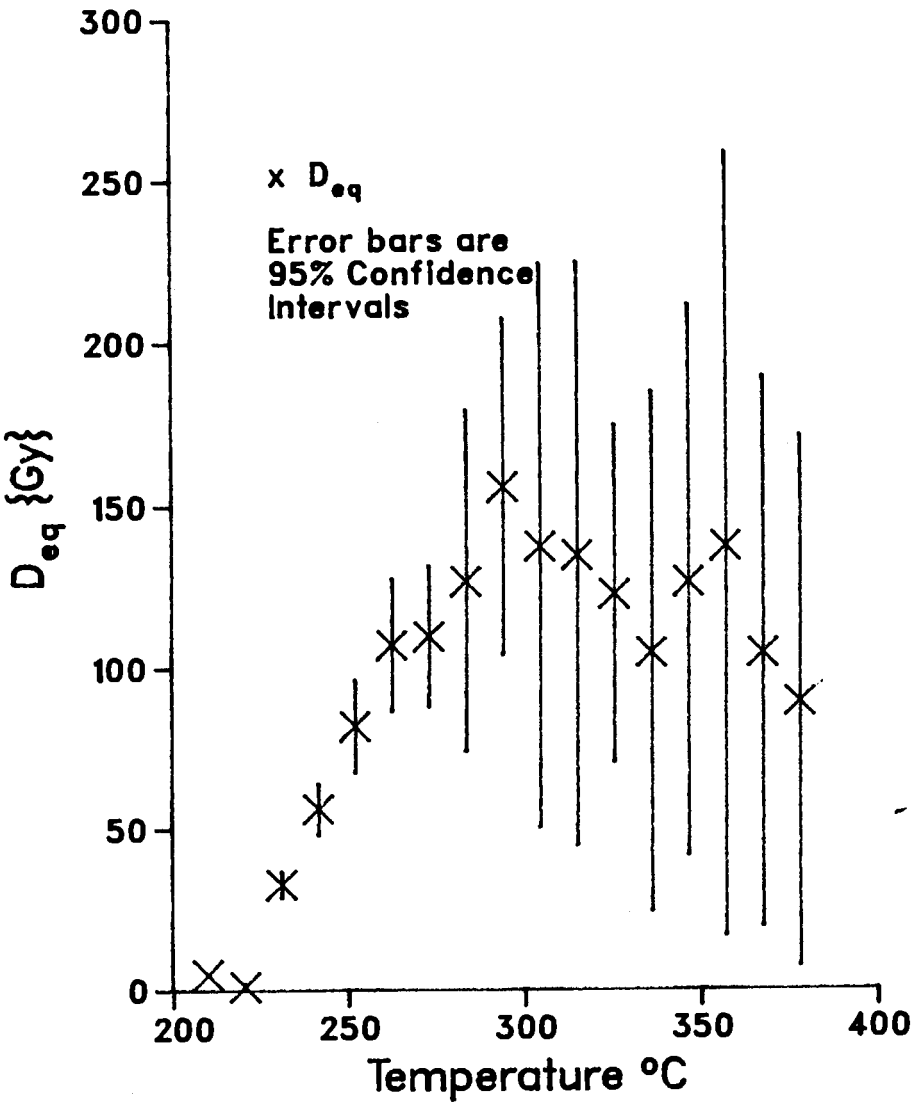

Figure 4.5e

Plateau test, SESA–30, (200 ka)
D_{eq} vs Temperature

Exponential fits to unbleached and bleached data.

Table 4.1

D_{eq} Partial Bleach Method

SESA #	Grain Size (Microns)	D_{eq} Minutes in Gamma Cell	Gy/Minute in Gamma Cell	D_{eq} (Gy)* (from plateau test)	Corrected D_{eq}**
17	100	2 ± .6	1.55	3.1 ± .9	
20	100	.5 ± .5	1.55	.8 ± .8	
13	150	25 ± 4	1.58	40 ± 6	36 ± 8
1	100	58 ± 8	1.50	87 ± 12	82 ± 16
30	200	90 ± 30	1.50	135 ± 40	125 ± 45

* This value was obtained from the plateau tests (Figures 4.5a-e) which are plots of the the Deq as a function of temperature. The error bars for specific temperature ranges of 5 °C were approximate 95% confidence intervals. The final Deq value was obtained by looking at the figures and deciding which value was consistent with the data for temperatures from ≈300°C - 370°C. The error limits were also estimated by eye, and cannot be represented statistically as no formal analysis was done.

** These values were corrected due to errors inherent in the fitting routine. Please see Figure 4.3.

Note the low values obtained for SESA-17 and SESA-20. Low D_{eq} values are a check on the validity of the method chosen to date the samples (Wintle and Huntley, 1982).

The values obtained for SESA-36 should be treated with caution. The growth curve (Figure 4.4c) was near saturation. The data were very scattered, and this made it difficult to fit an exponential curve to the data. More data at higher doses may have been useful, but doses ranging from 0 - 300 Gy were adequate for all the other younger samples, so it is unlikely that more data at higher doses would have helped the fit. Due to the small amount of sample available (Table 3.2), this experiment could not be repeated. Also, from Figure 4.1 the ratio for the natural TL from SESA-36 to SESA-17 is about 10:1. This should be the ratio of the intercept of the bleached and unbleached curves from SESA-36 and the natural TL (lab dose=0) from the unbleached curve, but it is more like 2:1. The sample may have been overbleached, although it was exposed to less than one hour of sunlight. The problem was most likely due to the difficulty in fitting a curve to the saturating exponential. If one did not know from previous work that such growth curves should be fitted with exponentials (Section 4.1.2.1) a linear fit would appear to be the best choice. This would yield D_{eq} of $\simeq$600 Gy. But linear fits are not acceptable for quartz which has experienced large (>200 Gy) doses. As the fit is evidently inappropriate, the D_{eq} value obtained was discarded.

The results obtained from the extrapolation test (Section 4.1.1.2, Figure 4.3) indicate that some correction should be made to the D_{eq} shown in Figure 4.5. For example, if Figure 4.3a indicated that the computer extrapolation for a sample at 330°C with an expected D_{eq} of 15 Gy gave a value which was 5 Gy too large, then 5 Gy was subtracted from the 330°C value of the appropriate plateau shown in Figure 4.5. This process was continued for the rest of the temperatures, then a value for the "corrected" plateau was chosen.

To a certain extent, the final value was arbitrarily chosen, as shall be discussed for some specific examples. Plateaus are found from measurements of the D_{eq} from about 300°C - 370°C, so the calculated D_{eq} of 40 Gy for SESA-13 (83 ka) is about 5 Gy too large. For SESA-1 (120 ka), the calculated D_{eq} for temperatures from 250-350°C should be reduced by $\simeq$ 15 Gy, while the D_{eq} above this should not change. This decreases the overall (plateau averaged) D_{eq} of 87 Gy by about 4 Gy, and increases the error. A similar procedure should be followed for SESA-30 (200 ka). In this case, the error limits of the D_{eq} used in the plateau were large, and lowering the D_{eq} for temperatures less than $\simeq$350°C slightly improved the plateau. The large scatter in the results of Figure 4.3 means that these correction factors cannot be applied exactly, but they do lower the calculated D_{eq}.

The D_{eq} values obtained for the modern samples were not "corrected" as these values give the lower limit of the accuracy of this technique.

SESA-1 (Woakwine, 120 ka) was studied more than once. Three samplings were done at the site, SESA-1, -40 and -1/2, the latter was taken from the same hole as the first. The preliminary work done on the sample gave a smaller D_{eq} than the final value used in this thesis, but all the values were within one standard deviation of each other. This, and the ages derived from the various values, are discussed in Chapter 6.

4.2 The Growth Curve Matching {GCM} Method

4.2.1 Introduction

The difficulties experienced with the curve fitting in the partial-bleach method led to experimentation with a new method. Assuming that one is working with similar samples which have similar TL growth characteristics, a composite curve can be constructed with the growth curves (TL intensity vs. Dose) from various samples. The growth curve from the modern sample is used to indicate the response of the samples for doses from 0 to 300 Gy. An older sample would have received a dose in nature so its growth curve (with lab doses from 0 to 300 Gy) would be similar in shape to that of the modern sample, but without the low dose values. If the older sample's growth curve was shifted along the dose axis, the amount of shift being equal to the dose received by the sample in nature, the curves should overlap (Figure 4.6). Given two growth curves, the amount of shift on the dose axis necessary to make them overlap would indicate the dose the

Figure 4.6
Model For The Growth Curve Matching Technique
TL Intensity vs. Dose

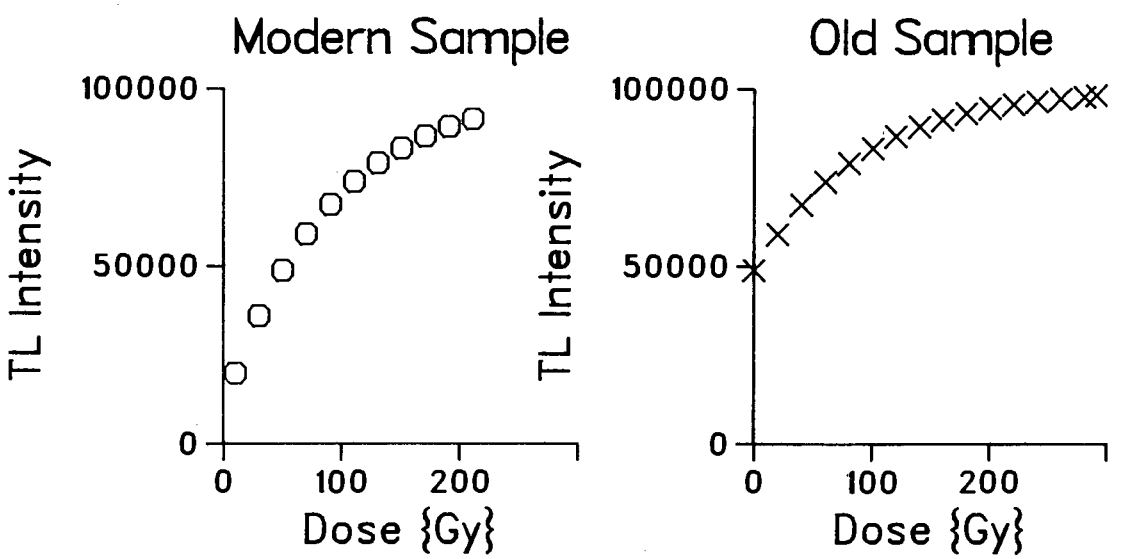

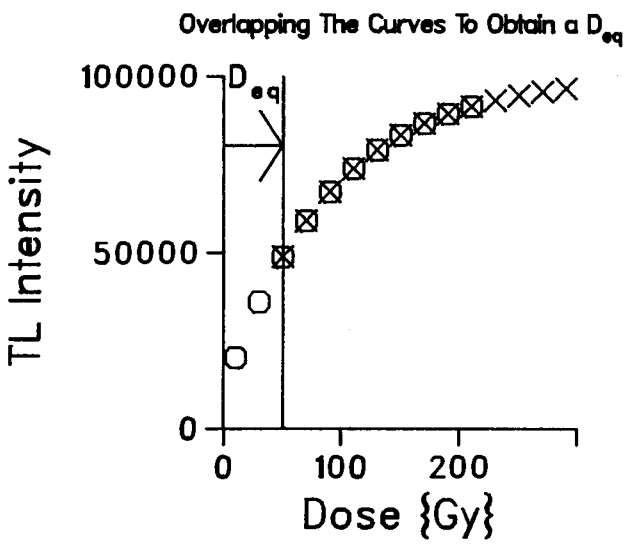

The growth curves of the modern and old samples are overlapped to obtain a 'best fit'. The amount of shift along the dose axis necessary to obtain this fit gives a measure of the D_{eq}.

sample had received in nature - it would be a measure of the D_{eq}.

An estimate of the error involved could be calculated from the range of fits. Scatter in the data would ensure that the curves would not overlap exactly, so the minimum and maximum "acceptable" shifts would give some idea of the error limits.

This method assumed that the samples had identical histories and received identical bleaching prior to deposition.

It was hoped that this method could be used on samples which were close to saturation. Such growth curves are difficult to fit with exponential curves. As well, it would eliminate the need for the bleaching of any samples, a source of potential error in most of the previous methods of TL dating.

Before this investigation began, it was not known if such a curve could be constructed, if the the technique would be sensitive enough to resolve the various growth curves, and if useful age estimates could be found.

4.2.2 Background work

Previous work done for the the partial-bleach method was used to see if the GCM technique could work. If the growth curves were similar, then the technique would warrant further investigation. In the partial-bleach method, exponential curves were fitted to the various Natural+Dose growth curves. The equation used was:

$$y = Y_o \left(1 - \exp(-(x + D_e)/ D_o)\right)$$

Y_o = saturation value

D_e = dose axis intercept value

D_o = rise parameter of the curve .

Figure 4.7a and b give the fitting parameters Y_o and D_o as a function of temperature for the samples which were dated using the partial-bleach method. With the GCM method, the growth curves were to be overlapped, and the amount of shift along the dose (x) axis necessary to give this overlap would be an estimate of D_{eq}. If the Y_o and D_o parameters for different samples were dissimilar, the GCM technique would require further work, perhaps the use of scaling factors. As Figure 4.7 indicates, there were variations in the fitting parameters, but it was hoped that the curves would be similar enough that reasonable fits could be obtained.

4.2.3 Results and Discussion

4.2.3.1 Unscaled Data

Figure 4.8a shows the growth curves from various samples. The data has not been scaled. The x-axis (dose) shift for the various samples shown in the figure was calculated from known results. This was done by taking the ages from Schwebel (1978) and multiplying by the dose-rate data (Table 5.2) to give an estimate of the dose in Gy received by a sample in nature prior to collection. The growth curve for an older sample was then

shifted by this amount relative to the modern growth curve. In other words, the curves shown in Figure 4.8a have been shifted on the dose axis (overlapped) where they "should" be, not necessarily where they would be placed if only the data shown in Figure 4.8a was used to determine the amount of shift.

This was done because some of the growth curves (especially SESA-43, -36, and -10) were quite different from the modern growth curve, and it was very difficult to decide where the overlap should have been done.

The D_{eq} shown in Table 4.2 were calculated by shifting the old and modern growth curves over each other until a best fit was found. The limits of the match (the error) were estimated by eye. The old and modern growth curves were shifted back and forth along the x (dose) axis to find the range of acceptable fits.

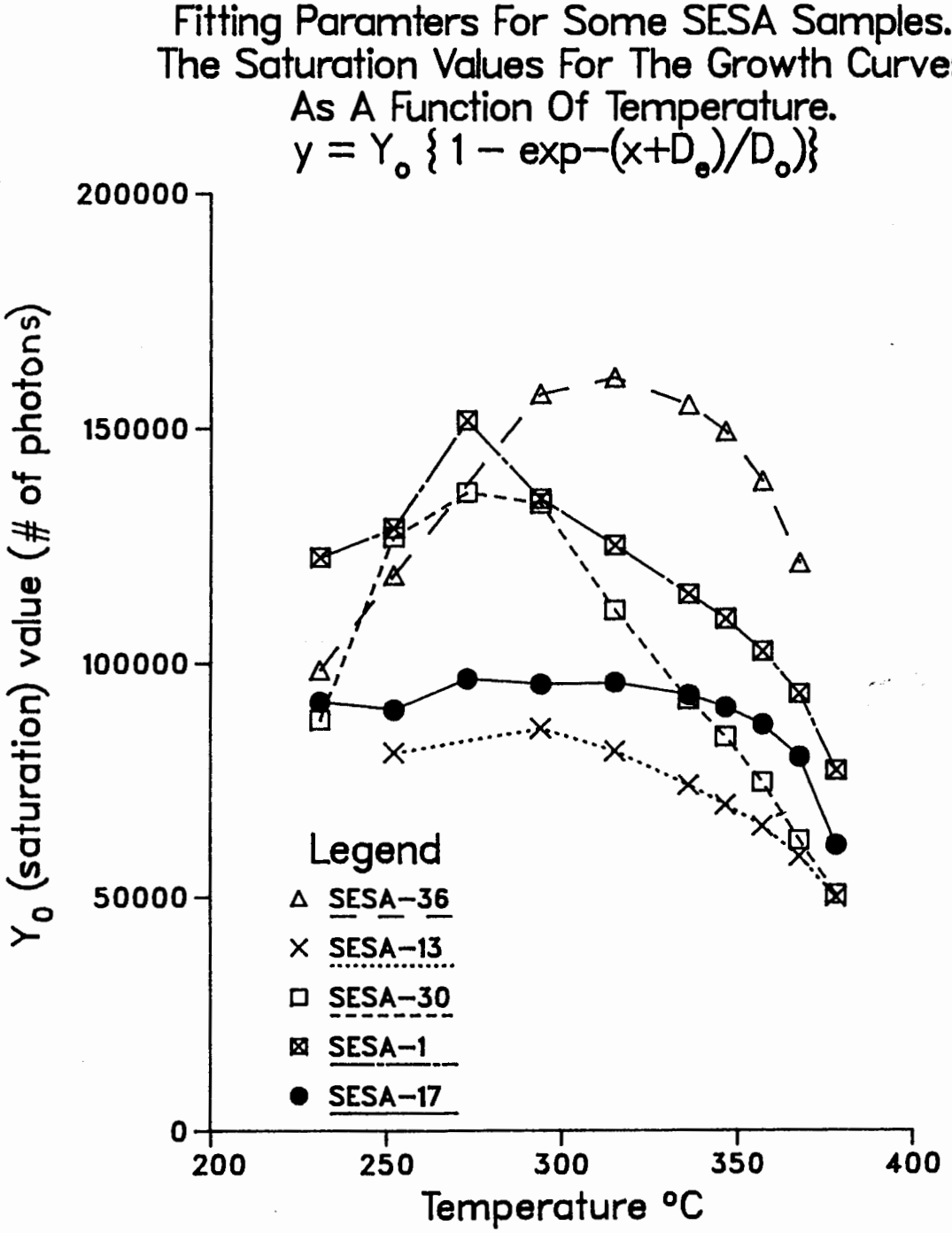

Figure 4.7a

The computer program outlined in Appendix B was used to fit exponential curves to the Natural+Dose growth curves. This is a plot of the Y_o (saturation) values. There are some similarities at higher temperatures, but the curves do not appear to saturate at the same values. The samples were from a sediment sequence so it was expected that the fitting parameters would be similar.

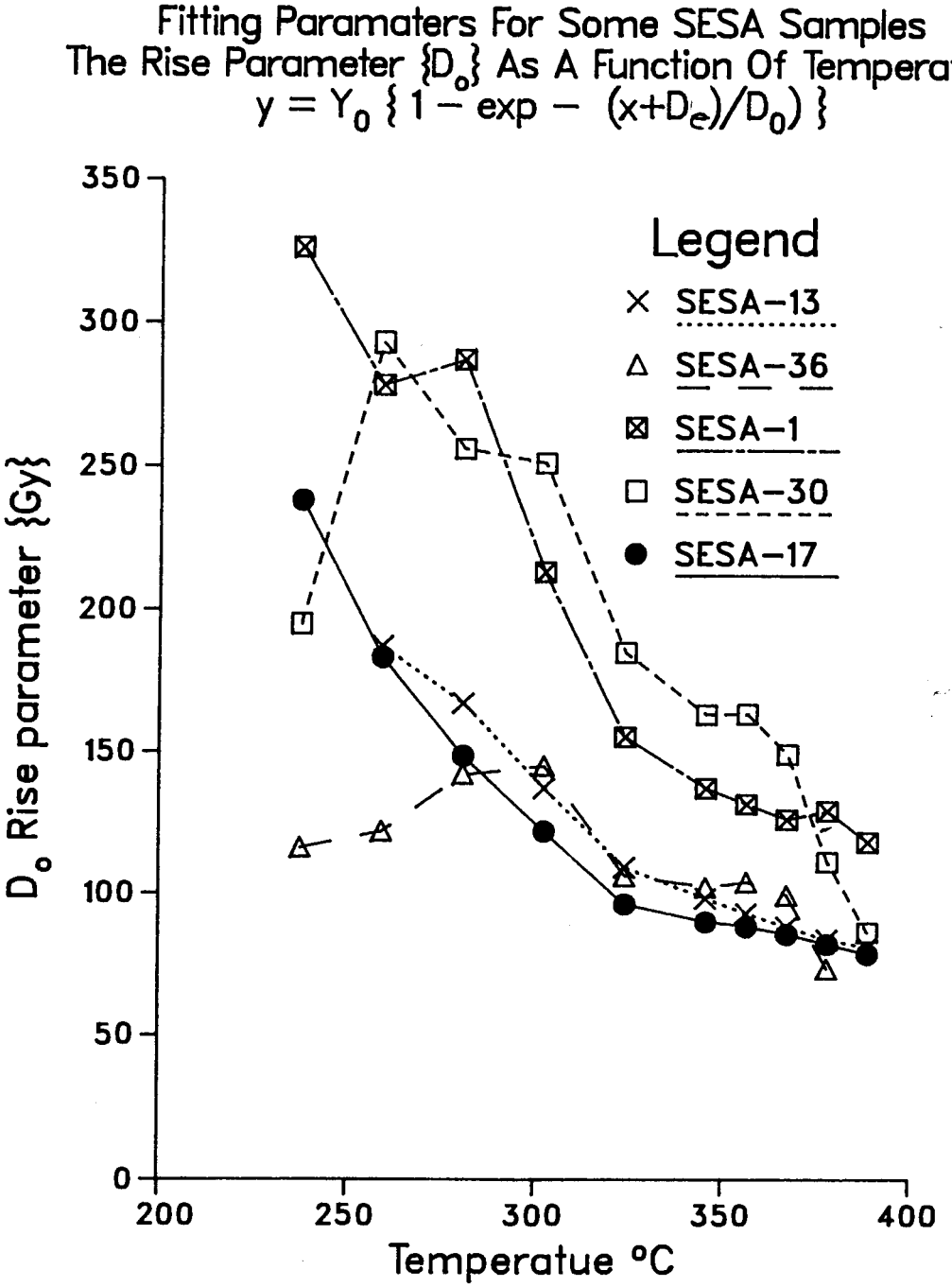

Figure 4.7b

Same as in Figure 4.7a, but in this case D_o, the rise parameter is plotted as a function of temperature. The values become similar at higher temperatures.

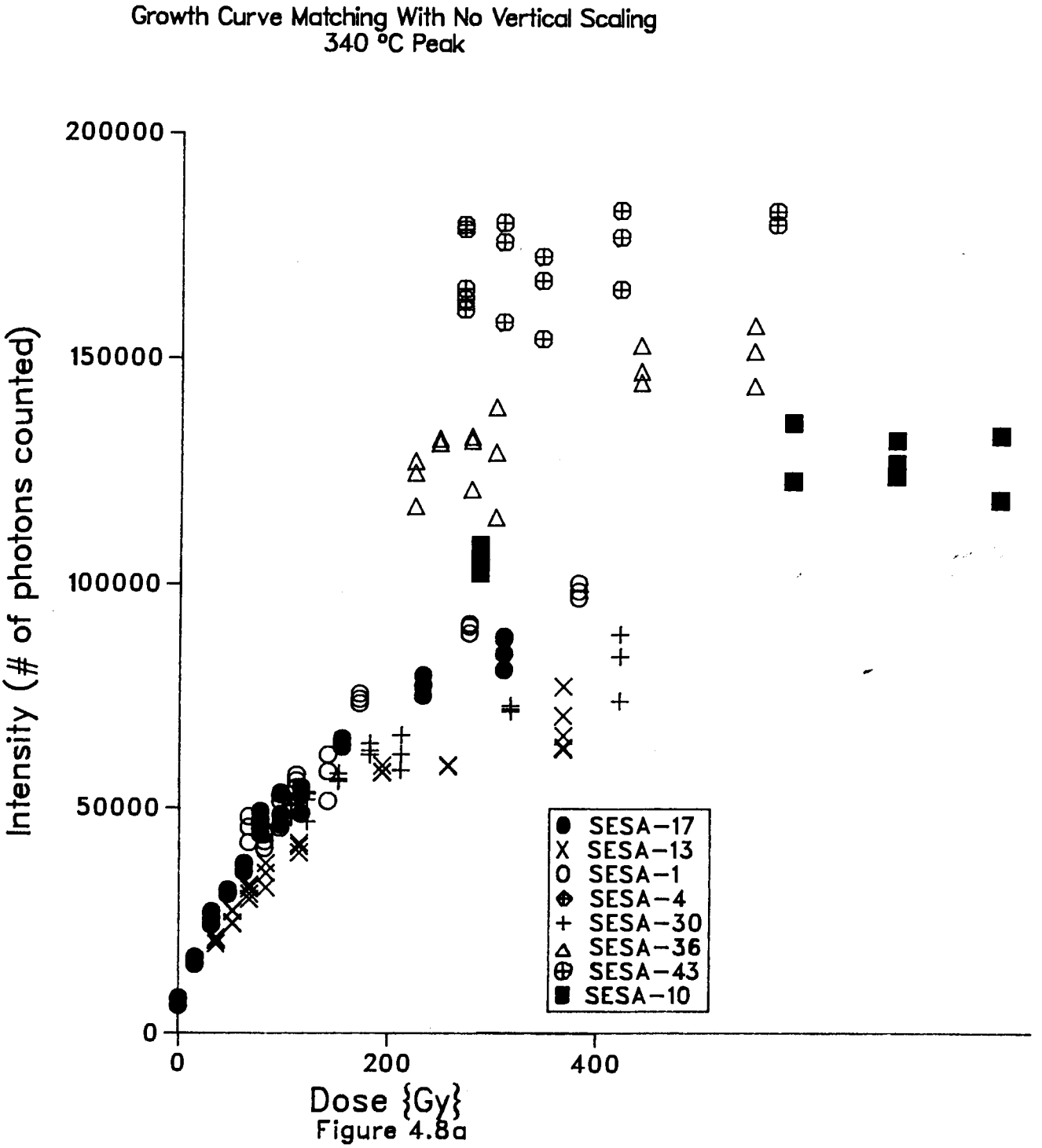

Figure 4.8a

Data from various SESA samples, the natural+dose growth curves.No vertical scaling, but the horizontal shift was chosen so as to give the expected Deq. This was calculated by multiplying the known age {Table 3.1} by the dose-rate {Table 5.6}.

This method worked best with SESA-13 and SESA-1. With SESA-13, the growth curves overlapped very well, resulting in an D_{eq} of 25 ± 5 Gy. The growth curve from SESA-1 overlapped the modern growth curve well, giving an D_{eq} of 90 ± 10 Gy. Unfortunately, these D_{eq} were to give age estimates which were lower than expected. (This will be discussed further in Chapter 6.)

4.2.3.2 Scaled Data

The poor overlaps shown in Figure 4.8a indicate that scaling factors were needed if this technique was to be generally applicable. It was felt that the use of a vertical scaling factor could be justified on the grounds of possible differences in the response of the samples to natural vs. laboratory radiations, or differences in the TL sensitivity between samples. Such effects could have been the cause of the large variations between the growth curves.

The arbitrary scaling was done so as to give the "best fit". Two growth curves were studied at a time: the modern (SESA-17) and a curve from an older sample. As described previously, the horizontal shift was chosen to give the correct D_{eq} calculated from the known age and dose-rate data. The two curves were plotted with this known x-axis shift. Then the y-axis data (TL intensity) from the older curve was multiplied by an arbitrary number until it overlapped the data from the modern curve. The "quality" of the overlap was judged by eye.

After the data was scaled, the procedure outlined in Section 4.2.3.1 (Unscaled Data) was followed. The GCM method was applied to growth curves from four different temperatures: 300°C, 340°C, 360°C and 370°C. For the same sample, the scaling factors for these four temperatures varied by as much as ±15%.

The error in the D_{eq} was found in the same manner as for the unscaled data.

Figure 4.8b shows the results of scaling, and the D_{eq} calculated from this figure are listed in Table 4.2. Scatter in the data points and the similarity of the curves at large doses (near saturation) combined to produce a large error for the old samples.

4.2.3.3 General Discussion of the GCM

The GCM technique does not require the use of bleaching to obtain a D_{eq}. For samples with similar sensitivities, it furnishes another check on the D_{eq} obtained from other methods. Samples which are near saturation (with flat growth curves) are as difficult to deal with in this method as in the partial-bleach method; the same type of error is involved.

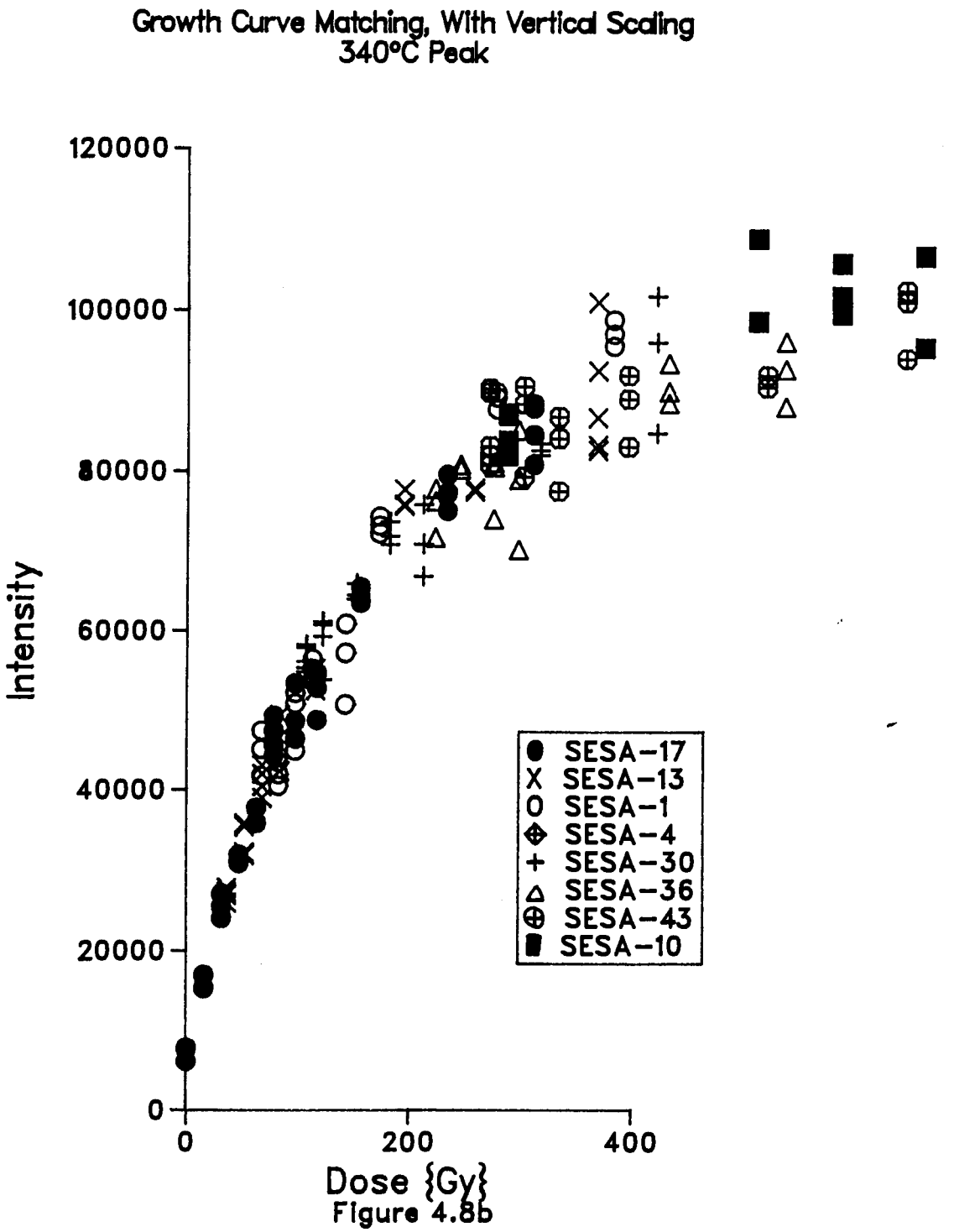

Figure 4.8b

Same data as in Figure 4.8a, but with vertical scaling. The scaling factors were chosen to give the 'best fit'. The horizontal shift was calculated from the expected Deq – the known age was multiplied by the dose-rate.

Table 4.2

D_{eq} Growth Curve Matching (GCM) Method

SESA	D_{eq} (Gy) Unscaled	D_{eq} (Gy) Scaled
17	By def'n=0	By def'n=0
13*	25 ± 5	not scaled
1	90 ± 10	not scaled
30	poor fit	85 ± 25
4	poor fit	85 ± 15
36	poor fit	220 ± 30
43	poor fit	270 ± 50
10	poor fit	160 ± 40

*The growth curves from SESA-17 and -13 overlapped very well, without the need for scaling. SESA-13 gave the "best fit" of all the samples. Unfortunately, as will be discussed later in Chapter 6, the age determined from this result was too low.
The grain sizes used in these experiments were the same as shown in Table 4.1.

It is difficult to decide how to fit/overlap a saturating exponential with a gently curved, almost horizontal line. This means that the upper age limits on the two methods are about the same.

The GCM technique has several added difficulties. The need for arbitrary scaling factors is the most serious objection. In the case of some of the SESA sands, if the "right answer" had not been known beforehand, it would have been difficult to obtain the "proper" scaling factors.

In the case of the SESA samples, this technique does not appear to offer any great advantages over the partial-bleach method.

For this technique to work well, one should really have a modern and old sample of the same type. Young samples in the same sequence are not always obtainable. The difficulties experienced with the SESA samples make it highly unlikely that the GCM method can be used for samples with different depositional histories, different source material, different origins. The technique is obviously of limited use.

4.3 Pre-dose Dating

As mentioned in the introduction, three separate techniques were used in an attempt to determine the D_{eq}. Using the two techniques outlined above, reliable D_{eq} could not be obtained

for samples more than about 200,000 years old. The pre-dose effect is the name given to the change in sensitivity samples often undergo after receiving a large radiation dose and heating. It was hoped that this effect could be used to measure the dose received by by the older samples, but the attempt was unsuccessful. The results were erratic. An effective method for determining the dose was not developed, and there was no obvious reason why the method did not work.

As no meaningful dates were obtained, the work done for this part of the investigation is presented in greater detail in Appendix B.

CHAPTER V

DOSE-RATES

5.1 Introduction

TL can be used to find the radiation dose to which a sample has been exposed. To determine the age, the dose-rate must be evaluated. This often proves to be as subtle, difficult and fraught with errors as the dose determination.

In TL dating, one is primarily concerned with radioactive isotopes with half lives that are long compared to the sample age (Appendix A). These provide an almost constant dose-rate. In most samples, the doses from the naturally-occurring radioactive isotopes of potassium, thorium and uranium are approximately equal, with a small additional cosmic-ray contribution (Aitken, 1985). In the case of the SESA dunes, with their low concentrations of U, Th ($\simeq$1 ppm) and K ($\simeq$.1% by weight), cosmic rays contribute $\simeq$30% of the total dose-rate.

The concentrations of the various radionuclides were determined by alpha counting, and in a few cases, neutron activation analysis, γ- and α-spectrometry, and XRF. Atomic absorption was used to determine the potassium content, though γ-spectrometry and XRF analysis were done on a few of the samples.

The following sections will review some of the concepts used to calculate the dose-rate.

Infinite Matrix Assumption

The "infinite matrix assumption" is a consequence of the law of conservation of energy. Within a volume having dimensions greater than the range of the radiation, the rate of energy absorption = rate of energy emission. If the matrix is uniform, then the absorption of energy per unit mass = emission of energy per unit mass. It is then easy to evaluate the dose-rate. In this case the specific activity, the number of disintegrations per second in 1 kg of sample, is the same for all the members of the decay chain. The rate of energy emission is the energy per disintegration times the activity. The dose-rates for each of the main emitters is given in Table 5.1.

5.2 Alpha

5.2.1 Attenuation

Even the most energetic alpha emission (^{212}Po in the thorium series, Energy = 8.75 MeV) has a path of only ≃45 μm in quartz (Fleming, 1979). Large grains, such as those studied in this thesis, have an inner core that experiences no radiation at all. Only a fraction of the α-radiation available from the Th and U decay chains is absorbed by a grain. For a 100 μm grain, the attenuation factor is .21 (Fleming, 1979).

Table 5.1

Dose-rate Determination Factors

Dose-rate (Gy/ka) for 1 ppm by Weight of Parent and by Percentage Weight for Potassium Oxide

	Alpha	Beta	Gamma
Thorium Series			
No radon loss	.738	.0286	.0514
100% radon loss*	.309	.0103	.0208
Uranium Series			
No radon loss	2.783	.1462	.1148
100% radon loss*	1.262	.0609	.0056
Rubidium	-	.000464	-
Potassium			
1% K_2O	-	.6893	.2069

Dose-rate (Gy/ka) per Counted Alpha Particle per ($cm^2 \cdot ks^{-1}$)

	Alpha	Beta	Gamma
Thorium Series	20.55	.797	1.432
Uranium Series	22.74	1.194	.938

(Bell, 1977,1979)

*Radon occurs in the decay chains of U and Th (See Appendix A). It is a gas and can diffuse away from the sample. If this occurs, the radiation from the subsequent daughter products is "lost" to the sample, and the dose-rate will decrease.

5.2.2 Ionization Density, Low TL Efficiency

The heavy α particles are not scattered as they pass through the crystal, they travel in straight lines, gradually slowing as their energy decreases. The dose is concentrated in a cylindrical area with a diameter of about .1 μm and a length of 20 μm. There is a very high ionization density within the cylinder, so high that the electron traps are saturated. This means that much of the alpha particle's energy is "wasted". Alpha particles do not produce TL efficiently. The energy from an alpha particle produces from .05 to .5 of the TL an equivalent amount of energy from beta or gamma rays would. As the tracks are so short and narrow, they tend not to overlap at low doses. The TL caused by α particles is directly proportional to the total track length. With γ and β particles, the ionization has a relatively continuous spatial distribution and the TL is in proportion to the general level of ionization.

5.2.3 Etching

As the alpha particles have such a short range, sample preparation techniques which remove the outer edge of a grain also remove part of the sample which has been exposed to alpha radiation. In the case of the SESA sands, the HF treatment (See Chapter 3) etched away the outer layer ($\simeq$ 6 μm) of the quartz grains which were used for the TL measurements. Such etching reduces the alpha-dose by a factor of $\simeq$2 (Fleming, 1979 and Goedicke, 1984). Such treatment does not etch the surface

evenly, it depends on the grain morphology. Even if the etching is not uniform, the alpha-dose is still reduced by a significant factor (Goedicke, 1984). Large etched grains receive less than 1% of the dose received by fine (less then ≃5 μm) grains.

5.2.4 Presence of Heavy Minerals

If the radionuclides are not uniformly distributed, the short range of the alpha particles makes the alpha contribution to the dose-rate decrease even further.

5.2.5 Quartz

Quartz has very low natural concentrations of uranium and thorium (Harmon and Rosholt, 1982) and was expected to have received a negligible self-dose. To test this, quartz grains from SESA-1 which had undergone the sample preparation techniques described in Chapter 3 were alpha-counted. The results were barely discernible above the background count rate.

Because of these factors, the alpha-contribution to the dose-rate was ignored.

5.3 Beta - Including Corrections due to the Presence of Heavy Minerals

Unlike γ and α radiation which are emitted from the nucleus with discrete energies, β particles emerge with a spectrum of energies. As the β particles pass through matter, they are scattered and lose energy as they produce secondary electrons

and X-rays via Bremsstrahlung radiation.

β particles have ranges on the order of mm. If the radionuclides are concentrated in a small fraction of the total sample, which can occur if there are heavy minerals present, the distribution of the beta dose can be effected. The usual techniques used to determine the U, Th and K in a sample measure the total amounts of the elements in the sample, not their distribution. The inhomogeneity of the beta dose was a concern as the SESA dune sands have very low concentrations of U and Th, with strong evidence that at least some of the heavy minerals carry most of the U and Th (Hutton, personal communication, 1985, Colwell 1979).

5.3.1 Corrections due to the presence of heavy minerals

It was felt that some sort of correction would have to be made to the β-dose rate, but the number of variables (size of the heavy minerals, percentage of U and Th in them, etc.) and the lack of quantitative data about them made a detailed analysis a daunting prospect.

A model which would give some idea of the effect for a range of reasonable values was developed to find the ratio of bright (TL saturated) to dim (unsaturated) quartz grains in the SESA samples. If this ratio was large (>5%) then a more thorough calculation would have to be done.

The dose (radiation energy in Joules per kg) around a zircon grain was calculated as a function of the distance from the grain. This was done by calculating the distance from the centre of the zircon grain (which was assumed to be a point source) where the energy density was X Gy (1 Gy = 1 Joule/kg). The energy densities studied ranged from $5\text{-}10^4$ Gy.

This section will outline the details of this calculation. Various important parameters (number of zircon grains, the amount of uranium per zircon grain, etc.) were estimated by using reasonable values for grain sizes and concentration data. J. Hutton (personal communication, 1985) used XRF to determine the concentration of zirconium in some of the SESA samples. A typical value was 20 ± 5 ppm (See Table 5.3a). The molecular weight of zirconium (Zr) is 91.22, while zircon ($ZrSiO_4$) has a molecular weight of 183.30. The zircon concentration is 183.3/91.22 ≃ 2.01 of the zirconium concentration. This gives a zircon concentration of ≃ 40 ppm.

The mass of a single zircon grain can be calculated if the diameter of the grain is known. A reasonable value for the diameter of a zircon grain is 50 ± 20 μm (J. Hutton, personal communication, 1985). The density of zircon is 4.56 g/cm^3 (CRC Handbook, 57th Edition).

The total number of zircon grains per kg of sample

$$= \frac{\text{Total mass of zircon}}{\text{Mass of 1 zircon grain}}$$

$$= \frac{40 \times 10^{-6} \text{ kg}}{4/3\ \pi\ (25 \times 10^{-6} \text{ m})^3\ 4560 \text{ kg/m}^3}$$

$$\simeq 1.34 \times 10^5 \text{ grains / kg of SESA sample}$$

To calculate the distance between the zircon grains, the density of the sample must be known.

Composition of SESA = 75% Calcium Carbonate ($CaCO_3$)
Density = 2.710 g/cm^3
25% Quartz (SiO_2)
Density = 2.65 g/cm^3

Density of SESA = .75 * 2.710 + .25 * 2.65 g/cm^3
= 2.70 g/cm^3

In 1 m^3 of SESA, which has a mass of 2700 kg, there will be 3.6×10^8 zircon grains. Assuming the zircon grains are point sources, and are arranged in a cubic lattice, there would be $\simeq$ 1.4 mm between them. The ratio of the diameter of the zircon grain to the spacing is 50×10^{-6}:1.4×10^{-3}, so the point source assumption is reasonable.

To calculate the mass of uranium per zircon grain, the concentration of uranium in the overall sample must be known. With a concentration of $\simeq$ 1 ppm, the mass of uranium per cubic meter of SESA is 2.7×10^{-3} kg, which with 3.6×10^8 zircon grains per m^3 of sample, gives a mass of 7.5×10^{-12} kg of uranium per zircon grain.

Natural uranium has an activity of 13 Bq/mg (Aitken, 1985), which gives an activity per zircon grain of 9.75×10^{-5} Bq. The

energy per disintegration ranges from 0-≃2 MeV. Assuming an energy release of 1 MeV, the energy release per zircon grain is:

$$9.75 \times 10^{-5} * 1 \times 10^{6} \text{ eV} * 1.6 \times 10^{-19} \text{ J/eV} = 1.56 \times 10^{-17} \text{ J/sec.}$$

$$100 \text{ ka} = 3.16 \times 10^{12} \text{ seconds}$$

The total energy release per zircon grain in 100 ka = 4.93×10^{-5} J.

This is the total energy release from the zircon grain point source; E(r=0) or just E(0). Once the total energy release is known, it is necessary to calculate the energy distribution throughout the sample. To calculate the energy deposited in a given volume of sample, one needs to know the rate of change of the energy flux.

$E(x)$ = Radiation energy flux

$$E(x) = E(0)\, e^{-\mu x}$$

$$\frac{dE}{dx} = E(0) \{ -\mu\, e^{-\mu x} \}$$

$|dE|$ = energy deposited in a slab of thickness dx

$$E_{Density} = \frac{d|E|}{d(Mass)} = \text{Dose}$$

$$= \frac{\mu\, E(0)\, e^{-\mu r}\, dr}{4\pi\, r^2\, dr * (\text{Sample Density})}$$

where r is the distance from the centre of a zircon grain.

Rearranging,

$$r^2 e^{\mu r} = \frac{\mu\, E(0)}{4\pi * (\text{Sample Density}) * \text{Dose}}$$

From Aitken (1985) $\mu \simeq 1.73$ per mm. This is the μ value for aluminum oxide. For comparison, the μ values for pottery were experimentally determined (Aitken, 1985) to be 1.32 per mm (thorium series) and 1.14 per mm (uranium series). The value of 1.73 was chosen as aluminum oxide has a beta attenuation similar to that of quartz.

$$= \frac{1.73\ \text{mm}^{-1} * 4.94\text{x}10^{-5}\ \text{J}}{4\pi * 2.7\text{x}10^{-6}\ \text{kg/mm}^3 * \text{Dose}}$$

$$= \frac{2.51\ \text{mm}^2}{\text{Dose (J/kg)}}$$

The E_{Density} is the energy deposited per unit mass, the dose (1 Gy=1 J/kg). The above equation can be rearranged to give the beta dose as a function of the distance from the centre of a zircon grain in mm.

$$\text{Dose (Gy)} = \frac{2.51\ \text{mm}^2}{r^2 e^{1.73*r}}$$

The radii corresponding to doses from $5\text{-}10^4$ Gy were calculated in steps of 5 Gy. Figure 5.1 illustrates the dose dependence as a function of the distance from a centre of a zircon grain for doses from 0-600 Gy.

Beta Dose Dependence As a Function Of The Distance From A Single Zircon Grain

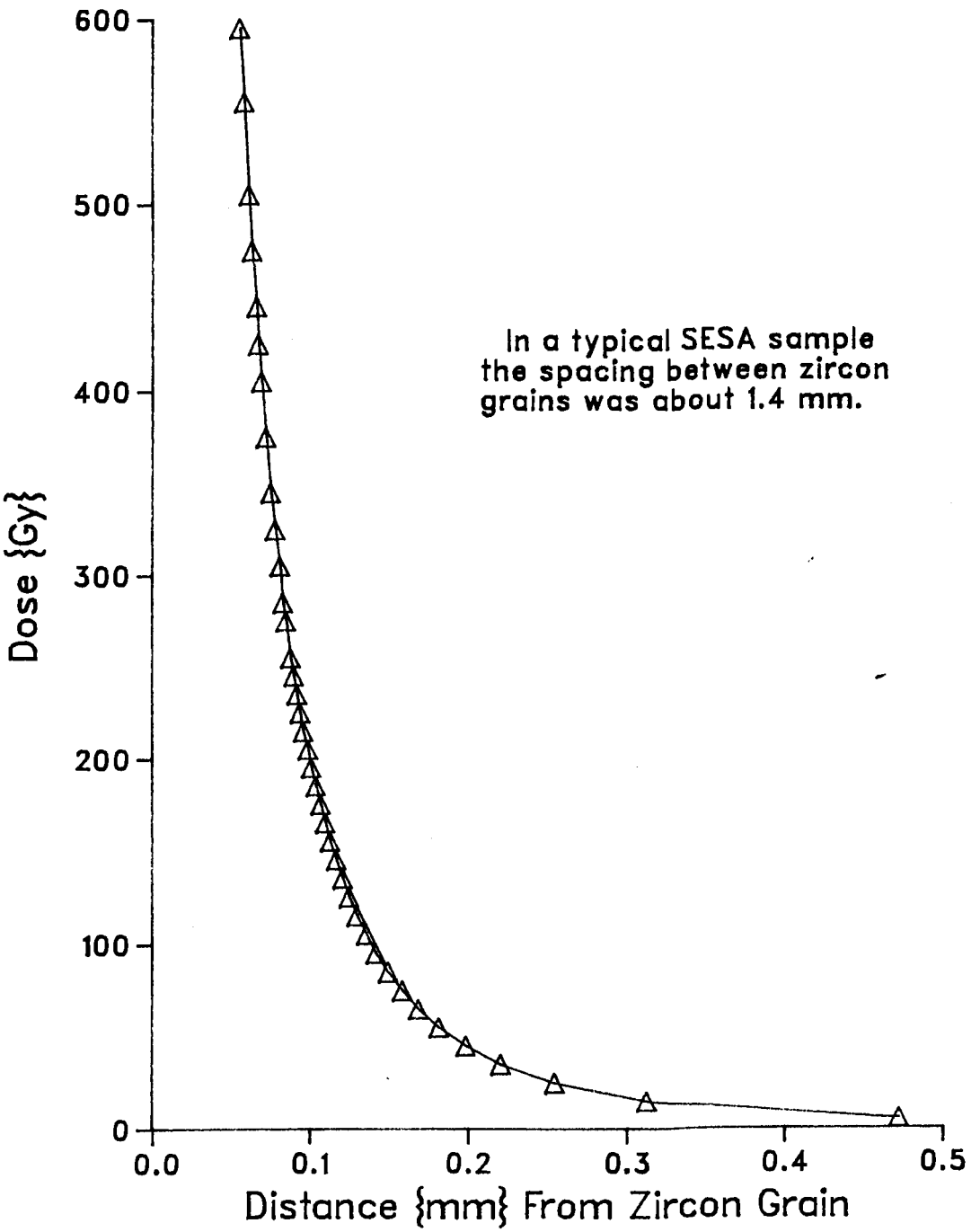

Figure 5.1

In order to determine the fraction of quartz grains in the total sample which had received certain doses, the radii corresponding to doses from 0-10^4 Gy were calculated in steps of 5 Gy (as described above). From this data, the volume of a "shell" within which the dose was X to X + 5 Gy could be calculated. A list of volumes (V_1 = Volume which has experienced a dose of 5-10 Gy, V_2 = Volume which has experienced a dose of 10-15 Gy, ...) was made. Assuming the zircon grains were arranged in a cubic lattice, the spacing between the grains was 1.4 mm. Each zircon grain had a volume $V_z=(1.4)^3$ = 2.74 x 10^{-9} m^3 around it. The ratio of the V_i to V_z was an indication of the fraction of quartz grains in the total sample which had received a certain dose. These values are displayed as a histogram in Figure 5.2, and tabulated in Table 5.2. The 0-5 Gy value was calculated from the volume remaining after the sum of the volumes corresponding to doses from 5-10^4 Gy had been subtracted from V_z.

A dose of 5 Gy occurs at .47 mm from the centre of a zircon grain. As the zircon spacing is about 1.4 mm, there is not a significant amount of overlap between the beta rays from different zircon grains. The results presented in Figure 5.2 assumed no overlap. If some overlap occurred, the relative heights of the low dose (<50 Gy) values would change, but unless most of the zircon grains were very close together (about .2 mm) the high dose values would not change significantly.

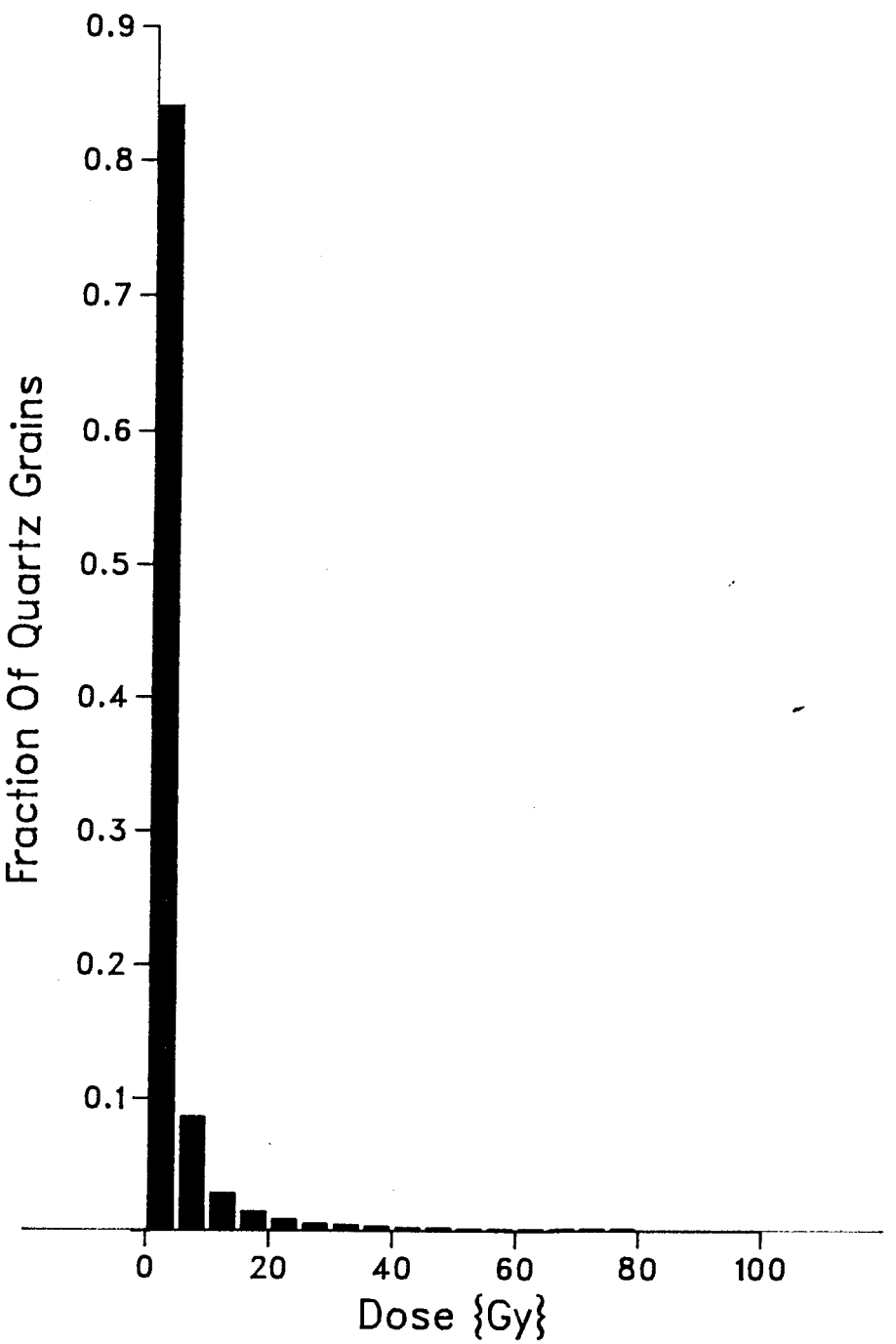
Fraction Of Quartz Grains
Receiving Different Beta Doses
Fraction Of Quartz Grains
0.9
0.8
0.7
0.6
0.5
0.4
0.3
0.2
0.1
0
20
40
60
80
100
Dose {Gy}

Figure 5.2

Table 5.2

Fraction of Quartz Grains Receiving Different Beta Dose Values

Dose (Gy)	Fraction	Cumulative Total
0-5	.83985	.83985
5-10	.08575	.92560
10-15	.02804	.95363
15-20	.01357	.96721
20-25	.00787	.97508
25-30	.00508	.98017
30-35	.00352	.98370
35-40	.00257	.98626
40-45	.00195	.98821
45-50	.00152	.98973
50-55	.00122	.99095
55-60	.00099	.99195
60-65	.00082	.99275
65-70	.00069	.99344
70-75	.00059	.99403
75-80	.00050	.99453
80-85	.00044	.99497
85-90	.00038	.99535
90-95	.00033	.99569
95-100	.00030	.99598
100-105	.00027	.99625
105-110	.00023	.99650
110-115	.00021	.99670
115-120	.00019	.99689
120-125	.00017	.99707
125-130	.00016	.99723
130-135	.00015	.99737
135-140	.00013	.99750
140-145	.00012	.99763
145-150	.00011	.99774
150-155	.00011	.99785
155-160	.00010	.99794
160-165	.00009	.99804
165-170	.00008	.99812
170-175	.00008	.99820
175-180	.00007	.99827
180-185	.00007	.99834
185-190	.00006	.99839
190-195	.00006	.99844
195-200	.00006	.99850

This is a table of the values plotted in Figure 5.2. Please refer to the two previous figures for an explanation of this data.

This is a simple model, but it does show that less than .2% of the grains will have received a dose >200 Gy, and will be saturated (bright). A more thorough analysis would be useful, but this rather naive one is adequate. The most important parameter in this model is the zircon size.

All the dose-rate equations give the beta dose assuming a uniform distribution of the radionuclides. A quantitative expression is needed for the fraction of the beta dose to which most of the grains in the the SESA samples have been exposed.

$$\text{overall average dose} = \int_0^{\infty} (\text{fraction})\,(\text{dose})$$

= same dose the grains would have received if the uranium had been evenly distributed

$$= .401 \qquad \{1\}$$

$$\text{average dose of unsaturated grains} = \int_0^{50\ \text{Gy}} (\text{fraction})\,(\text{dose})$$

$$= .332 \qquad \{2\}$$

$$\frac{\{2\}}{\{1\}} = \text{factor to multiply the "uniform" dose rate by}$$

$$= .83$$

This dose-rate factor is applied only to the beta dose from the uranium and thorium which is tied up in the heavy minerals. The rest of the radionuclides were assumed to be uniformly distributed. Approximately 80% of the "uniform" beta dose is available to the quartz grains. But only about 75% of the uranium and thorium is tied up in the heavy minerals (J. Hutton,

personal communication, 1985) which gives a factor of .25 + .83*.75 = .87. The estimates used in these calculations have an associated error of at least ± 10%, so .85 ± .10 was the factor by which the beta dose from the uranium and thorium was multiplied to get the total dose-rate values listed in Table 5.8.

5.3.2 Effect of TL Saturated Grains on the Calculated D_{eq}

When glowed, there is mixture of bright and dim grains in the samples (See Appendix C and D). If some of the grains have become TL saturated (perhaps due to a non-uniform dose distribution) then the calculated D_{eq} may be different than that from a sample where all the grains are of the same brightness and have identical dose histories.

$$I_{total} = \Sigma\, I_{individual\ grains}$$

$$I_{indiv} = I_{saturated} \{ 1 - e^{-(D_{nat} + D_{lab}\} / D_o} \}$$

D_{nat} = Dose received before the sample was collected, the natural dose

If some of the grains are saturated, then exposure to the lab dose will not increase their TL intensity.

$$I = I_{saturated\ grains} + I_{unsaturated\ grains}$$

$$I = I_{sat} N_{sat} + I_{sat} \{ 1 - e^{-(D_{nat}^{*} + D_{lab})/D_o} \} N_{unsat}$$

Here, D_{nat}* is the natural dose received by the unsaturated grains in the environment. It equals the dose-rate the grains have been exposed to times the age of the overall sample.

The two types of grains (saturated and unsaturated) have been exposed to different doses in the past. The TL from the saturated grains is constant. The growth curve (the change of intensity with dose) is a function of the unsaturated grains only. The growth curve will be a combination of a saturating exponential (from the unsaturated grains) plus a constant contribution (from the saturated grains).

A computer simulation was done to quantify this effect. A series of growth curves was constructed assuming different mixtures of grains. As the fraction of saturated grains increased, so did the calculated D_{eq}. From the simulation, it was found that if 1% of the grains were saturated, the calculated D_{eq} would increase by about 1 Gy. The best "guesstimate" for the percentage of saturated grains in the SESA sands is .5% (from J.T. Hutton). The scatter in the experimental data is on the order of ±5%, and the errors in the calculated D_{eq} of the older samples are greater than ± 5 Gy. An increase of 1 Gy is not significant and would not be noticed in the extrapolations used to determine the D_{eq}.

5.4 Gamma

Gamma rays have penetration depths on the order of 10 cm. Samples should be collected a reasonable distance (≃30 cm) away from a surface or inhomogeneous section of the site to ensure that gamma rays from different layers with different radioactive contents do not affect the dose rate. Rocks and pebbles can cause local areas of high radioactivity and it is difficult to quantify the effect on the dose-rate.

Gamma rays do not directly induce TL. As they pass through matter, they produce electrons via photoelectric, Compton and pair production processes. These electrons collide with atoms, slowing down and releasing more electrons.

5.5 Radon

Radon is formed when $^{226}Ra \Rightarrow {}^{222}Rn + \alpha$ (in the U-238 decay chain). As the alpha particle is emitted, the nucleus recoils with an energy of .1 MeV. The range of the recoil is ≃ .02 μm. This is long enough that there is a non-negligible probability of the atom ending up in the pore between the solid particles. As radon is a gas, it can diffuse away. If all the Rn escapes, the annual dose due to the U chain decreases.

If the sample is wet, the radon loss is greater than in a totally dry sample. Radon has a shorter recoil path in water than in air, and this increases the probability of the radon

ending up in between the grains.

As radon loss can affect the dose rate, information about the amount of radon being lost is quite important.

During the alpha-counting, described below, a simple test for radon loss is done. First, the sample is counted without being sealed, then the container is tightly sealed to prevent gases from escaping. If the sealed rate shows a significant increase over over the unsealed rate, then this is an indication that radon loss is occurring (Table 5.4d). Few of the samples showed a significant increase (>5%) upon sealing. The counting time was a minimum of one week.

5.6 Methods for Determining the Concentrations of the Radioactive Elements and the Results

5.6.1 Concentration Data

The techniques used to determine the concentrations of the various radiogenic elements were atomic absorption, α-counting, γ-ray spectroscopy, and neutron activation analysis. To determine the weight percentage of K_2O, the most common technique used was atomic absorption; the data was obtained from various commercial laboratories.

The α-counting procedure which was done in the course of this thesis is detailed below.

5.6.2 Alpha counting

Following the method developed by Cherry (1963) and refined by D. Huntley and A. Wintle (1981), a layer of sample was spread on an α-scintillator. The thickness of the sample is such that it is greater than the largest range of the α-particles - on the order of mm. One quarter of the α - particles which are emitted within a layer of thickness equal to the range of of the particle will make it to the scintillator screen, produce a light flash and be counted. The total count and pair count rates can be used to calculate the concentrations of U and Th in the sample (Huntley and Wintle, 1981).

The sample holder used for α-counting was a clear plastic "bowl" which could be sealed air-tight. The sample was spread on a plastic screen which had ZnS[1] applied to it. The scintillations were counted with an EMI 6097 photomultiplier tube. The pulses were fed through a discriminator to eliminate any pulses due to β, γ and noise.

5.6.2.1 Pairs technique to determine Thorium Concentrations

Typical α count rates are $\simeq$ 1 per 100 sec. In the Thorium chain, $\simeq$ 3% of these occur as pairs, with an average separation of $\simeq$ .2 sec. This is due to the decay of ^{216}Po which has a half life of .145 seconds.

$$^{220}\mathrm{Rn} \xrightarrow{\alpha} {}^{216}\mathrm{Po} \xrightarrow{\alpha} {}^{212}\mathrm{Bi}$$

---

[1]Wm. B. Johnson & Associates, Montville, New Jersey, U.S.A.

If the α-counting is done with a time discriminator, the number of pairs occurring within .4 seconds of each other gives an indication of the Th content of the sample.

The number of coincidence pairs can be a significant fraction of the total pair counts. This must be calculated and allowed for when the Th content is determined.

5.6.3 Results

Table 5.4 lists the values obtained for the K_2O, uranium and thorium concentrations by the various methods described above.

The results from alpha-counting, which are expressed as the number of counts per unit time and area can be used to directly calculate the dose-rate, with the factors listed in Table 5.1, or they can be used to calculate the concentrations of U and Th which are present in the sample. For ease of comparison with the other concentration data, the latter was done and the results shown in Table 5.4b and c. For the actual dose-rate calculations, the former method was used.

The next section will describe how this data was used to calculate the dose-rate which the quartz grains have received.

5.7 Correction Factors to the Dose-rate Calculations

This section will discuss the correction factors used in the calculations which will be described in the next section.

5.7.1 Alpha

As mentioned earlier in this chapter, the alpha-contribution is negligible for etched 100μm quartz grains, and was not taken into account in the dose-rate calculations.

5.7.2 Effect of Water

On a weight to weight basis water absorbs more radiation energy than rock, so water decreases the radioactivity per unit mass when compared to the dry situation. Nuclear tables must be used to determine the quantitative affect on the various types of radiation, which yield the set of correction factors listed in Table 5.5.

The sands were quite dry when they were collected, containing less than 10% water (Table 5.4).

5.7.3 Beta attenuation

Beta particles have ranges on the order of mm, and the quartz grains have diameters of about 100μm. They absorb a certain fraction of the beta rays. As the concentration of radionuclides inside the quartz is much less than that in the rest of the sample, the self-dose percentage is quite low.

Table 5.3a

Concentrations of Potassium Oxide, Rubidium, Zirconium and Water

(Ages from Schwebel, 1978)

SESA #	Ages (ka)	Sampling Depth (m)[1]	Potassium Oxide (Percentage by Weight) Atomic[2] Absorption ±5%	Gamma-[3] Spec. ±10%	XRF[4] ±5%	Rb[4] (ppm)	Zr[4] (ppm)	Water[5] Conc.
17	0	0			.17	7	24	.07
20	4	1	.15		.16	4	21	.025
13	83	1	.17,.18		.10	5	21	.052
1	120	1.5	.15	.16	.10	4	15	.041
30	200	1	.07		.06	3	14	.01
4	248	2	.25	1.03	.27	10	25	.018
33	309	4	.84		.14	7	22	.04
36	380	3	.22		.2	11	29	.004
6	500	1			.12	7	58	.060
43	510	3	.14		.20	8	32	.04
10	<700	3	.14	.16	.09	4	29	.03

[1] From D.J. Huntley, J.T. Hutton, and J. Prescott; field notes and personal communication.

[2] Atomic absorption was done commercially by Chemex, 212 Brooksbank Avenue, North Vancouver, Canada, V7J 2C1.

[3] From T.J. Lewis of the Pacific Geoscience Centre, Department of Energy, Mines and Resources.

[4] From J.T. Hutton, Dept. of Physics, University of Adelaide, Australia. The measurements were done on similar samples.

[5] The weight of the water in the sample divided by the dry weight of the sample. Some of the values were measured by C. Hearty and D.J. Huntley, SFU.

Table 5.3b

Concentration of ^{232}Th (ppm) from Various Methods

SESA #	Atomic[1] Absor. ±.2	Gamma[2] Spec. ±10%	Alpha[3] Spec.	XRF[4] ±.2	Alpha[5] Counting
17	.9			1.8	.87±.12; 2.2*
20	1.5		.98±.05	1.1	1.3*;1.16±.21**
13	.8			1.1	.97±.15; 1.20±.42**
1	.8	.92	.64±.04	.9	1.0*; .7±.2**†
30				1.0	.99±.27; .5*
33				1.2	1.5*
4	1.1	2.47	.78±.02	1.7	1.3*; 1.28±.21**
42W				1.0	1.3*
36				.4	1.79±.18; 1.4*
6	1.8			2.0	1.8*;1.89±.43**
43				2.6	2.93±;25†, 2.0*
8					3.52±.34
10	1.2	1.21	1.24±.07	1.3	1.2*; 1.17±.18**

† significant increase on sealing
* alpha counted by J.T. Hutton, Univ. of Adelaide
** alpha counted by C. Hearty and D.J. Huntley, SFU

[1] From the Australian Atomic Energy Commision.

[2] From T.J. Lewis, Pacific Geoscience Centre, Department of Energy, Mines and Resources. Thorium equivalent gamma-spectrometry was used to measure peaks from near the end of the chain.

[3] From A. Latham of the Geology Dept., McMaster University, Canada. These values are not absolute, they are included for comparison only.

[4] From J. Hutton, Department of Physics, University of Adelaide, Australia. The measurements were done on similar samples.

[5] These values are included for comparison only. The dose-rates were calculated from the data listed in Table 5.3d.

Table 5.3c

Concentrations of ^{238}Uranium (ppm) from Various Methods

SESA #	D.N.A.A.[1] ±.2	Gamma[2] Spec. ±10%	Alpha[3] Spec	XRF[4] ±.2	Alpha[5] Counting
17	.8;1			.8	.98±.04;.6*
20	.96		.90±.02	1.5	1.3*; 1.17±.07**
13	.9			1.0	1.27±.05; 1.39±.14**
1	.87	.97	1.07±.06	.8	.9*,1.10±.06**†
30				.8	1.21±.09;.7*
33				.2	.6*
4	.51	.90	.61±.02	.5	.8*; .80±.07**
42W	1.4			.6	1.3*
36				.4	.79±.06;.7*
6	.5			.6	.4*;.56±.13**
43				.4	1.06±.08†
8					1.31±.12†
10	.45	.55	.46±.02	.8	.9*; .64±.06**

† significant increase on sealing
* alpha counted by J. Hutton, Univ. of Adelaide
** alpha counted by C. Hearty, D.J. Huntley, SFU

[1] Delayed Neutron Activation Analysis, from the Australian Atomic Energy Commision.

[2] From T.J. Lewis of the Pacific Geoscience Centre. This is the uranium equivalent from the 5 peaks of ^{214}Bi and ^{214}Pb.

[3] From A. Latham of the Geology Dept., McMaster University, Canada. The values listed are not absolute, they were included for comparison only.

[4] From J.T. Hutton, Physics Dept., University of Adelaide, Australia. The measurements were done on similar samples.

[5] Included for comparison only. The dose-rates were calculated directly from the data listed in Table 5.3d.

Table 5.3d

Alpha-counting Data

Counts per ($cm^2 \cdot ks^{-1}$)

SESA #	Total Count Rate	Thorium Count Rate	Uranium Count Rate
17	.155 ± .003	.033 ± .004	.125 ± .005
20	.192 ± .004*	.043 ± .008	.149 ± .009
13	.199 ± .003	.036 ± .006	.163 ± .006
	.222 ± .008*	.044 ± .015	.178 ± .017
1	.166 ± .004†*	.025 ± .007	.141 ± .008
30	.191 ± .005	.037 ± .010	.154 ± .011
4	.150 ± .005*	.048 ± .008	.102 ± .009
36	.167 ± .003	.067 ± .007	.101 ± .007
6	.142 ± .006*	.070 ± .016	.072 ± .017
43	.244 ± .003†	.109 ± .009	.135 ± .010
8	.279 ± .004†	.148 ± .013	.131 ± .014
	.303 ± .005*	.136 ± .014	.167 ± .015
10	.125 ± .003*	.043 ± .007	.082 ± .008

† significant increase on sealing.

* Counted by C. Hearty and D.J. Huntley at SFU.

The beta dose calculated for a small grain must be multiplied by an attenuation factor. The values depend on the grain size, but for a 100 μm quartz grain, the factor for K_2O is .975, for uranium is .9 and for thorium is .85. For 150 μm grains the factors are .95, .875 and .825 respectively and for 200 μm grains the factors are .935, .85 and .795. (Fleming, 1979, Figure 2.7).

5.7.4 Presence of Heavy Minerals

As detailed in Section 5.3.1, the uranium and thorium was not evenly distributed and the beta dose from these radionuclides should be corrected by a factor of .85 ± .10.

5.7.5 Disequilibrium

Due to the nature of the SESA sample - lightly consolidated sands - it was considered highly probable that the uranium series decay chain would be in disequilibrium. The principal disequilibrium occurs between ^{234}U and ^{230}Th and is caused by the solubility of uranium, which leaches relativily easily, and the 75 ka half-life of the insoluble ^{230}Th. Table 5.4c lists the uranium concentrations from a variety of methods for the different samples. The results do vary, but a general trend can be seen. There is little decrease for samples from 0 to 200 ka, but the uranium decreases by a factor of about two over the whole 700 ka age range.

Table 5.4

Correction Factors Due to Water Contents

$$\Delta = \frac{\text{Mass of Water in Sample}}{\text{Mass of Dry Sample}}$$

$$D_{\alpha\ \text{true}} = \frac{D_{\alpha\ \text{Dry}}}{\{1 + H_{\alpha}\Delta\}}$$

$$D_{\beta\ \text{true}} = \frac{D_{\beta\ \text{Dry}}}{\{1 + H_{\beta}\Delta\}}$$

$$D_{\gamma\ \text{true}} = \frac{D_{\gamma\ \text{Dry}}}{\{1 + H_{\gamma}\Delta\}}$$

H_{α} = the ratio of the specific stopping power of water
to the stopping power of the dry sediment for alpha particles.
= 1.50

H_{β} = the ratio of the specific stopping power of water
to the stopping power of the dry sediment for beta particles.
= 1.25

H_{γ} = the ratio of the absorption coefficients of water
to sediment for gamma rays.
= 1.14

(c.f. Huntley and Wintle, 1981)

A. Latham used alpha-spectrometry to determine the $^{230}Th/^{234}U$ ratio for four samples. For the three samples with ages less than $\simeq$ 300 ka, the ratio decreased slightly with age, while the ratio in the fourth sample ($\simeq$ 700 ka) doubled. This indicates that there is probably some disequilibrium occurring over the total age range of the samples (0-700 ka) but that the effect is small for the younger (less than 200 ka) samples.

No corrections were made for disequilbrium effects in the dose-rates listed in Tables 5.7 and 5.8.

5.8 The Dose-rate Calculations

The following is a description of the calculations used to obtain the results listed in Tables 5.7 and 5.8. The concentration and alpha-counting data from Table 5.4 were multiplied by the appropriate factors from Table 5.1, then corrected for factors such as the water, beta attenuation and the presence of heavy minerals. The results are presented in Table 5.7. The alpha-counting and concentration results are listed separately for the purpose of comparison. The final results are presented in Table 5.8. The following sections give examples of these calculations.

5.8.1 K_2O

To determine the dose-rate due to K_2O in the sample, an average of the values listed in Table 5.4a was calculated. For example, SESA-13 (150 μm grains):

Values: .17 ± .0085, .18 ± .009

.10 ± .005 % weight

Weighted average = .130 ± .004 % weight

The data is inconsistent with the quoted uncertainities, so a value of .14 ± .03 was used.

Using the factors from Table 5.1, with a water content of Δ= .052 and the beta attenuation factors for 150 μm grains (Section 5.7.3), the dose rates (Gy/ka) are:

Beta: .086 ± .018 Gy/ka

Gamma: .0273 ± .0058 Gy/ka

5.8.2 Uranium and Thorium

5.8.2.1 Concentration Data

A similar procedure was followed for the uranium and thorium concentration data shown in Tables 5.4b and c. For example, SESA-13:

Thorium .8 ± .2, 1.1 ± .2 ppm

Weighted Average = .95 ± .14 ppm

Uranium .9 ± .2, 1.0 ± .2 ppm

Weighted Average = .95 ± .14 ppm

Rubidium = 5 ± 1 ppm

From Table 5.1, with corrections due to water and beta

attenuation:

Beta: Thorium = .021 ± .003 Gy/ka

Uranium = .114 ± .017 Gy/ka

Rubidium = .002 ± .004

This is included here for completeness and to demonstrate the neglible contribution of Rubidium to the overall dose-rate.

Gamma: Thorium = .046 ± .007 Gy/ka

Uranium = .103 ± .015 Gy/ka

The beta contributions were further corrected by a factor of .85 ± .10 due to the presence of heavy minerals (From Section 5.3.1).

Beta (Corrected) = .12 ± .03

For the results presented in Table 5.7, the beta dose has not been corrected for the presence of heavy minerals. This is done in Table 5.8, where the total dose rates, including beta uncorrected and corrected, are shown.

5.8.2.2 Alpha Counting

The results of the alpha-counting are listed in Table 5.4d. Some of the samples had been counted more than once - at the SFU lab by J. Kirkey as well as C. Hearty and D. Huntley, and at the University of Adelaide by J. Hutton. Where possible, an average of these values was calculated. As outlined in the previous sections, the data was multiplied by various factors to obtain the dose-rate. For example, SESA-13:

Total count rate = .199 ± .003 ks^{-1} cm^2.

Thorium count rate = .036 ± .006 ks^{-1} cm^2.

Uranium count rate = .163 ± .006 ks^{-1} cm^2.

Total count rate = .222 ± .008 ks^{-1} cm^2.

Thorium count rate = .044 ± .015 ks^{-1} cm^2.

Uranium count rate = .178 ± .017 ks^{-1} cm^2.

Weighted averages:

Thorium count rate = .037 ± .006 ks^{-1} cm^2.

Uranium count rate = .165 ± .006 ks^{-1} cm^2.

After corrections for water and beta attenuation, the calculated dose-rates were"

Beta: Thorium = .023 ± .003 Gy/ka

Uranium = .162 ± .006 Gy/ka

Gamma: Thorium = .050 ± .007 Gy/ka

Uranium = .146 ± .005 Gy/ka

The beta-dose correction due to the presence of heavy minerals, gave a beta-dose rate of

Beta (Corrected) = .16 ± .03 Gy/ka.

5.8.3 Cosmic Rays

Cosmic Rays

Cosmic rays originate almost exclusively outside the solar system, and are predominantly protons with an average energy of a few GeV. Rays are influenced by the earth's magnetic field; more cosmic rays reach the top of the atmosphere near the poles, than at the equator.

The cosmic ray flux on the earth's surface is determined not only by the geo-magnetic field, but by the atmosphere, which has a density of ≃1000 g/cm^2. The cosmic ray flux has a "hard" (mostly muons) and a "soft" (mostly electrons) component. About two-thirds of the cosmic ray flux at sea level is from the hard component. At depths below the surface of ≃50 cm, only the hard component remains.

The dose-rate due to the cosmic ray flux at ground level at 40° latitude is about .280 Gy/ka. Below ground level, there is a rapid initial fall off with depth in the first 50 cm as the soft component (the electrons) get absorbed. The hard component (the muons) penetrates much further, and this flux halves at a depth of approximately 5 m (Table 5.6, Prescott and Stephan, 1982).

For example, the annual dose underneath .5 metres of soil is 185 ± 11 μGy/a and under 1 metre is ≃ 150 μGy/a.

The flux is attenuated 8.5% per 100 g/cm^2 of rock and 10% per 100 g/cm^2 of water.

5.8.4 In Situ

For a few of the dunes, in situ measurments were done by J. Prescott and J. Hutton of the University of Adelaide. A TL dosimeter ($CaSO_4$) and a gamma scintillator was used. The calcium sulphate capsules were shielded to prevent alpha and beta rays from reaching the dosimeter. After zeroing, they were buried about half a metre deep for periods of time on the order of one

year. Such capsules measure the gamma and cosmic ray contributions to the overall dose rate, not the beta or alpha.

A gamma scintillator (URTEC model UG-140)[2] was used for fast on-site analysis of the gamma dose rate; cosmic ray contributions were not measured. This portable differential gamma ray spectrometer with an external crystal detector (NaI) was used to simultaneously measure ^{232}Th, ^{214}Bi and ^{40}K. It had a .3 MeV low cutoff and a high cutoff to get rid of cosmic rays. The spectrometer was placed in the sampling hole for a few minutes, and a reading taken. The short sampling times (few minutes) were convenient, but do not give seasonal averages of the gamma dose-rate.

It must be noted that the present day dose-rate was measured, which does not necessarily equal the dose-rate received by the grains in the past. The dosimeters were placed within a few meters of the surface of a dune. A site which was once at the centre of a dune may now be only a few metres below the surface, due to the digging of drainage ditches or road construction. As the cosmic ray flux is highly dependent on the depth below the surface, the present day cosmic and calcium sulphate in situ rate could be higher than it was in the past.

---

[2]URTEC Instrument Sales Ltd. 131 Telson Road, Markham (Toronto) Ontario L3R 1E4

Table 5.5 a

Cosmic Dose Rate as a Function of Depth

Below Ground Level

Depth Below Surface ($g.cm^{-2}$)	Dose Gy/ka
0	.28 ± .1
50	.20 ± .2
100	.18 ± .2
150	.16 ± .2
200	.15 ± .2
250	.14 ± .2
300	.13 ± .2

These values were extrapolated from Figure 4, Stephan and Prescott, 1982.

Table 5.5b

Cosmic Dose Rate as a Function of Depth For Depths Greater Than 1 Metre

Depth Below Surface (m)	Fraction of Dose Remaining
1	1
2	.84
3	.71
4	.6
6	.43
10	.22
15	.09

The density of soil was taken as ρ = 2 g/cm^3 (Aitken, 1980).

5.9 Results And Discussion

Tables 5.7 and 5.8 list the results calculated as described above. The final errors in Table 5.7 are from the sums of the individual variances. The results have been arranged for ease of comparison.

In Table 5.7, the contributions from K_2O were calculated from the data listed in Table 5.4a. The U and Th contributions were calculated in two ways - from the concentration data listed in Tables 5.4b and c, and from the alpha-counting data listed in Table 5.4d. The cosmic ray contribution was calculated from the sampling depths (Table 5.4a and Table 5.6). The in-situ measurements gave the present day gamma plus cosmic ray dose-rates.

Table 5.8 gives the overall dose-rate calculated in various ways. Firstly, "Concentration data", is a total of the beta and gamma contributions from K_2O, U, Th and Rb whose values in Table 5.7 were calculated from concentration data, plus the cosmic ray contribution from Table 5.7. The second, "Alpha-counting", totals the beta and gamma from K_2O (which was calculated using only concentration data), the beta and gamma contributions from U and Th calculated from alpha-counting data and the cosmic ray contribution. Thirdly, "Beta (Concentration Data) + In-situ", is the sum of the beta contributions from K_2O, U and Th from concentration data and the in-situ value. The last "Beta (Alpha-counting) + In-situ" contains the beta contribution from

K_2O (concentration data) plus the beta from U and Th which was calculated from alpha-counting, and the in-situ contribution.

A final value was chosen which was consistent with the various totals. Due to the small amount and inter-correlation of the data, no method of formal statistical analysis was applicable. The smaller error on the in-situ results meant that the final results were often weighted toward these values. Then, the beta contribution from U and Th was reduced by a factor of .85 ± .15 due to a non-uniform distribution of the beta dose, and the final value was shown in Column 7. The first three columns of Table 5.8 indicate that the results from concentration and alpha-counting data are similar though the alpha-counting results tend to be larger than the concentration data results. As alpha-counting is an easy and relatively inexpensive procedure, it is encouraging to see that it gives results which are consistent with other methods.

The in-situ results are in agreement with the concentration and alpha-counting results, though the match could be better. The high accuracy of these results is useful. As explained earlier in this section, such measurements record the present day dose rate, which is probably larger than the dose received by the sample in the past.

More specifically, the dose-rate calculations from different methods for SESA-17, -20, -1, -4, and -10 are within 1 standard deviation of each other. For SESA-13 and -30, the results are

within 2 standard deviations. This agreement is acceptable. For SESA-36, the results from concentration data are much lower than that from the alpha-counting. The concentration of U & Th ($\simeq$ .4 ppm) were from only one source, and were lower than the other SESA samples. The alpha-counting results ($\simeq$1 ppm) are from 2 sources, and agree better with the results from the other samples. In the case of SESA-43, the large result from alpha-counting data can be explained by the significant (10%) increase in the count rate after the sample was sealed.

The affect of the beta-dose correction factor is shown in the final column. The presence of heavy minerals decreased the total dose rate by less than 5%. While the affect should not be ignored, it is within the other experimental errors in the age calculation. The beta dose contributes approximately one-third of the total dose, so a correction of 30% to the beta dose-rate would cause a 10% correction in the total dose-rate, which would still be consistent with the errors involved in determining the D_{eq}.

The dose-rates for the various samples are similar. Given the deposition history of these samples, this is not surprising. The errors quoted here give a lower limit on the accuracy of the dose-rate, as it is extremely difficult to quantify exactly the various correction factors used in the calculations, and as no corrections were made for radon loss or disequilibrium affects.

Table 5.6

Dose Rate in Gy/ka

Contributions From Different Types Of Radiation

SESA #	BETA			GAMMA			COSMIC[3]	IN SITU[4] $CaSO_4$
	K_2O	U & Th Conc.[1]	U & Th Alpha[2] Count.	K_2O	U & Th Conc.[1]	U & Th Alpha Count.		
17	.105 ±.006	.14 ±.02	.14 ±.01	.033 ±.002	.16 ±.01	.15 ±.01	.28 ±.01	
20	.101 ±.004	.19 ±.02	.18 ±.01	.031 ±.001	.20 ±.02	.20 ±.01	.15 ±.03	
13	.086 ±.02	.14 ±.02	.19 ±.01	.027 ±.006	.15 ±.02	.19 ±.01	.15 ±.03	.403 ±.01
1	.083 ±.01	.14 ±.01	.16 ±.01	.026 ±.004	.15 ±.01	.16 ±.01	.13 ±.03	.384 ±.007
4	.171 ±.006	.12 ±.02	.14 ±.02	.053 ±.002	.14 ±.02	.16 ±.01	.12 ±.03	.426 ±.004
30	.041 ±.002	.12 ±.03	.18 ±.01	.013 ±.001	.14 ±.03	.20 ±.02	.15 ±.03	
36	.140 ±.005	.07 ±.03	.15 ±.01	.043 ±.001	.07 ±.03	.19 ±.01	.11 ±.03	.351 ±.01
43	.11 ±.01	.11 ±.03	.21 ±.01	.033 ±.004	.17 ±.02	.27 ±.02	.11 ±.03	
10	.08 ±.02	.12 ±.01	.11 ±.01	.026 ±.006	.12 ±.01	.13 ±.01	.11 ±.03	

The dose rates listed in this table were calculated for 100 μm quartz grains, except for SESA-13 (150 μm) and SESA-30 (200 μm).

[1] Calculated from the concentration data listed in Tables 5.3b and c.
[2] Calculated from the alpha-counting data listed in Tables 5.3d.
[3] Calculated from Table 5.5 and the depths listed in Table 5.3a.
[4] This data is from J. Prescott and J. Hutton of the Physics Department, University of Adelaide, Australia. The $CaSO_4$ in situ dosimeter measured the gamma and cosmic ray components of the overall dose.

Table 5.7

Total Dose Rates (Gy/ka)

SESA #	DOSE RATES FROM DIFFERENT METHODS: Conc. Data [1]	Alpha-Counting Data [2]	Beta Conc. Data +In situ [3]	Beta From Alpha-Counting +In situ [4]	AVERAGES: Value Consistent With Columns 2-5 [5]	After Corrections to the Beta Dose-rate [6]
17	.72 ±.03	.71 ±.03			.72 ±.03	.70 ±.04
20	.67 ±.04	.66 ±.03			.66 ±.03	.65 ±.05
13	.55 ±.04	.65 ±.04	.62 ±.03	.68 ±.02	.62 ±.04	.60 ±.04
1	.53 ±.04	.57 ±.04	.61 ±0.02	.63 ±.02	.60 ±.03	.58 ±.04
4	.62 ±.04	.65 ±.04	.72 ±.02	.74 ±.02	.69 ±.02	.67 ±.02
30	.47 ±.05	.58 ±.04			.52 ±.05	.50 ±.06
36	.42 ±.05	.63 ±.03	.56 ±.03	.64 ±.01	.56 ±.06	.54 ±.05
43	.54 ±.05	.73 ±.04			.64 ±.05	.62 ±.05
10	.46 ±.04	.47 ±.04			.47 ±.04	.45 ±.05

These values are calculated from the data in Table 5.6.

[1] Concentration data results: Totals of beta and gamma from K_2O, U & Th concentration values plus the cosmic ray contribution.

[2] Alpha-Counting results: Totals of beta and gamma from K_2O, U & Th contributions from the alpha-counting results and the cosmic ray contribution.

[3] Beta contributions from K_2O and U & Th from concentration data plus the in situ results.

[4] Beta contributions from K_2O concentration data and U & Th from the alpha-counting data plus the in situ results.

[5] The final values were chosen to be consistent with the data shown in columns 2-5.

[6] The beta dose from the U & Th contribution was reduced to .85 ± .15 of its uncorrected value, due to the presence of heavy minerals. The values decreased by less than 5%.

CHAPTER VI

RESULTS AND DISCUSSION OF THE TL DATING METHODS

Table 6.1 lists the ages calculated by taking the D_{eq} values determined by the partial-bleach method (Table 4.1) and the growth curve matching (GCM) method (Table 4.2) and dividing them by the dose-rate (Table 5.8).

6.1 Partial-bleach Method

This technique worked well for the younger samples. TL ages from 0-200 ka were obtained for samples which had been independently dated. As outlined in the review section of Chapter II, TL dates in the 100,000 year range are rare, and there have been few opportunites to check the validity of those dates.

The low age obtained for SESA-17, the modern sample, is very encouraging. SESA-20 is supposed to be 4 ka old, but it could very easily be a modern sample - the sand was taken from the top of the dune, it was not consolidated, and could have been a recently reworked (by wind) sample.

The TL age for SESA-13 is low, but is within two standard deviations of the expected answer. The TL ages of SESA-1 and SESA-30 are within the error limits of the expected ages.

Table 6.1

TL Dating Age Estimates of the SESA Dunes

Ages in ka

SESA #	Expected Age (ka) (Schwebel, 1978)	Partial-Bleach Method	Growth Curve Matching Method
17	0	4.4 ± 1.4	By definition = 0
20	4	1.2 ± 1.2	
13	83	60 ± 14	42 ± 9
1	120	141 ± 29	160 ± 20
30	200	250 ± 94	170 ± 50*
36	380		410 ± 80*
43	510		440 ± 100*
10	>700		350 ± 100*

*Required the use of scaling factors

The D_{eq} are listed in Table 4.1 and 4.2
The dose rates are from Table 5.7. The beta dose contribution to the overall dose-rate has been corrected for the presence of heavy minerals.

Several D_{eq} were obtained for the Woakwine dune (SESA-1) but all were within one standard deviation of each other. The first result, calculated from highly scattered data, was ≃70 ± 30 Gy. The sample preparation procedures outlined in Chapter 3 had not yet been developed. In fact, it was the large scatter in this data that led to the development of these preparation techniques. After the scatter had been greatly reduced, the experiment was repeated. The data was analyzed with an exponential fitting program which gave no estimate of the error. The error was estimated by eye, the range of acceptable fits to the data being decided by the experimenter, to give a D_{eq} = 71 ± 11 Gy. Preliminary dose-rate calculations (which did not take into account all the data which was finally available, nor correct for such things as beta-attenuation; presence of heavy minerals, etc.) gave a dose-rate of .663 ± .03 Gy/ka, for an age of 112 ± 19 ka, which was highly encouraging. Other work used up most of the SESA-1 and SESA-40 samples. When more sample from the same hole (called SESA-1/2) was sent to S.F.U. from Prescott, et al., the experiment was repeated yet again. The data was analyzed with the computer program outlined in Appendix B, and a value of 80 ± 13 Gy was found. Further analysis with correction factors due to extrapolation errors, etc. led to the final D_{eq} value of 82 ± 16 Gy, and a dose-rate of .58 ± .04 Gy/ka to give the age of 141 ± 29 ka shown in Table 6.1.

The error limits for all the TL ages are large. This is due to uncertainty in both the D_{eq} and the dose-rate values. It is not immediately obvious how these limits could be reduced significantly. With the D_{eq}, the errors are due to uncertainties in the extrapolations and the difficulty in evaluating the intersection of two exponential curves. In the dose-rates, different methods yielded slightly different answers and there is uncertainty about the exact quantitative effect of such things as the presence of heavy minerals and disequilibrium effects. But the results indicate that the partial-bleach method of TL dating with large (100-150 μm) quartz grains can be used to date sand dunes in the 0-200 ka age range. This is significant as it pushes the upper age of reliable TL dating of quartz beyond 100 ka. Unfortunately, the older samples could not be dated using the partial-bleach method.

6.2 Growth Curve Matching Method

As mentioned in Chapter 4, the need for scaling factors means that the results from this technique are somewhat uncertain.

If the "right answer" had not been known beforehand, it would have been very difficult to obtain these results. The D_{eq} values obtained do fall within the same range though, and this is encouraging.

The growth curves from SESA-13 and SESA-1 overlapped the SESA-17 (modern) growth curve well enough that scaling factors were not necessary. But the D_{eq} obtained from these two values, when combined with the dose-rate calculations, gave ages which were much too low for SESA-13, and too high for SESA-1. The rest of the samples required scaling factors, which were chosen with a knowledge of the expected answer in mind. This technique did not work well with this particular set of samples.

The need for scaling factors has shown that this technique is sample dependent. The technique may prove more useful with a set of samples which does not exhibit different saturation values for samples from the same sequence. In other words, while this technique did not work well with these particular samples, it may be of use at another time.

6.3 Summary

Using the partial-bleach method, a known technique, acceptable TL ages in the 0-200 ka age range were obtained. In an attempt to date the older samples (200-700 ka), two new techniques were tried. The growth curve matching technique had limitations similar to the partial-bleach method, plus some added difficulties. While it did not work well with this sample, it may prove useful at another time,

with a different sample. The pre-dose dating method using the high temperature (375 °C) peak did not yield any meaningful dates, the results were not as expected.

6.4 Suggestions for Further Work

6.4.1 General

TL must prove itself a reliable dating technique before it will be routinely used and fully accepted as a tool in the geological community. The best way of proving TL is to work with sediments which have a well determined age and demonstrate that TL can reproduce those ages with a minimum of "fudge factors" and fuss. While there are few, if any, sediment sequences quite like the SESA sands there are several loess sediments which range back approximately 1 million years, such as those in China and Tadzhikistan, U.S.S.R. Such sites should be studied and TL dating attempted.

6.4.2 Specific

Only 15 of the SESA dunes were sampled. As there are many more dunes, it would be very interesting to do more sample collections. Large samples (more than 2 litres) should be collected so that a variety of measurements could be done on the same sample. It would be good to have different samples from the same dunes to see what differences, if any, exist between them.

The partial-bleach method has proven to be useful and reliable with the sands in the 0-200 ka year range. The experiments should be continued and expanded - this would require more samples from the sequence.

The GCM method deserves more work, as it is an interesting idea. The different behaviour of the dunes (need for scaling factors) meant that GCM was not a particularly good technique for this sample, though it is possible that not all sequences will require such scaling factors. As the method does not involve bleaching, it would eliminate one problem which the other dating methods have. While I do not feel that the GCM method works well with this sample, it would be useful to have a few more growth curves, extending out to higher doses, to further test the technique.

The pre-dose effect did not yield an effective dating method, and there is no obvious reason why it did not work. More study might shed some light on this problem, though a clear path of investigation does not present itself.

While I do not feel that it is truly necessary, an anomalous fading test on the quartz grains used in this work should be done.

The investigation into the effect of zircon on the dose-rate should be continued, so that more definite numbers can be given to the model outlined in Chapter Five. The dose-rate calculations could be more thoroughly done. More

alpha, beta and gamma spectroscopy on all the dunes, longer alpha counting times, etc. would help clarify differences in the dose-rates obtained from alpha-counting and concentration data. The effect of disequilibrium should be studied. Regarding the alpha counting, some of the samples could be made into glass, and then counted. Radon escape did not appear to be a problem, but further investigation could prove interesting.

Much more work must be done on the question of intrinsic vs. extrinsic scatter of the data. The large sample to sample variability suggests just how little is known about TL. Improved sample preparation techniques should be developed to reduce the scatter as much as possible, but until a clear picture emerges of the intrinsic scatter, and ways to reduce it are found, curve fitting programs and extrapolations will be plagued by large error bars.

The scatter experiments should be redone, with a larger number of glow curves, samples, etc. The modelling was done on approximately 100 grains, which is not a large statistical sample. The tediousness and length of time required to do this is somewhat daunting, but the exercise would be valuable.

The same comments apply to the image intensifier work.

The SESA dunes are unique, and this work has barely scratched the surface of their potential for TL dating. Even these suggestions for further work fail to do justice to the possibilities available.

APPENDIX A

Radioactive Decay Schemes

The following tables outline the radioactive decay schemes which are of interest in TL dating.

Table A.1

Radioactive Decay Schemes of Uranium-238

(from CRC Handbook, 57th ed.)

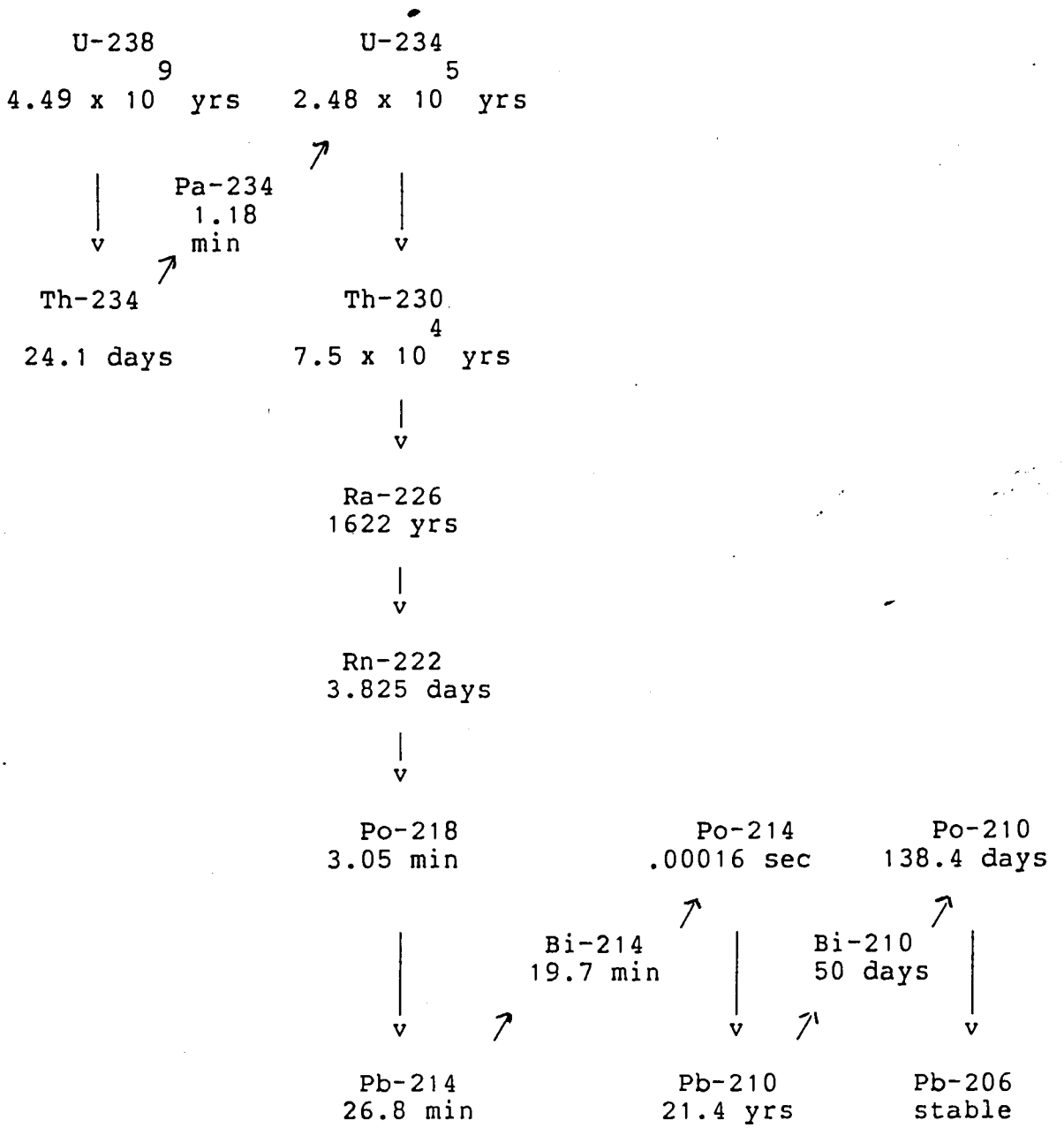

Table A.2

Radioactive Decay Schemes of Uranium-235

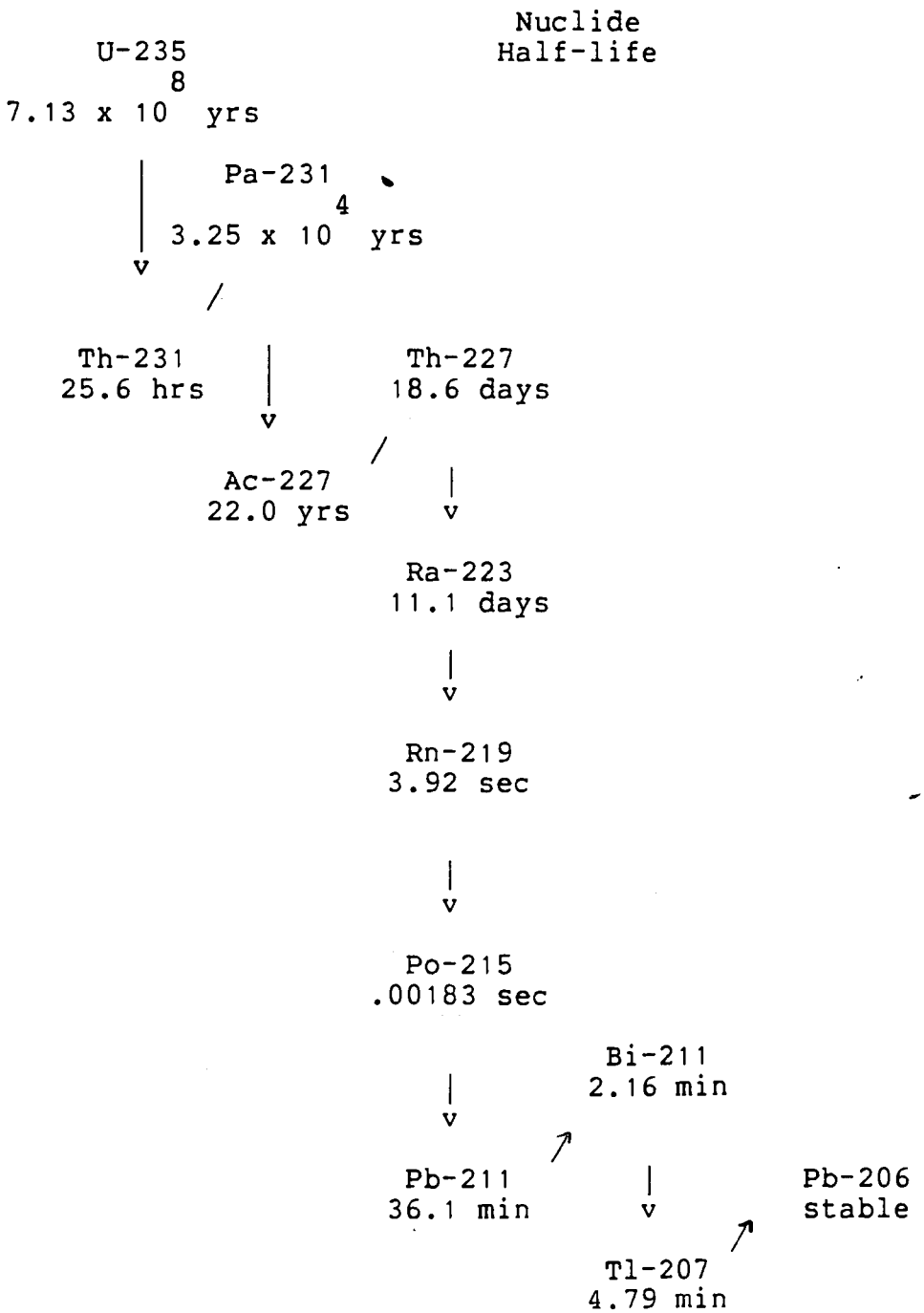

Table A.3

Radioactive Decay Schemes of

Thorium-232 and Potassium-40

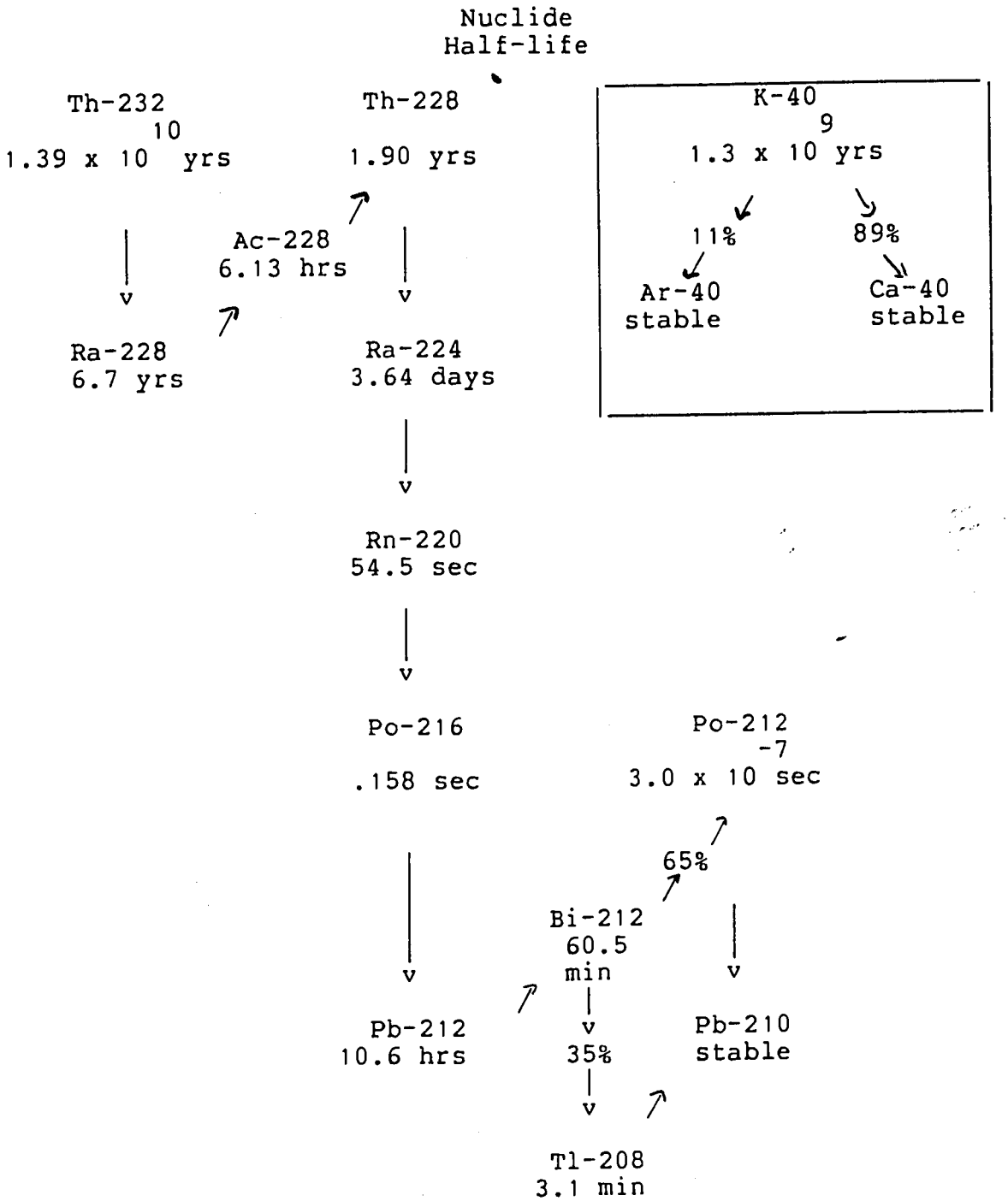

APPENDIX B

B.1 Effect Of Large Doses On TL Intensity

Large doses affect the TL intensity in dramatic ways. It was hoped that a pre-dose effect could be used to date sediments which had reached the saturation level of their first glows. Although no meaningful ages were obtained, the results were interesting, and shall be presented here.

Very large doses can cause sensitivity changes which can be observed as follows. One starts with two identical samples, A and B. B is given a large ($\simeq$100 Gy) dose and then both samples are glowed, which releases all of the trapped electrons in the two samples. Both samples are then given a small, identical test-dose, less than 10 Gy, and then reglowed. B will have a larger TL intensity than A. The large pre-dose has made B more sensitive to radiation than A.

B.2 Pre-dose And The 110° Peak

The 110° peak in quartz exhibits this change in sensitivity. It has been used to measure small D_{eq} and has proven to be especially useful in the authentifcaiton of art objects (Fleming, 1979). A model which qualitatively explains much of the behaviour of this peak has been developed (Zimmerman, 1977)

but as the behaviour of this low temperature (110 °C) peak is different from the high temperature (375 °C) it will not be discussed here. Thorough explanations can be found in the references cited above and in Aitken's books (1974, 1985).

B.3 The Pre-dose Effect With The High Temperature, 375° Peak

No dating work had been done with the high temperature peak prior to this thesis. Its behaviour has been documented (Aitken et al., 1968 and Fleming, 1970) but no model exists to help explain this behaviour.

Fleming (1970) published a curve showing the sensitivity changes of the high-temperature 365° peak following large pre-doses. There was little or no change observed with pre-doses from 0-200 Gy, but a startling, almost quadratic increase in sensitivity for doses above about 400 Gy was observed. A distinct "knee" was formed in the sensitivity curves, which occurred at about 300 Gy.

It was felt that this could form the basis of a technique for dating sediments which had received a large environmental dose. Such sediments have often reached the saturation point in the first glow growth curves; an increasing lab dose does not cause a corresponding increase in the observed TL, which means that such sediments cannot be dated using regular methods.

It was hoped that pre-dose dating using the high-temperature peaks could be used to provide a way to date these sediments. The modern and old samples would have similar sensitivity changes, but the "knee" of the older sample would occur at lower lab doses than the modern sample, as the older sample would have received a substantial environmental dose. The difference in the position of the knees would yield D_{eq} (Figure B.1).

Initally, four samples were measured: SESA-17 (modern), SESA-36 (380 ka), Sesa-43 (510 ka) and SESA-35 (greater than 700 ka). 45 planchets of each sample were made, and divided into 15 groups of 3 planchets each. The groups of planchets were given doses from 0 - 2250 Gy, in steps of about 250 Gy. The samples were then glowed (heated to 450°C). After a two day wait, the samples were given a small "test dose" of 15 Gy. They were left to sit for 24 hours, then glowed. Due to the large numbers of planchets, it was impossible to glow all the samples on the same day. The four samples were split into two groups; SESA-17 and -35, SESA-36 and -43. Each group was irradiated and glowed on the same day to reduce possible differences caused by changes in the equipment.

There was no noticeable sensitivity change in the planchets which had received a pre-dose of less than about 400 Gy, with a rapid increase as a function of pre-dose occurring for larger doses. The second-glow intensities, with the distincitive "knee" occurring at a pre-dose of about 500 Gy is shown in Figure B.2a.

Model For The Pre-Dose Dating Technique
Using The High Temperature {375°C} Peak

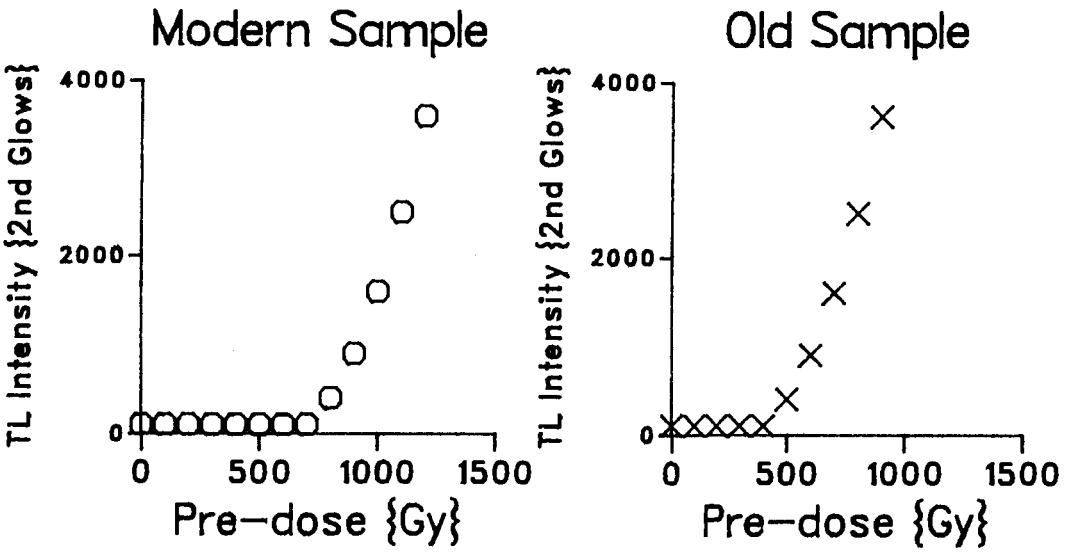

Figure B.1A

Figure B.1B

Large doses can have a dramatic effect on the TL intensity. A 2nd glow curve is constructed by 1) Irradiating with a series of doses {eg. 0-1200 Gy, the pre dose}. 2) Glowing - heating to 450 all the samples with a small {eg. 10 Gy} test dose 4) Re-glowing 5)Plotting the TL intensity of the 2nd glows as a function of the pre-dose.

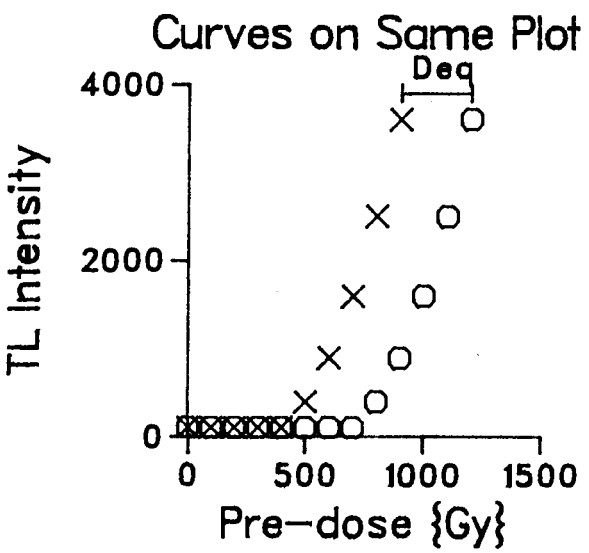

Figure B.1C
The old samples should undergo the sensitivity change at a lower pre-dose than the modern sample as they would have received a substantial dose in the environment. The two curves could be plotted on the same graph, and the Deq would be measured as the shift along the dose axis necessary to overlap the modern and old curves.

All the samples did yield similarily shaped curves, but the position of the knee did not appear to be a function of the age of the sample. SESA-35, the oldest sample, should have had its "knee" occurring at a point more than 700 Gy before SESA-17, not after it.

As well, each sample appeared to have a different initial sensitivity (Figure B.2b). For similiar samples, it was expected that the initial second glow intensity would be the same. Differences of ±15% were observed, greater than the intrinsic disc to disc variability.

Even when the data was arbitrarily scaled so that the initial sensitivities were the same (Figure B.3), the results did not improve. In fact, all of the old curves were then below the modern curve. The "knee" occurred in approximately the same place for all the samples, but the rate of increase of the sensitivity was not the same. There does not appear to be an obvious method of overlapping these curves.

To see if there was any correlation between the second-glow sensitivities after a large (1500 Gy) pre-dose and age, eleven samples (from 0 to 700 ka old) were studied. Four planchets of each type were glowed, and the curves shown in Figure B.4 are the average of the results. The second-glow intensities do not appear to follow any obvious pattern.

B.4 Discussion

The results were not as expected; no method of obtaining meaningful D_{eq} presents itself. The results were presented here because they are still of interest. The high temperature pre-dose effect does not appear to yield much hope as a method of TL dating for older sediments at this time. Hopefully, further work will help explain what is happening with this effect.

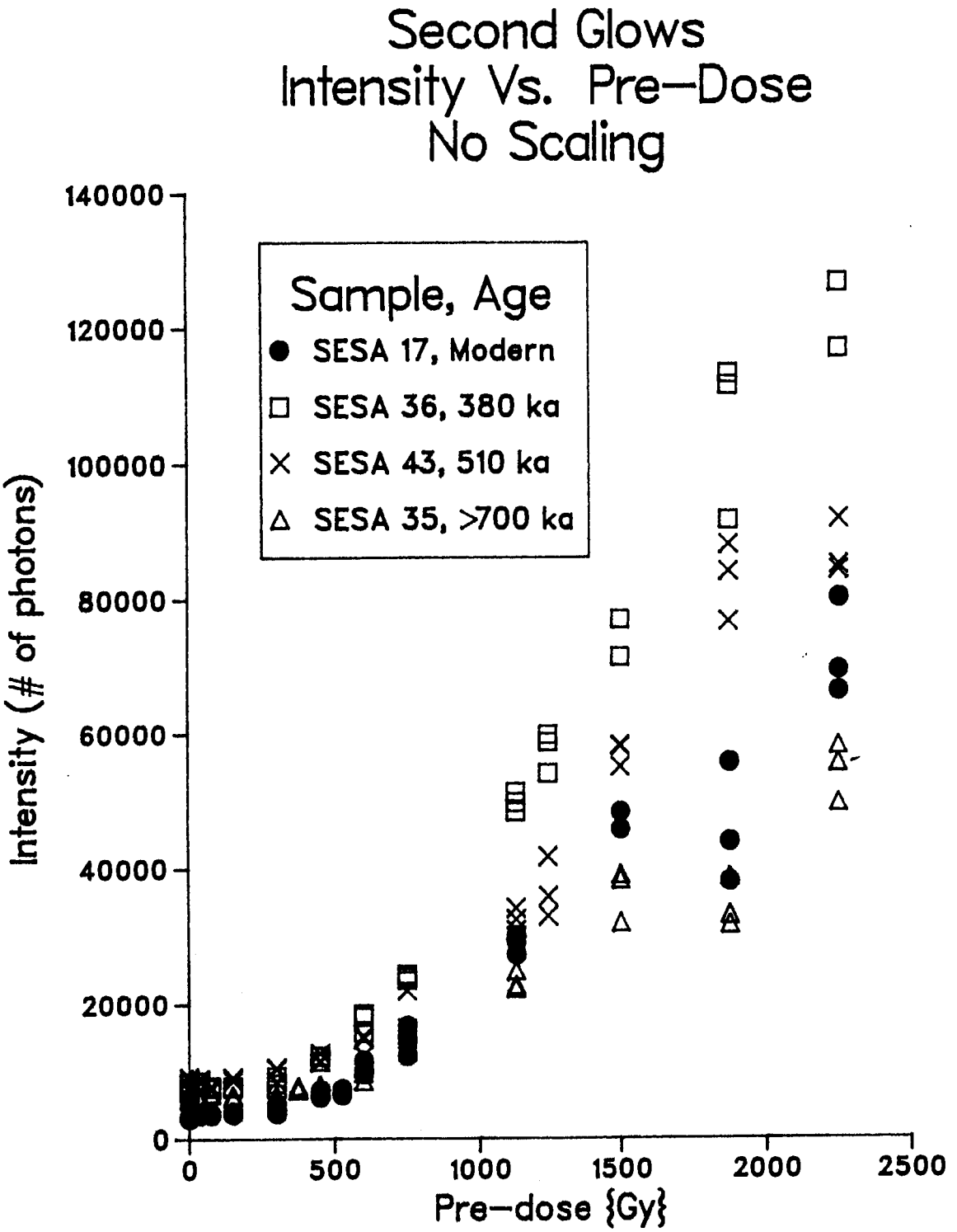

Figure B.2A
Results of the Pre-Dose Dating method. The above is a plot of the second glow intensities (unscaled) as a function of the pre-dose. The samples ranged in age from 0 to 700 ka.

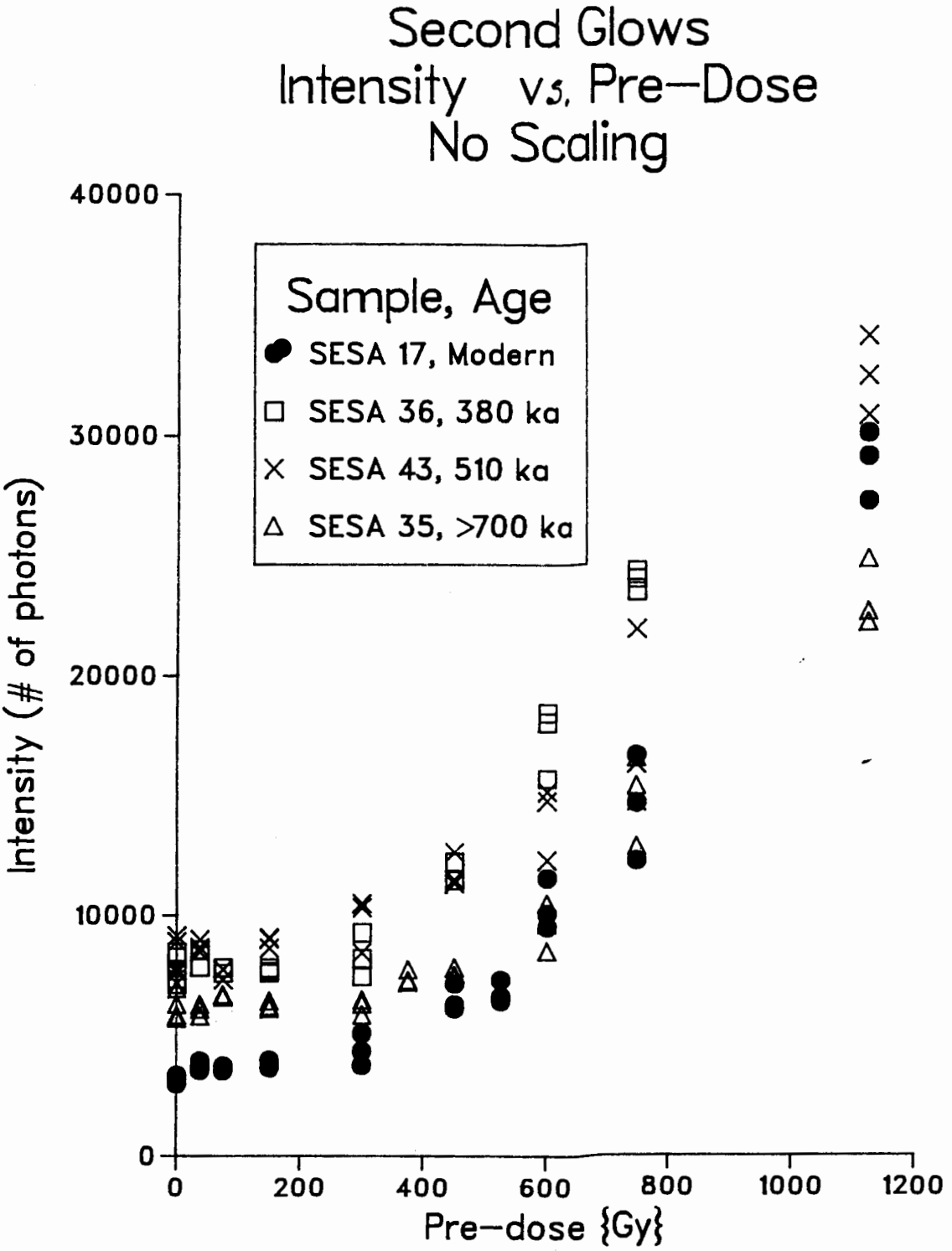

Figure B.2B
This is the same data as in Figure B.2A, but only pre-doses less than 1200 Gy are shown. This shows the different initial intensities. The data was unscaled.

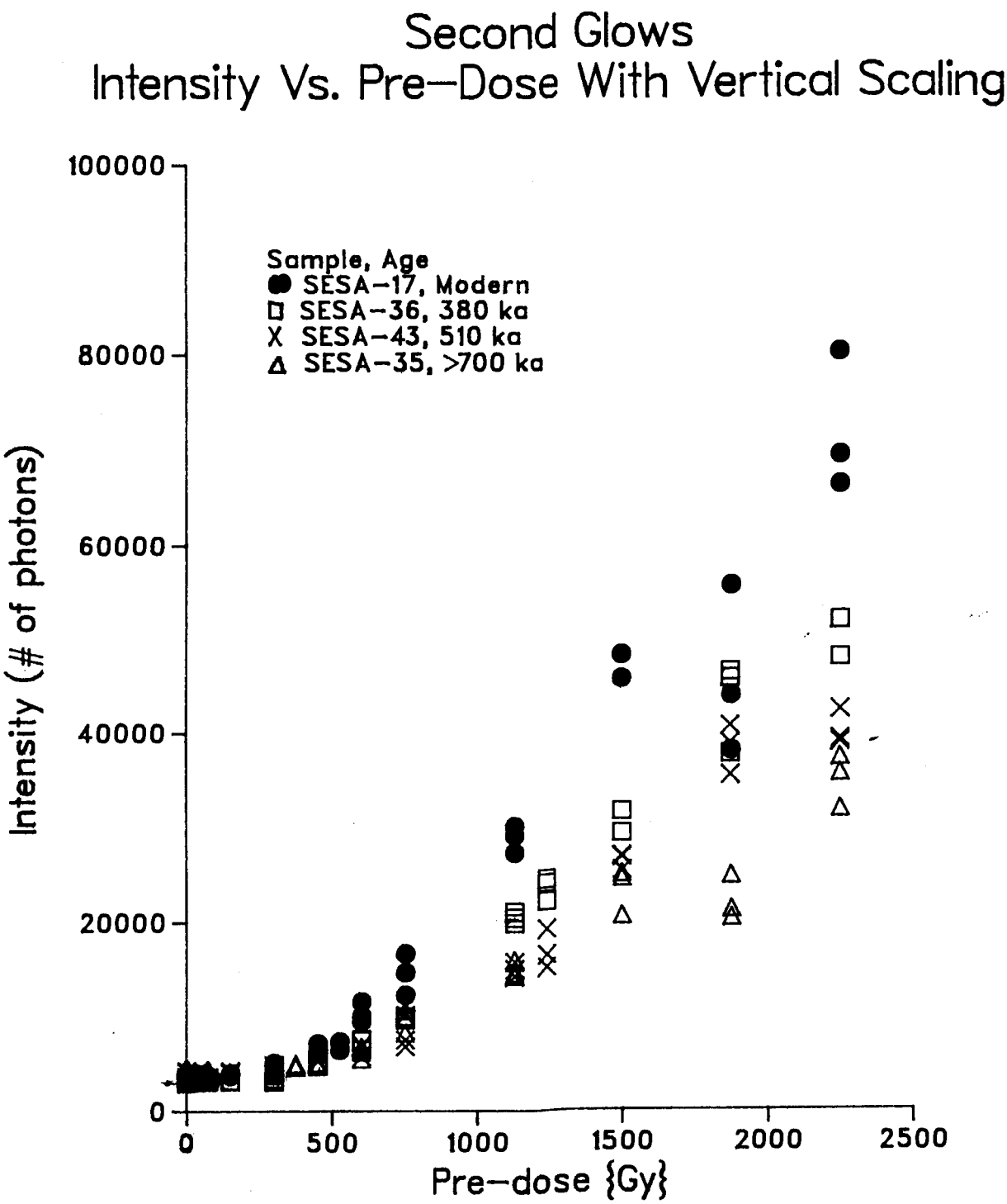

Figure B.3
Same data as in Figure B.2, but the data has been scaled vertically so that the initial sensitivities are the same. The results were not as expected, please see Figure B.1.

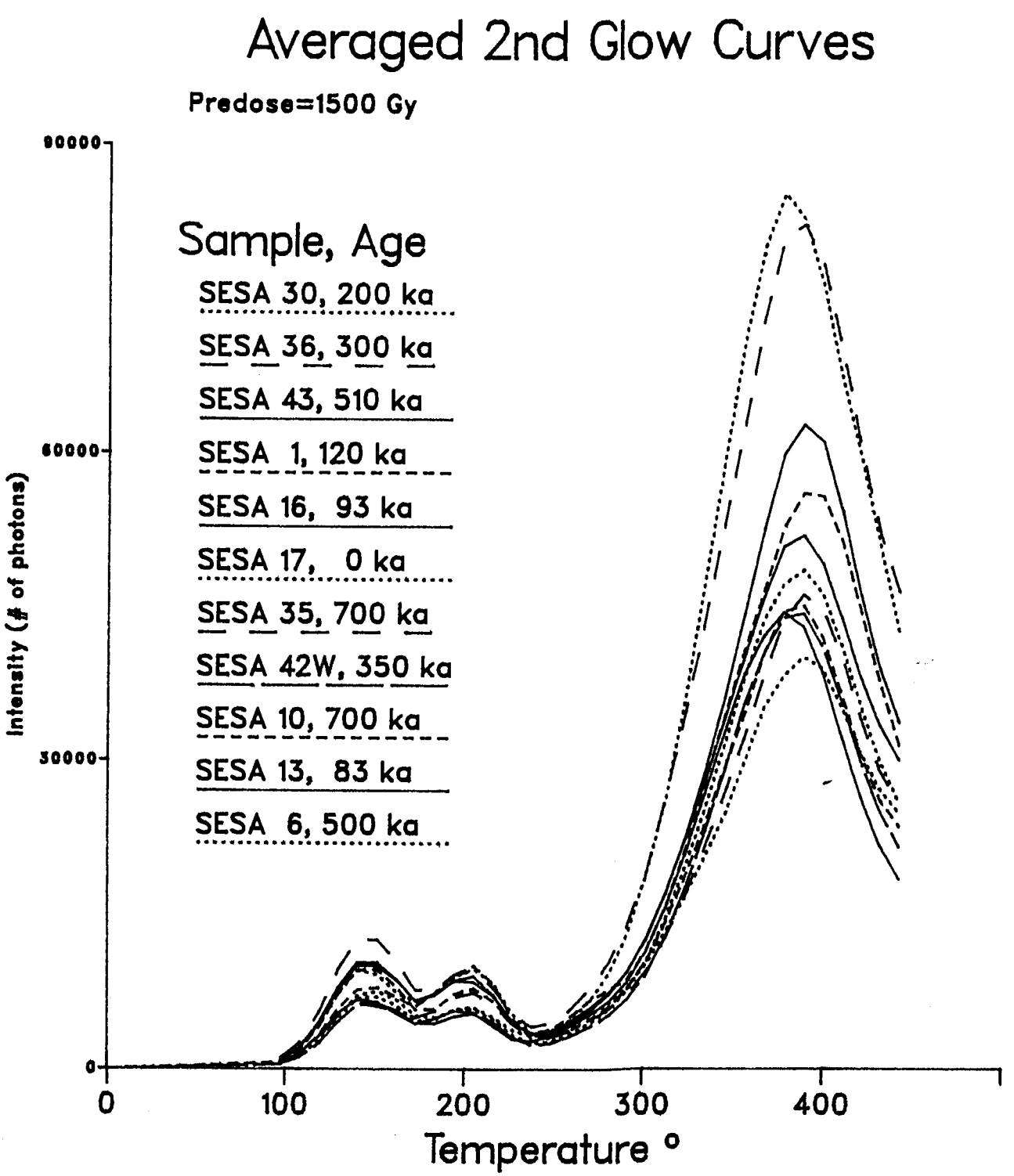

Figure B.4

The SESA samples, which range in age from 0 to 700 ka years old were given a pre-dose of 1500 Gy. The second glow intensities were expected to increase with age. The results above show no obvious correlation between the second glow intensities and the sample age.

APPENDIX C

Curve Fitting Routines

These programs were written by Stuart Cowan during the summer of 1985. The work he did was greatly appreciated. The main reference for this work was a book entitled Regression: A Second Course in Statistics, by R.J. Wonnacott and T.H. Wonnacott.

The following is an outline of the algorithm used to fit exponential and quadratic curves to the data obtained during the course of the research for this thesis. Error estimates for the intersections of the bleached and unbleached curves (in the partial-bleach method) were also obtained from these programs.

Multiple Regression

Multiple regression is the extension of simple regression, it takes account of more than one independent variable x. It is used to investigate the effects on Y of several variables simultaneously.

$$Y_i = \alpha + \beta x_i + \gamma z_i + \epsilon_i$$

where α, β and γ are the fitting parameters, x_i and z_i are the independent variables, and ϵ_i is the difference between the observed and expected values of Y_i. It is the stochastic, or error term.

As the true model is not known, the best that can be done is an estimated fit.

$$Y_i = \hat{\alpha} + \hat{\beta}x_i + \hat{\gamma}z_i + \epsilon_i$$

where $\hat{\alpha}$, etc. are the estimated values of the fitting parameters.

Non-Linear Regression

The aim of these programs was to estimate the set of parameters that minimized the sum of the squared deviations between the observed and fitted values of of Y.

As long as the parameters appear in a linear way, the estimating equations could be solved relatively simply by redefining the regressors. A model that is linear in the parameters can be handled with ordinary least squares, even if the variables enter non-linearly.

The Algorithm

The first model was,

$$Y_i = y_o + y_1 (1 - e^{-x_i}) + \epsilon_i$$

Where ϵ_i had a normal distribution with mean 0 and standard deviation σ_i and where the σ_i could be distinct. Dividing by the

scaling factor $k\sigma_i$,

$$\frac{Y_i}{k\sigma_i} = \frac{1}{k\sigma_i} y_o + y_1 \frac{(1 - e^{-x_i})}{k\sigma_i} + \epsilon$$

where each ϵ had a normal distribution with mean 0 and the same standard deviation σ. Redefining

$$Y_i^* = \frac{1}{k\sigma_i} Y_i$$

$$Z_1 = \frac{1}{k\sigma_i}$$

$$Z_2 = \frac{1}{k\sigma_i} (1 - e^{-x_i})$$

The new model is obtained:

$$Y_i^* = y_o Z_1 + y_1 Z_2 + \epsilon$$

Since this was a regression with linear estimating parameters on two variables, it was possible to apply standard least squares techniques to find maximum-likelihood estimates of y_o and y_1. The 95% confidence intervals were constructed by multiplying the standard errors by $t_{.025,\delta}$ where δ is the number of degrees of freedom in the statistical model under consideration (Wonnacott, p. 527). The critical points used were taken from a table in Wonnacotts' book.

Assumptions

The model for the data was

$$Y_i = y_o (1 - \exp(-(D_i + D_e)/ D_o)) + \epsilon_i$$

where ϵ_i had a normal distribution with mean 0 and standard deviation proportional to Y_i.

Maximum-likelihood estimates of D_o, y_o, and D_e can be found by using nonlinear regression (see below). In general, these parameter estimates will not be normally distributed so that the t-test does not fully apply. However, as the number of sample points increases, the distributions of the parameter estimates each approach a normal distribution. Thus, it was reasonable to assume that the parameter estimates $\hat{D}_o$, $\hat{y}_o$, and $\hat{D}_e$ each had normal distributions.

With this last assumption, 95% confidence intervals could be obtained for D_o, y_o and D_e. In addition, a joint confidence interval for D_o, y_o and D_e could be formed which took into account the covariance of the parameters.

$\bar{B}$ was the vector of parameters, $\hat{\bar{B}}$ was the vector of estimates for the parameters, and X'X was the covariance matrix of the parameters. The 95% confidence region for D_o, y_o and D_e could be written

$$(\bar{B} - \hat{\bar{B}})' \; X'X \; (\bar{B} - \hat{\bar{B}}) \leq s^2 k \; F_{.05}$$

Where k was the number of variables, s^2 was the estimated variance, $F_{.05}$ was the F-statistic with k and (n-k) degrees of freedom, and n was the number of observations.

The 95% confidence region defined in the equation above was a k-dimensional ellipsoid. For the analysis done in this thesis,

the bleached and unbleached data generated two different 3-dimensional ellipsoids in the parameter space which formed good approximations to the actual confidence regions.

The bleached and unbleached parameter estimates were assumed to be independent, so 95% of the time D_o, y_o, D_e and D_o', y_o', and D_e' were within their respective 97.5% ($\sqrt{95\%}$) confidence regions. Each choice of D_o, y_o, D_e; D_o', y_o', D_e' defined an intersection point of the bleached and unbleached curves. D_{min} and D_{max} were defined to be the minimum and maximum value of $D_{intersection}$ for the parameters in the 97.5% confidence regions. In at least 95% of all cases,

$D_{min} \leq D_{intersection} \leq D_{max}$.

In practise, it was difficult to determine D_{min} and D_{max}. To approximate D_{min} and D_{max} 100 pairs of points were chosen, one in the bleached ellipsoid and one in the unbleached ellipsoid, then the maximum and minimum observed $D_{intersection}$ values were found using these values.

By assuming that D_{min} and D_{max} could be approximated closely by taking a large, but finite sample of the two confidence regions, then the values of D_{min} and D_{max} thus generated formed an acceptable approximation to the 95% confidence interval for $D_{intersection}$, and gave an estimate of the error involved in the the intersection term.

For a model of the form,

$$Y_i = y_o \left(1 - \exp(-(D + D_e)/ D_o)\right) + \epsilon_i$$

then

$$Y = f\ (B_1, B_2,\ldots,B_n; x_1, x_2,\ldots,x_k) + \epsilon \qquad (1)$$

where ϵ has the same standard deviation for each point.

Here the B_i are parameters (y_o, D_i and D_o in our case) and the x_i are the independent variables (D_e in our case).

$B_1^*,\ldots\ldots,B_n^*$ is an initial guess at the correct values $B_1,\ldots\ldots,B_n$. If B^* is close enough to B the multivariate Taylor expansion will give a reasonable approximation.

$$f\ (B_1,\ldots,B_n;x_1,\ldots,x_k) = f\ (B_1^*,\ldots,B_n^*; x_1,\ldots,x_k) + \frac{\partial f}{\partial B_1}\ (B_1 - B_1^*) + \ldots\ldots + \frac{\partial f}{\partial B_n}\ (B_n - B_n^*) + e_{Taylor} \qquad (2)$$

Substituting (2) into (1) we obtain

$$Y = f(B_i^*;x_i) + \frac{\partial f}{\partial B_1}\ (B_1 - B_1^*) + \ldots. + \frac{\partial f}{\partial B_n}\ (B_n - B_n^*) + e_{combined} \qquad (3)$$

Where the partials in (3) were evaluated at B*.

Rewriting,

$$Y - f(B_i^*;x_i) + \frac{\partial f}{\partial B_1} B_1^* + ... + \frac{\partial f}{\partial B_n} B_n^*$$

$$= B_1 \frac{\partial f}{\partial B_1} + ... + B_n \frac{\partial f}{\partial B_n} + e_{combined}$$

Letting

$$Y_c = Y - f(B_i^*;x_i) + \frac{\partial f}{\partial B_1} B_1^* + ... + \frac{\partial f}{\partial B_n} B_n^*$$

$$Z_i = \frac{\partial f}{\partial B_i}$$

We find,

$$Y_c = B_1 Z_1 + ... + B_n Z_n + e_{combined}$$

Since Y_c and the Z_i were known, a linear regression could be performed to find a new, presumably better estimate of the B_i. Letting the new estimate be B*, the process detailed above can be repeated. The method converges quadratically to the correct value $B_i,....,B_n$ provided that the initial guess was close enough. With a poor initial guess, convergence is definitely problematic.

APPENDIX D

The Reproducibility Investigations

Reproducibility problems are caused by a combination of two things; the intrinsic variations in brightness among the grains, and differences in the sample and disc preparation (e.g. uneven spreading of grains on the disc). In an effort to reduce this problem, both types of scatter were studied.

The intrinsic scatter was investigated by using an image intensifier to study the behaviour of individual grains. The grains varied in brightness by more than a factor of 10. 15% of the grains were "bright" while 2% of the grains were "very bright". It was found that a grain which was bright at a low temperature was not necessarily bright at a higher one. A more detailed explanation of the Image Intensifier and some results are given in Appendix D.

Over 100 grains were individually glowed. A histogram of their brightness is shown in Figure D.1. From this data, the intrinsic scatter could be calculated as a function of the number of grains/disc. A "theoretical" value for the expected scatter could be determined from this data (Figure D.2).

TL measurements using standard experimental equipment were done on discs with 1, 10, 100, 1000 ... grains/disc. The observed scatter could then be analyzed in terms of its

intrinsic and extrinsic parts.

Initially, the experimental scatter was a large fraction of the total, so ways to reduce it were studied. This was the motivation for studying and improving planchet preparation techniques, which are described in Chapter 3.

Figure D.1 bears some relationship to Figure 5.2. The variations in brightness amongst the planchets were most likely caused by variations in the beta-dose they received. Heavy minerals concentrated the uranium and thorium in the sample, making the beta-dose non-uniform.

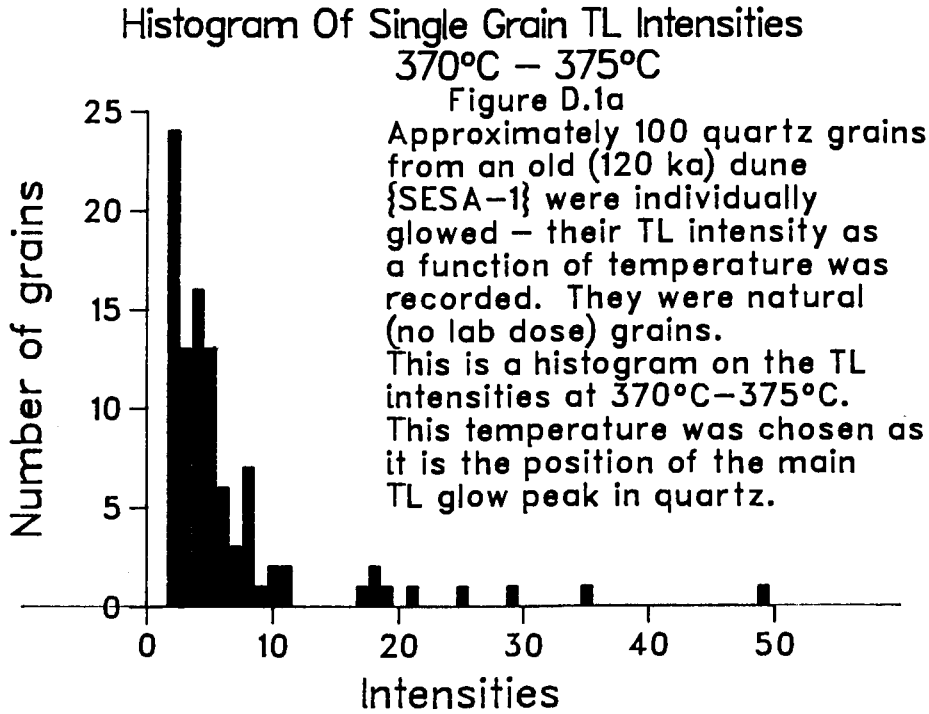

Figure D.1a
Approximately 100 quartz grains from an old (120 ka) dune {SESA–1} were individually glowed – their TL intensity as a function of temperature was recorded. They were natural (no lab dose) grains.
This is a histogram on the TL intensities at 370°C–375°C. This temperature was chosen as it is the position of the main TL glow peak in quartz.

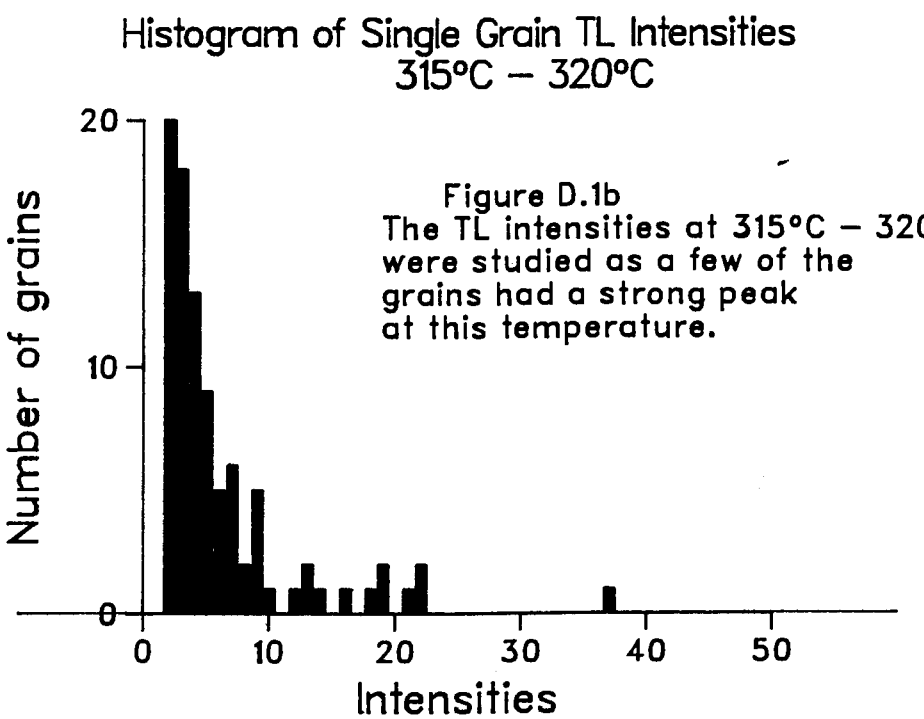

Figure D.1b
The TL intensities at 315°C – 320° were studied as a few of the grains had a strong peak at this temperature.

These histograms should be compared with Figure 5.1. While some of the variations in the TL intensities of the grains could be caused by non–uniform dose–rates, it does not appear that this is the only cause of the variations.

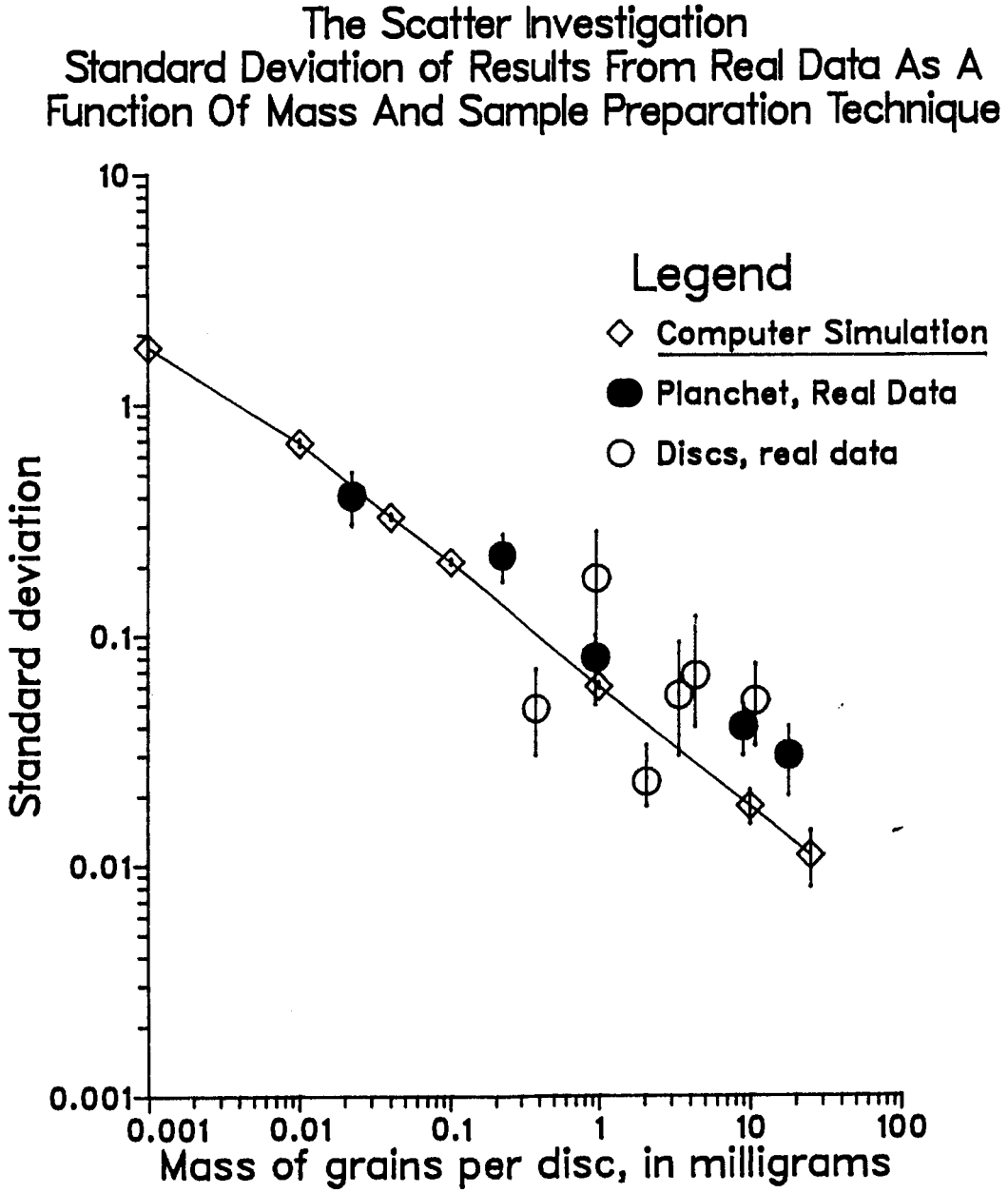

Figure D.2

Theoretical and actual scatter plotted as a function of the mass of the sample on the disc or planchet.

This demonstrates that not all the scatter in the data is due to sample preparation techniques, there is some 'intrinsic' scatter.

APPENDIX E

The Use Of An Image Intensifier To Study The TL Intensity Variability Of Individual Grains

The following is an article which appeared in Ancient TL, in July 1985.

When using 100μm quartz grains in TL dating a difficultly commonly experienced is poor disc-to-disc reproducibility, a major cause of which is intrinsic sample variability. Because this occurs when there are several hundred grains per disc, it can be deduced that most of the TL must arise from only a few percent of the grains.

In order to test this deduction we have constructed a simple apparatus that gives a semi-quantitative light intensity distribution of a large number of grains and permits sorting the grains for further study.

The apparatus is shown in Figure 1. The sample chamber was an Oxford-style glow oven with a Wild BG-38 filter (pass band 320-630 nm) to remove the incandescence emission. Above this an f1.4 camera lens was mounted with a reverse adapter on the bottom of a bellows unit. At the top of the bellows an image intensifier was placed and its position adjusted so that an image of the sample was focused on its input.

Figure 1

Figure 2a

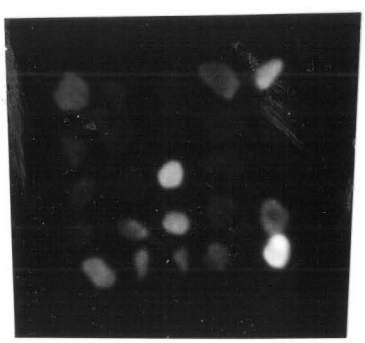

Figure 2b

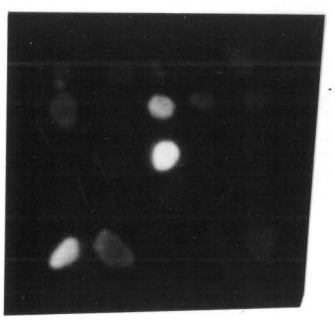

The glowing grains were readily visible at the upper phosphor surface of the intensifier and could easily be photographed with the camera shown in the upper part of the figure.

The image intensifier used was a Varo model 3603 from Varo Inc., 2203 Walnut Street, P.O. Box 469014, Garland, Texas 75046-9014 U.S.A. It had a gain of $\simeq>10^5$ from 400-800 nm, operated on two 1.5V cells and cost $\simeq$ US $2000.

Small chips of CaF_2:Dy dosimeter crystals were used for set-up and focusing. After being given a large dose (> 1kGy) their phophorescence was visible for over two weeks.

Figures 2a and 2b are photographs of the intensified natural TL of 25 quartz grains, 0.5-1mm in diameter, extracted from a 120 ka South Australian beach dune. Figure 2a is the TL from 250-400°C and Figure 2b the TL from 400-450° C. Although many grains are visible, most of the light is coming from 2 or 3 grains. It is also interesting to note that the brightest grain (upper left) in the first picture is barely visible in the second one. Photographs of discs containing several hundred 100μm quartz grains of the same sample also indicate that the TL is dominated by a few bright grains.

We know of only two previous attempts to determine an intensity distribution, those of McKerrell and Mejdahl (1981) and Benko (1983) who measured the TL of individual grains. Because of the small number that they measured they could have missed the important bright grains. The idea that only a small percentage of the grains contribute significantly to the measured TL was put forth several years ago by D. Zimmerman (D. Stoneham, private communication, 1983) yet has received little discussion in the literature. The cause and implications of this variability remain to be investigated.

A sensitive apparatus for photographing TL has been described previously by Debenham and Walton (1982); our system is much cheaper, simpler to construct and easier to use.

Acknowledgement

We thank A. Walton for assisting with a pilot experiment using his image intensifier in Oxford in 1983, M.L.W. Thewalt for the loan of the Varo image intensifier, and P.M. Hobler for the loan of some of the photographic equipment. The work was supported by the Natural Sciences and Engineering Research Council.

References

Benko, L. (1983) TL Properties of Individual Quartz Grains. Pact 9, 175-181.

Debenham, N.C. and Walton, A.J. (1982) Image Intensifier Studies of Pottery TL. Pact 6, 539-541

McKerrell, H. and Mejdahl, V. (1981) Progress and Problems with Automated TL Dating. Symposium on Archaeometry and Archaeological Prospection, Edinburgh, March 24-27, 1976. Published as report Risø-M-2265.

BIBLIOGRAPHY

Aitken, M.J., 1974, Physics And Archaeology, Clarendon Press, Oxford.

Aitken, M.J., 1985, Thermoluminescence Dating, Academic Press, New York.

Aitken, M.J., Thompson, J. and Fleming, S.J., 1968, Proceedings Of The Second International Conference On Luminescence Dosimetry, Conference 680920, Oak Ridge National Laboratory, U.S.A.E.C., p.364

Bell, W.T., 1977, Thermoluminescence Dating: Revised Dose-Rate Data: Archaeometry, v.19, p. 99-100.

Bell, W.T., 1979, Thermoluminescence Dating: Radiation Dose-rate Data: Archaeometry, v.21, p. 243-246.

Berger, G.W., 1984, Thermoluminescence Dating Of Glacial Silts From Ontario: Canadian Journal of Earth Sciences, v. 21, p.1393-1399.

Berger, G.W., 1985, Thermoluminescence Dating Studies Of Rapidly Deposited Silts From South-central British Columbia: Canadian Journal of Earth Sciences, v.22, p.704-710.

Berger, G.W., 1985, Thermoluminescence Dating Applied To A Thin Winter Varve Of The Late Glacial South Thompson Silt, South-central British Columbia: Canadian Journal of Earth Sciences, v.22, p.1736-1739.

Berger, G.W., 1986, Dating Quaternary Deposits By Luminescence - Recent Advances: Geoscience Canada, v.13, p.15-21.

Berger, G.W. and Huntley, D.J., 1982, Thermoluminescence Dating Of Terrigenous Sediments: PACT Journal, Council of Europe, v.6, p.495-504.

Berger, G.W., and Huntley, D.J., 1983, Dating Volcanic Ash By Thermoluminescence: PACT Journal, Council of Europe, v.9, p. 581-592.

Berger, G.W., Huntley, D.J. and Stipp, J.J., 1984, Thermoluminescence Studies On A ^{14}C Marine Core: Canadian Journal of Earth Sciences, v.21, p.1145-1150.

Blackburn, G., Bond, R.D. and Clarke, A.R.P., 1965, Soil Development Associated With Stranded Beach Ridges In South-east South Australia, Commonwealth Scientific and Industrial Research Organization, Australia, Soil Publication no.22.

Broecker and Bender, 1972, Age Determinations On Marine Strandlines. Calibration Of Hominid Evolutions. Scottish Academic Press, Edinburgh.

Chen, R., 1976, Methods For Kinetic Analysis Of Thermally Stimulated Processes: Journal of Material Science, v.11, p.1521-1541.

Cherry, R.D., 1963, The Determination Of Thorium And Uranium In Geological Samples By An Alpha-Counting Technique: Geochimica et Cosmochimica Acta, v. 27, p.183-189.

Colwell, J.B., 1979, Heavy Minerals In The Late Cainozoic Sediments Of Southeastern South Australia And Western Victoria. BMR Journal of Australian Geology & Geophysics, v.4, p.83-97.

Covey, C. and Schneider, S., 1984, Models For Reconstructing Temperature And Ice Volume From Oxygen Isotope Data: Milankovitch And Climate, Part 2. NATO ASI Series, D. Reidel Publishing Co., Dordrecht, Holland, p.699-705.

Divigalpitiya, W.M.R., 1982, Thermoluminescence Dating Of Sediments: unpublished M.Sc. Thesis, Simon Fraser University, Burnaby, British Columbia.

Dreimanis, A., Hutt, G., Raukas, A. and Whippey, P.W., 1978, Dating Methods Of Pleistocene Deposits And Their Problems - 1. Thermoluminescence Dating: Geoscience Canada, v.5, p.55-60.

Fleming, S.J., 1970, Thermoluminesce Dating: Refinement Of The Quartz Inclusion Technique: Archaeometry, v.12, p.133-146.

Fleming, S.J., 1979, Thermoluminescence Techniques in Archaeology, Clarendon Press, Oxford.

Goedicke, C., 1984, Microscopic Investigations Of The Quartz Etching Procedure: Nuclear Tracks and Radiation Measurements, v.9, p.87-93.

Grootes, P.M., 1978, Carbon-14 Time Scale Extended: Comparison Of Chronologies: Science, v.200, p.11-15.

Hamilton, E.I., 1965, Applied Geochronology, Academic Press, London.

Hamilton, R.E. and Farquhar, R.M., editors, 1968, Radiometric Dating For Geologists, John Wiley & Sons, London.

Harmon, R. and Rosholt, J., 1982, Igneous Rocks: Uranium Series Disequilibrium: Applications To Environmental Problems Ivanovich, M. and Harmon, R.S. (eds) Clarendon Press, Oxford, p.149-150.

Huntley, D.J., 1985, On The Zeroing Of The Thermoluminescence Of Sediments: Physics and Chemistry of Minerals, v.12, p.112-127.

Huntley, D.J., Berger, G.W., Divigalpitiya, W.M.R. and Brown, T.A., 1983, Thermoluminescence Dating Of Sediments: PACT Journal, Council of Europe, v.9, p.607-618.

Huntley, D.J., Hutton, J.T. and Prescott, J.R., 1985, South Australian Sand Dunes: A TL Sediment Test Sequence: Preliminary Results: Nuclear Tracks and Radiation Measurements, v.10, p.757-758.

Huntley, D.J. and Johnson, H.P., 1976, Thermoluminescence As a Potential Means Of Dating Siliceous Ocean Sediments: Canadian Journal of Earth Sciences, v.13, p.593-596.

Huntley, D.J. and Kirkey, J.J., 1985, The Use Of An Image Intensifier To Study The TL Intensity Variability Of Individual Grains: Ancient TL, v.3, p.15-18.

Huntley, D.J., Godfrey-Smith, D.I. and Thewalt, M.L.W., 1985, Optical Dating Of Sediments: Nature, v.313, p.105-107.

Huntley, D.J. and Wintle, A.G., 1981, The Use Of Alpha Scintillation Counting For Measuring Th-230 And Pa-231 Contents Of Ocean Sediments: Canadian Journal Of Earth Sciences, v.18, p.419-432.

Idnurm, M. and Cook, P., 1980, Palaeomagnetism Of Beach Ridges In South Australia And The Milankovitch Theory Of Ice Ages: Nature, v.286, p.699-702.

Imbrie, J., and Imbrie, K., 1979, Ice Ages, Solving The Mystery, Enslow Publishers, New Jersey, USA.

Imbrie, J., Hays, J.D., Martinson, D.G., McIntyre, A., Mix, A.C., Morley, J.J., Pisias, N.G., Prell, W.L. and Shackleton, N.J., 1984, The Orbital Theory Of Pleistocene Climate: Support From A Revised Chronology Of The Marine $\delta^{18}O$ Record: Milankovitch and Climate. Berger, et al. (eds.), D. Reidel Publishing Company, New York, p.269-305.

Jungner, H., 1983, Prelimary Investigations On TL Dating Of Geological Sediments From Finland: PACT Journal, Council of Europe, v.9, p.565-572.

Libby, W.F., 1955, Radiocarbon Dating, 2nd Edition, The University of Chicago Press.

Libby, W.F., 1967, History Of Radiocarbon Dating: Radioactive Dating And Methods Of Low-Level Counting, Proceedings of a Symposium organized by the International Atomic Energy Agency, Vienna, p.3-26.

Masters, P. and Bada, J., 1978, Amino Acid Racezimation Dating: Archaeological Chemistry - II. G.F. Carter, ed., Advances in Chemistry Series No.171.

Mejdahl, V. and Wintle, A.G., 1984, Applications To Archaeological And Geological Dating: Thermoluminescence And Thermoluminescent Dosimetry, Horowitz, Y.S. ed., CRC Press, Boca Raton, U.S.A., p.133-190.

McKeever, S.W.S., 1984, Thermoluminescence In Quartz And Silica: Radiation Protection Dosimetry, v.8, p.81-98.

McKeever, S.W.S., 1985, Thermoluminescence Of Solids, Cambridge University Press, Cambridge.

Pethick, J., 1985, An Introduction To Coastal Geomorphology. Edward Arnold, London, p.126-143.

Prescott, J.R., 1983, Thermoluminescence Dating Of Sand Dunes At Roonka, South Australia: PACT Journal, Council of Europe, v.9, p.505-512.

Prescott, J.R. and Stephan, L.G., 1982, The Contribution Of Cosmic Radiation To The Environmental Dose For Thermolumiscent Dating - Latitude, Altitude And Depth Dependence: PACT Journal, Council of Europe, v.6, p.17-25.

Readhead, M.L., 1984, Thermoluminescence Dating Of Some Australian Sedimentary Deposits: unpublished Ph.D. thesis, Australian National University, Canberra, 696 p.

Rosholt, J.N., 1967, Open System Model For Uranium-Series Dating Of Pleistocence Samples: Radioactive Dating And Methods Of Low-Level Counting, Proceedings Of A Symposium organized by the International Atomic Energy Agency, Vienna, p.299-312.

Schwebel, D.A., 1978, Quaternary Stratigraphy Of The Southeast Of South Australia: unpublished Ph.D. Thesis. School of Earth Sciences, The Flinders University of South Australia.

Singhvi, A.K., Sharma, Y.P. and Agrawal, D.P., 1982, Thermoluminescence Dating Of Sand Dunes In Rajasthan, India: Nature, v.295, p.313-315.

Singhvi, A.K. Sharma, Y.P., Agrawal, D.P. and Dhir, R.P., 1983, Thermoluminescence Dating Of Dune Sands - Some Refinements: PACT Journal, Council of Europe, v.9, p.498-504.

Southgate, G.A., 1985, Thermoluminescence Dating Of Beach And Dune Sands: Potential Of Single-grain Measurements: Nuclear Tracks and Radiation Measurements, v.10, p.743-747.

Sprigg, R.C., 1979, Stranded And Submerged Sea-Beach Systems Of Southeast South Australia And The Aeolian Desert Cycle: Sedimentary Geology, v.22, p.53-93.

Tarling, D.H., 1983, Palaeomagnetism, Chapman and Hall, London.

Taylor, R.E., Payen, L.A., Prior, C.A., Slota, P.J., Gillespie, R. Gowlett, J.A.J., Hedges, R.E.M., Jull, A.J.T., Zabel, T.H., Donahue, D.J. and Berger, R., 1985, Major Revisions In The Pleistocene Age Assignment For North American Human Skeletons By C-14 Accelerator Mass Spectrometry: None Older Than 11,000 C-14 Years B.P.: American Antiquity, v.50, p. 136-140.

Valladas, G., 1978, A Problem Encountered In Dating Quartz By Thermoluminescence: in the Proceedings of the 18th International Symposium on Archaeometry and Archaeological Prospection, Bonn, Germany.

Von der Borch, C.C., Bada, J.L. and Schwebel, D.L., 1980, Amino Acid Racemization Dating Of Late Quaternary Strandline Events Of The Coastal Plain Sequence Near Robe, Southeastern South Australia: Transactions of the Royal Society of South Australia, v. 104, p.167-170.

Wintle, A.G., 1973, Anomalous Fading Of Thermoluminescence In Mineral Samples: Nature, v.245, p.143-144.

Wintle, A.G., 1977, Detailed Study Of A Thermoluminescent Mineral Exhibiting Anomalous Fading: Journal of Luminescence, p.385-393.

Wintle, A.G., 1981, Thermoluminescence Dating Of Late Devensian Loesses In Southern England: Nature, v.289, p.479-480.

Wintle, A.G., 1980, Thermoluminescence Dating: A Review Of Recent Applications To Non-pottery Materials. Archaeometry, v.22, p.40-48.

Wintle, A.G. and Brunnacker, K., 1982, Ages Of Volcanic Tuff In Rheinhessen Obtained By Thermoluminescence Dating Of Loess: Naturwissenchaften v.69, p.181-183.

Wintle, A.G. and Huntley, D.J., 1979, Thermoluminescence Dating Of A Deep-sea Sediment Core. Nature, v.279 ,p.710-712.

Wintle, A.G. and Huntley, D.J., 1980, Thermoluminescence Dating Of Ocean Sediments: Canadian Journal of Earth Sciences, v.17, p.348-360.

Wintle, A.G. and Huntley, D.J., 1982, Thermoluminescence Dating Of Sediments: Quaternary Science Reviews, v.1, pp. 31-53.

Wonnacott, T.H. and Wonnacott, R.J., 1981, Regression, A Second Course In Statistics, John Wiley and Sons, Toronto.

York, D. and Farquhar, R.M., 1972, The Earth's Age And Geochronology, Pergamon Press, Oxford.